

Washington University in St. Louis

## Washington University Open Scholarship

---

All Theses and Dissertations (ETDs)

---

5-24-2012

### Investigation Into Modeling And Control Methods To Optimize The Power Output Of Wind Turbines

Robert Liebschutz

*Washington University in St. Louis*

Follow this and additional works at: <https://openscholarship.wustl.edu/etd>

---

#### Recommended Citation

Liebschutz, Robert, "Investigation Into Modeling And Control Methods To Optimize The Power Output Of Wind Turbines" (2012). *All Theses and Dissertations (ETDs)*. 711.

<https://openscholarship.wustl.edu/etd/711>

This Dissertation is brought to you for free and open access by Washington University Open Scholarship. It has been accepted for inclusion in All Theses and Dissertations (ETDs) by an authorized administrator of Washington University Open Scholarship. For more information, please contact [digital@wumail.wustl.edu](mailto:digital@wumail.wustl.edu).

WASHINGTON UNIVERSITY IN ST. LOUIS  
School of Engineering and Applied Science  
Department of Mechanical Engineering and Material Sciences

Thesis Examination Committee:  
Dr. David Peters, Chair  
Dr. Norman Katz  
Dr. Swami Karunamoorthy  
Dr. Mark Jakiela  
Dr. Guy Genin

INVESTIGATION INTO MODELING AND CONTROL METHODS TO  
OPTIMIZE THE POWER OUTPUT OF WIND TURBINES

by

Rob Liebschutz

A dissertation presented to the School of Engineering  
of Washington University in partial fulfillment of the  
Requirements for the degree of

DOCTOR OF SCIENCE

May 2012  
Saint Louis, Missouri

## ABSTRACT OF THE DISSERTATION

Investigation Into Modeling and Control Methods to Optimize the  
Power Output of Wind Turbines

by

Rob Liebschutz

Doctor of Science in Mechanical Engineering

Washington University in St. Louis, 2011

Research Advisor: Professor David Peters

Wind turbine power output is a function of not only wind speed but many other constraints such as attitude with respect to the wind and blade pitch settings. Optimizing power output with respect to these parameters is accomplished by optimizing the rotary system's power coefficient. A primary objective of this research is to optimize the power coefficient in a design space that includes collective and cyclic pitch in the presence of axial or yawed wind inflow. The model developed to perform this analysis uses blade element theory and a nonlinear version of the Pitt Peters dynamic inflow model. The model was compared to the National Renewable Energy Labs WT\_Perf wind turbine simulation and showed an acceptable match for the domain being analyzed. A secondary objective of this research is to investigate the effect of continuous cyclic pitch on the power coefficient when used to control the instantaneous moments of a wind turbine at a specific yaw angle with respect to the wind. Wind-turbine power output and attitude with respect to the wind is generally controlled through collective pitch and/or tower yaw, via a vane or actuator. Hohenemser suggested the possibility of control by means of rotor yaw via moments generated by cyclic pitch. (Wind turbines generally do not have cyclic pitch). For the purposes of this dissertation, the investigation focuses on the feasibility of Hohenemser's idea by evaluating the change of the optimal power coefficient when cyclic pitch is also being used to reduce the magnitude of the system's instantaneous moments.

Collective blade pitch control is an accepted practice to optimizing power output by setting the turbine to the optimal collective pitch settings as the wind magnitude changes. This research shows that the extension of using cyclic pitch can further increase the optimal power coefficient by using optimal values for collective and cyclic pitch in yawed inflow conditions. Secondly this research supports the feasibility of Hohenemser's idea that cyclic pitch can be used to simultaneously optimize the power coefficient and minimize the instantaneous moments in yawed inflow. The results present numerical values for the optimal collective and cyclic pitch values that can optimize the power coefficient and keep the system moments below a design threshold. The results also show that the optimal power coefficient is not seriously degraded when cyclic pitch is both minimizing system moments and optimizing the power coefficient.

# Acknowledgments

Special thanks goes to Dr. Peters, the many graduate students and distinguished faculty within and outside my department who have reviewed this work and helped support the related research. Dr. Peters has been supportive beyond belief as I tried to balance full time work, a family and writing a dissertation.

Much love and thanks goes to my family, parents, kids and wife. Before it was clear I would do doctoral research and write a dissertation, I took qualifying exams just to see if I could pass them (which I found out later I did). During the exams my wife was having contractions with our second child and, unbeknownst to me, was trying to hang on to give me time to finish the exams. After the tests we went straight to the hospital and our son was born 4 hours later. So my family has been incredibly supportive every step of the way. Love you all very much.

Rob Liebschutz

*Washington University in St. Louis*

*May 2012*

# Nomenclature

$a$	slope of lift curve
$b$	number of blades
$c$	chord length, (m)
$C_D$	drag coefficient, $F_D/(\rho\pi R^2 W^2/2)$
$C_L$	lift coefficient, $F_L/(\rho\pi R^2 W^2/2)$
$C_{LL}$	Roll Moment Coefficient
$C_M$	Pitch Moment Coefficient
$C_P$	Power coefficient, $P/(\rho\pi R^3 W^2/2)$
$dF_1$	thrust on blade element, which is normal to the plane of rotation, (N)
$dF_2$	drag on blade element, tangential to the circle swept by rotor, (N)
$dF_1^i$	thrust on element of the $i$ th blade, which is normal to the plane of rotation, (N)
$dF_2^i$	drag on element of $i$ th blade, tangential to the circle swept by the $i$ th blade, (N)
$F_D$	profile drag force parallel to the wind direction, (N)
$F_1$	thrust on blade, which is normal to the plane of rotation, (N)
$F_2$	drag on blade, which is tangential to the circle swept by the rotor, (N)
$F_L$	lift force on the rotor, (N)
$J$	normalized tip speed, $\Omega R/W$
$\dot{m}$	mass flow rate, (kg/s)
$L$	aerodynamic roll moment on rotor (N-m)
$M$	aerodynamic pitch moment on rotor (N-m)
$P$	power extracted from wind, (Watts)
$R$	radius of blade, (m)
$T$	thrust on the rotor, (N)
$v$	induced flow, (m/s)
$w$	induced flow coefficient, $v/W$
$W$	wind speed, (m/s)
$W_1$	component of the initial wind speed normal to the plane of rotation, (m/s)
$W_2$	component of the initial wind speed parallel to the plane of rotation, (m/s)

$W_p$	component of relative wind speed normal to plane of rotation, (m/s)
$W_T$	component of relative wind speed tangential to circle swept by rotor, (m/s)
$W_p^i$	component of relative wind normal to plane of rotation for ith blade (m/s)
$W_T^i$	component of relative wind tangential to the circle swept by ith blade, (m/s)
$x$	radial location of a blade element, (m)
$\rho$	density of air, (kg/m <sup>3</sup> )
$\alpha$	angle of attack, (rad)
$\gamma$	angle between the wind direction and the rotor axis, (rad)
$\theta$	blade pitch angle, (rad)
$\theta_o$	collective pitch angle, (rad)
$\theta_s$	lateral cyclic pitch angle, (rad)
$\theta_c$	longitudinal cyclic pitch angle, (rad)
$\theta_t$	blade twist angle, (rad)
$\phi$	angle between the relative wind and the plane of rotation, (rad)
$\Omega$	blade angular velocity, (rad/s)
$\psi^i$	angle between $W_2$ and the ith blade, (rad)
$\sigma$	rotor property parameter, $bc/(\pi R)$

# Contents

- Acknowledgments .....iv
- Nomenclature .....v
- Contents .....vii
- List of Tables ..... ix
- List of Figures .....x
- Chapter 1 Introduction..... 1
  - 1.1 Recent Growth in Wind Energy Research..... 1
  - 1.2 Problem Statement..... 2
  
- Chapter 2 Literature Review .....5
  - 2.1 Early Work in Wind Turbine Modeling ..... 5
  - 2.2 Applied Aerodynamics to Wind Turbines..... 7
    - 2.2.1 Dynamic Inflow and Yawed Flow ..... 8
    - 2.2.2 Optimizing the Power Coefficient without Fixed Boundary Conditions ..... 10
  - 2.3 Optimizing the Power Coefficient in Yawed Flow ..... 12
  - 2.4 Relevant Wind Turbine Codes ..... 13
  
- Chapter 3 Model Development..... 16
  - 3.1 Free Body Diagram ..... 16
  - 3.2 Blade Element Representation ..... 17
  - 3.3 Dynamic Inflow Model ..... 21
  - 3.4 Control Terms..... 24
  
- Chapter 4 Model Comparison to the WT Perf Simulation .....25
  - 4.1 Model Implementation ..... 27
  - 4.2 Case Study Description ..... 30
  - 4.3 Comparison of Results ..... 32
  
- Chapter 5 Preliminary Results ..... 41
  - 5.1 Parameter Sweeps of the Power Coefficient ..... 41
  - 5.2 Surface Plots of the Control Space ..... 56
  
- Chapter 6 Results for Optimal Power Coefficient with Varying Controls .....63
  - 6.1 Optimization Set up and Check out..... 63



6.2 Optimization Results .....	68
<b>Chapter 7 Results for Optimal Power Coefficient in Trimmed State .....</b>	<b>79</b>
7.1 Optimization Set up and Check out.....	80
7.2 Optimization Results .....	85
<b>Chapter 8 Conclusions and Future Work.....</b>	<b>96</b>
<b>Appendix A .....</b>	<b>99</b>
<b>Appendix B .....</b>	<b>100</b>
<b>References.....</b>	<b>102</b>
<b>Vita.....</b>	<b>106</b>

# List of Tables

Table 4.1 Input Variables required to run WT_3DOF.....	29
Table 4.2 Simulation outputs from WT_3DOF.....	29

# List of Figures

Figure 3.1 Physical system of wind flowing into the rotor plane with (a) a top view, (b) front view.....	16
Figure 3.2 Airflow over airfoil of one blade element for (a) front view of blade, (b) top view.....	18
Figure 4.1 Sign Conventions for WT_3DOF .....	28
Figure 4.2 Sample WT_Perf input file used for case study .....	31
Figure 4.3 Comparisons of (a) $C_p$ and (b) Power as a function of tip speed for $C_D=0.00$ , $\theta_o=3$ .....	34
Figure 4.4 Comparisons of (a) $C_p$ and (b) Power as a function of tip speed for $C_D=0.04$ , $\theta_o=3$ .....	34
Figure 4.5 Comparisons of (a) $C_p$ and (b) Power as a function of tip speed for $C_D=0.08$ , $\theta_o=3$ .....	34
Figure 4.6 Comparisons of (a) $C_p$ and (b) Power as a function of tip speed for $C_D=0.00$ , $\theta_o=1$ .....	35
Figure 4.7 Comparisons of (a) $C_p$ and (b) Power as a function of tip speed for $C_D=0.04$ , $\theta_o=1$ .....	35
Figure 4.8 Comparisons of (a) $C_p$ and (b) Power as a function of tip speed for $C_D=0.08$ , $\theta_o=1$ .....	35
Figure 4.9 Comparisons of (a) $C_p$ and (b) Power as a function of tip speed for $C_D=0.00$ , $\theta_o=-1$ .....	36
Figure 4.10 Comparisons of (a) $C_p$ and (b) Power as a function of tip speed for $C_D=0.04$ , $\theta_o=-1$ .....	36
Figure 4.11 Comparisons of (a) $C_p$ and (b) Power as a function of tip speed for $C_D=0.08$ , $\theta_o=-1$ .....	36
Figure 4.12 Comparisons of CP as a function of theta for tip speed $J = 2$ and $C_D=0.08$ .....	38
Figure 4.13 Comparisons of CP as a function of theta for tip speed $J = 4$ and $C_D=0.08$ .....	38
Figure 4.14 Comparisons of CP as a function of theta for tip speed $J = 5$ and $C_D=0.08$ .....	39
Figure 4.15 Comparisons of CP as a function of theta for tip speed $J = 7$ and $C_D=0.08$ .....	39
Figure 5.1 CP as a function of tip speed, $\gamma=0^\circ$ , $\theta_o=0^\circ$ , $\theta_s=0^\circ$ , $\theta_c = 0^\circ$ .....	42
Figure 5.2 CP as a function of tip speed, $\gamma=0^\circ$ , $\theta_o=2^\circ$ , $\theta_s=0^\circ$ , $\theta_c = 0^\circ$ .....	43
Figure 5.3 CP as a function of tip speed, $\gamma=0^\circ$ , $\theta_o=4^\circ$ , $\theta_s=0^\circ$ , $\theta_c = 0^\circ$ .....	43
Figure 5.4 CP as a function of w, $\gamma=0^\circ$ , $\theta_o=0^\circ$ , $\theta_s=0^\circ$ , $\theta_c = 0^\circ$ .....	44
Figure 5.5 CP as a function of w, $\gamma=0^\circ$ , $\theta_o=2^\circ$ , $\theta_s=0^\circ$ , $\theta_c = 0^\circ$ .....	44
Figure 5.6 CP as a function of w, $\gamma=0^\circ$ , $\theta_o=4^\circ$ , $\theta_s=0^\circ$ , $\theta_c = 0^\circ$ .....	45
Figure 5.7 CP as a function of $\theta_o$ , $J=2$ , $\gamma=0^\circ$ , $\theta_s=0^\circ$ , $\theta_c = 0^\circ$ .....	46
Figure 5.8 CP as a function of $\theta_o$ , $J=4$ , $\gamma=0^\circ$ , $\theta_s=0^\circ$ , $\theta_c = 0^\circ$ .....	46
Figure 5.9 CP as a function of $\theta_o$ , $J=6$ , $\gamma=0^\circ$ , $\theta_s=0^\circ$ , $\theta_c = 0^\circ$ .....	47
Figure 5.10 CP as a function of $\theta_s$ , $J=2$ , $\gamma=0^\circ$ , $\theta_o=0^\circ$ , $\theta_c = 0^\circ$ .....	47

Figure 5.11	CP as a function of $\theta_s$ , $J=4$ , $\gamma=0^\circ$ , $\theta_o=0^\circ$ , $\theta_c = 0^\circ$ .....	48
Figure 5.12	CP as a function of $\theta_s$ , $J=6$ , $\gamma=0^\circ$ , $\theta_o=0^\circ$ , $\theta_c = 0^\circ$ .....	48
Figure 5.13	CP as a function of $\theta_c$ , $J=2$ , $\gamma=0^\circ$ , $\theta_o=0^\circ$ , $\theta_s = 0^\circ$ .....	49
Figure 5.14	CP as a function of $\theta_c$ , $J=4$ , $\gamma=0^\circ$ , $\theta_o=0^\circ$ , $\theta_s = 0^\circ$ .....	49
Figure 5.15	CP as a function of $\theta_c$ , $J=6$ , $\gamma=0^\circ$ , $\theta_o=0^\circ$ , $\theta_s = 0^\circ$ .....	50
Figure 5.16	CP as a function of $\theta_s$ , $J=6$ , $\gamma=60^\circ$ , $\theta_o=0^\circ$ , $\theta_c = 0^\circ$ .....	51
Figure 5.17	CP as a function of $\theta_s$ , $J=4$ , $\gamma=0^\circ$ , $\theta_o=0^\circ$ , $\theta_c = 0^\circ$ .....	51
Figure 5.18	CP as a function of $\theta_s$ , $J=6$ , $\gamma=0^\circ$ , $\theta_o=0^\circ$ , $\theta_c = 0^\circ$ .....	52
Figure 5.19	CP as a function of $\theta_c$ , $J=2$ , $\gamma=60^\circ$ , $\theta_o=0^\circ$ , $\theta_s = 0^\circ$ .....	52
Figure 5.20	CP as a function of $\theta_c$ , $J=4$ , $\gamma=60^\circ$ , $\theta_o=0^\circ$ , $\theta_s = 0^\circ$ .....	53
Figure 5.21	CP as a function of $\theta_c$ , $J=6$ , $\gamma=60^\circ$ , $\theta_o=0^\circ$ , $\theta_s = 0^\circ$ .....	53
Figure 5.22	CP as a function of $\gamma$ , $J=2$ , $\theta_o = 0^\circ$ , $\theta_s=0^\circ$ , $\theta_c = 0^\circ$ .....	54
Figure 5.23	CP as a function of $\gamma$ , $J=4$ , $\theta_o = 0^\circ$ , $\theta_s=0^\circ$ , $\theta_c = 0^\circ$ .....	55
Figure 5.24	CP as a function of $\gamma$ , $J=6$ , $\theta_o = 0^\circ$ , $\theta_s=0^\circ$ , $\theta_c = 0^\circ$ .....	55
Figure 5.25	CP as a function of $\theta_s$ , $\theta_c$ with $J=3$ , $\theta_o = 4^\circ$ , for (a) $\gamma = 0^\circ$ (b) $\gamma = 40^\circ$ .....	56
Figure 5.26	CP as a function of $\theta_s$ , $\theta_c$ with $J=3$ , $\theta_o = 0^\circ$ , for (a) $\gamma = 0^\circ$ (b) $\gamma = 40^\circ$ .....	57
Figure 5.27	CP as a function of $\theta_s$ , $\theta_c$ with $J=3$ , $\theta_o = -4^\circ$ , for (a) $\gamma = 0^\circ$ , (b) $\gamma = 40^\circ$ .....	57
Figure 5.28	CP as a function of $\theta_s$ , $\theta_c$ with $J=5$ , $\theta_o = 4^\circ$ , for (a) $\gamma = 0^\circ$ , (b) $\gamma = 40^\circ$ .....	57
Figure 5.29	CP as a function of $\theta_s$ , $\theta_c$ with $J=5$ , $\theta_o = 0^\circ$ , for (a) $\gamma = 0^\circ$ , (b) $\gamma = 40^\circ$ .....	58
Figure 5.30	CP as a function of $\theta_s$ , $\theta_c$ with $J=5$ , $\theta_o = -4^\circ$ , for (a) $\gamma = 0^\circ$ , (b) $\gamma = 40^\circ$ .....	58
Figure 5.31	CP as a function of $\theta_o$ , $\theta_s$ with $J=3$ , $\theta_c = 4^\circ$ , for (a) $\gamma = 0^\circ$ , (b) $\gamma = 40^\circ$ .....	59
Figure 5.32	CP as a function of $\theta_o$ , $\theta_s$ with $J=3$ , $\theta_o = 0^\circ$ , for (a) $\gamma = 0^\circ$ , (b) $\gamma = 40^\circ$ .....	59
Figure 5.33	CP as a function of $\theta_o$ , $\theta_s$ with $J=3$ , $\theta_c = -4^\circ$ , for (a) $\gamma = 0^\circ$ , (b) $\gamma = 40^\circ$ .....	60
Figure 5.34	CP as a function of $\theta_o$ , $\theta_c$ with $J=3$ , $\theta_s = 4^\circ$ , for (a) $\gamma = 0^\circ$ , (b) $\gamma = 40^\circ$ .....	60
Figure 5.35	CP as a function of $\theta_o$ , $\theta_c$ with $J=3$ , $\theta_s = 0^\circ$ , for (a) $\gamma = 0^\circ$ , (b) $\gamma = 40^\circ$ .....	61
Figure 5.36	CP as a function of $\theta_o$ , $\theta_c$ with $J=3$ , $\theta_s = -4^\circ$ , for (a) $\gamma = 0^\circ$ , (b) $\gamma = 40^\circ$ .....	61
Figure 5.37	CP as a function of $\theta_o$ and $\theta_s$ with $J=5$ , $\theta_c = 0^\circ$ , for $\gamma = 0^\circ$ .....	62
Figure 6.1	CP as a function of $\theta_s$ and $\theta_c$ with $J=5$ , $C_D = 0.08$ , $\theta_o = -4^\circ$ , for (a) $\gamma = 0^\circ$ , and (b) $\gamma = 40^\circ$ .....	65
Figure 6.2	CP as a function of (a) $\theta_s$ , (b) $\theta_c$ with $J=5$ , $C_D = 0.08$ , $\theta_o = -4^\circ$ , $\gamma = 40^\circ$ .....	66
Figure 6.3	CP as a function of $\theta_o$ and $\theta_c$ with $J=5$ , $C_D = 0.08$ , $\theta_s = 0^\circ$ , for (a) $\gamma = 0^\circ$ , and (b) $\gamma = 40^\circ$ .....	66
Figure 6.4	CP as a function of (a) $\theta_o$ , (b) $\theta_c$ with $J=5$ , $C_D = 0.08$ , $\theta_o = 0^\circ$ , $\gamma = 40^\circ$ .....	67
Figure 6.5	Optimal CP as a function of tip speed, $J$ , for $C_D = 0.02$ , and (a) $\gamma = 0^\circ$ , (b) $\gamma = 20^\circ$ , (c) $\gamma = 40^\circ$ , (d) $\gamma = 50^\circ$ , (e) $\gamma = 60^\circ$ , (f) $\gamma = 80^\circ$ .....	69
Figure 6.6	Optimal CP as a function of tip speed, $J$ , for $C_D = 0.04$ , and (a) $\gamma = 0^\circ$ , (b) $\gamma = 20^\circ$ , (c) $\gamma = 40^\circ$ , (d) $\gamma = 50^\circ$ , (e) $\gamma = 60^\circ$ , (f) $\gamma = 80^\circ$ .....	70
Figure 6.7	Optimal CP as a function of tip speed, $J$ , for $C_D = 0.08$ , and (a) $\gamma = 0^\circ$ , (b) $\gamma = 20^\circ$ , (c) $\gamma = 40^\circ$ , (d) $\gamma = 50^\circ$ , (e) $\gamma = 60^\circ$ , (f) $\gamma = 80^\circ$ .....	71
Figure 6.8	Optimal CP as a function of Yaw Angle, $\gamma$ , for $C_D = 0.04$ , and (a) $J = 3$ , (b) $J = 5$ , (c) $J = 7$ and (d) $J = 8$ .....	73
Figure 6.9	Optimal CP as a function of Yaw Angle, $\gamma$ , for $C_D = 0.08$ , and (a) $J = 3$ , (b) $J = 5$ , (c) $J = 7$ and (d) $J = 8$ .....	74
Figure 6.10	Optimal Values as a function of tip speed, $J$ , for $C_D = 0.08$ , and $\gamma = 0^\circ$ .....	75
Figure 6.11	Optimal Values as a function of tip speed, $J$ , for $C_D = 0.08$ , and $\gamma = 20^\circ$ .....	76
Figure 6.12	Optimal Values as a function of tip speed, $J$ , for $C_D = 0.08$ , and $\gamma = 40^\circ$ .....	76

Figure 6.13	Optimal Values as a function of tip speed, J, for $C_D = 0.08$ , and $\gamma = 60^\circ$ ..	77
Figure 7.1	$M^2+L^2$ as a function of $\theta_s, \theta_c$ , for J=3, $C_D = 0.08$ , $\theta_o = 0^\circ$ and (a) $\gamma = 0^\circ$ and (b) $\gamma = 40^\circ$ .....	81
Figure 7.2	$M^2+L^2$ as a function of $\theta_s, \theta_o$ , for J=3, $C_D = 0.08$ , $\theta_c = 0^\circ$ and (a) $\gamma = 0^\circ$ and (b) $\gamma = 40^\circ$ .....	81
Figure 7.3	$M^2+L^2$ as a function of $\theta_o, \theta_c$ , for J=3, $C_D = 0.08$ , $\theta_s = 0^\circ$ and (a) $\gamma = 0^\circ$ and (b) $\gamma = 40^\circ$ .....	81
Figure 7.4	$f_o(x)$ as a function of $\theta_s, \theta_c$ , with $k=1e-7$ , for J=3, $C_D = 0.08$ , $\theta_o = 0^\circ$ and (a) $\gamma = 0^\circ$ and (b) $\gamma = 40^\circ$ .....	82
Figure 7.5	$f_o(x)$ as a function of $\theta_o, \theta_s$ , with $k=1e-7$ , for J=3, $C_D = 0.08$ , $\theta_c = 0^\circ$ and (a) $\gamma = 0^\circ$ and (b) $\gamma = 40^\circ$ .....	83
Figure 7.6	$f_o(x)$ as a function of $\theta_o, \theta_c$ , with $k=1e-7$ , for J=3, $C_D = 0.08$ , $\theta_s = 0^\circ$ and (a) $\gamma = 0^\circ$ and (b) $\gamma = 40^\circ$ .....	83
Figure 7.7	Moment design criteria as a function of $\log_{10}(k)$ for J=8, $C_D = 0.08$ , $\gamma = 40^\circ$ .....	84
Figure 7.8	Optimal CP as a function of tip speed, J, for $C_D = 0.02$ , and (a) $\gamma = 0^\circ$ , (b) $\gamma = 20^\circ$ , (c) $\gamma = 40^\circ$ , (d) $\gamma = 50^\circ$ , (e) $\gamma = 60^\circ$ , (f) $\gamma = 80^\circ$ .....	86
Figure 7.9	Optimal CP as a function of tip speed, J, for $C_D = 0.04$ , and (a) $\gamma = 0^\circ$ , (b) $\gamma = 20^\circ$ , (c) $\gamma = 40^\circ$ , (d) $\gamma = 50^\circ$ , (e) $\gamma = 60^\circ$ , (f) $\gamma = 80^\circ$ .....	87
Figure 7.10	Optimal CP as a function of tip speed, J, for $C_D = 0.08$ , and (a) $\gamma = 0^\circ$ , (b) $\gamma = 20^\circ$ , (c) $\gamma = 40^\circ$ , (d) $\gamma = 50^\circ$ , (e) $\gamma = 60^\circ$ , (f) $\gamma = 80^\circ$ .....	88
Figure 7.11	Optimal CP as a function of Yaw Angle, $\gamma$ , for $C_D = 0.04$ , and (a) J = 2, (b) J = 3, (c) J = 5 and (d) J = 7 .....	90
Figure 7.12	Optimal CP as a function of Yaw Angle, $\gamma$ , for $C_D = 0.08$ , and (a) J = 2, (b) J = 3, (c) J = 5 and (d) J = 7 .....	91
Figure 7.13	Optimal Values as a function of tip speed, J, for $C_D = 0.08$ , and $\gamma = 0^\circ$ ....	92
Figure 7.14	Optimal Values as a function of tip speed, J, for $C_D = 0.08$ , and $\gamma = 20^\circ$ ..	92
Figure 7.15	Optimal Values as a function of tip speed, J, for $C_D = 0.08$ , and $\gamma = 40^\circ$ ..	93
Figure 7.16	Optimal Values as a function of tip speed, J, for $C_D = 0.08$ , and $\gamma = 60^\circ$ ..	93
Figure 7.17	% Resultant Moment/(T*R) for Optimal Results Using Collective and Cyclic Pitch in Trimmed State .....	94
Figure B.1	Top Level Blocks of WT_3DOF .....	100
Figure B.2	Blade Element Theory Block in WT_3DOF .....	101

# Chapter 1

## Introduction

### 1.1 Recent Growth in Wind Energy Research

The United States Department of Energy published a report outlining the ambitious plan to make 20% of the total U.S. consumption of electricity supplied by wind energy by the year 2030 [1]. The report details the motivation for the ambitious initiative as that of reducing the country's reliance on fossil fuels, or specifically, “vulnerability to fluctuating prices, energy supply chain uncertainties and adverse environmental impacts”. The report concludes that it is feasible to increase wind energy's contribution to the U.S. electric supply to 20% by 2030. However major challenges must be overcome. Among them are improvements on how the electricity is absorbed into the country's electric supply chain, how the power could be transferred to regions with low wind—preventing new adverse environmental impacts—and, finally, improving wind turbine performance, both in terms of reducing cost and increasing efficiency.

This Department of Energy initiative began in the Bush administration and has gathered steam under the Obama administration. The DOE's 2008 Wind Technologies Market Report described how 16 billion dollars were spent to increase the country's capacity to harness wind energy and to make improvements through research [2]. The department also awarded additional tens of millions of dollars to various companies or research groups in 2009 all focused on improving wind turbine technology and electricity transmission. As a result of the department's financial investments and long term objectives, wind energy research has once again started to grow.

With this recent surge in political and financial investment, new and innovative approaches to harnessing wind energy have emerged. One promising area is that of High Capacity Wind Turbines (HCWTs), which are described as 4 Mega Watt (MW) or above. One example of such machines is a tethered turbine that is capable of absorbing the higher wind magnitudes at high altitudes and are connected to earth by tethers that both hold the turbine in place and transmit electricity to a plant. Feasibility studies have been conducted by companies such as Baseload Energy Inc. that indicate the HCWT configuration could make significant contributions to the Department of Energy's goal of increasing the contribution of wind energy to the overall electricity consumption of the United States[3]. Currently the company is still developing a prototype to collect data and validate their projections [4]. The company is using their own engineers with the contribution of researchers and faculty from The Georgia Institute of Technology to perform this work.

Wind power harnessed from a turbine, flying or fixed to a tower, is proportional to the velocity cubed. Thus the primary motivation of flying turbines is to put these machines where the wind speeds are the strongest - the jet stream. A general formula for computing the expected wind energy from a turbine is:

$$\text{Power in Watts (Joules per Second)} = 1/2 (\rho)(A)(V^3)(E) \quad (1.1)$$

where  $\rho$  is the air density,  $A$  is the area,  $V$  is the cubed of wind velocity, and  $E$  is the efficiency of capturing the wind energy. The technical term used to denote the efficiency for the wind turbine system is the power coefficient. The power coefficient is a non-dimensional measure of how well a turbine converts wind energy to electricity. Therefore regardless of all the system losses, optimizing the total energy that can be harnessed means optimizing the system's power coefficient.

## 1.2 Problem Statement

The focus of this research is to investigate how a windmill's power coefficient can be optimized by opening the control space of the wind turbine—that is, using both

collective and cyclic pitch to increase the optimal power coefficient. Traditionally, wind turbines only use collective pitch to regulate airflow and optimize power output. The use of cyclic pitch is relevant to wind turbine systems that want optimal power while controlling the wind turbine's orientation to the wind direction.

It is widely known that a wind-turbine rotor is designed to accommodate a specific range of wind speeds. Traditionally wind turbines run within a defined range of wind speeds with the understanding that if the inflow through the wind turbine disc becomes too low or high, the system would not be operating optimally. In very high winds, the system runs the risk of failure. To avoid damage, current wind turbine systems can apply brakes or turn the blades out of the wind such that it is turned off. Modern wind turbine designs have improved power output by implementing a controller. The controls can implement collective pitch or tower yaw via an actuator to limit the rotor's Revolutions Per Minute (RPMs) that can either run the system optimally or in adverse conditions, protect the system hardware.

To maximize power output, a wind turbine that operates continuously must optimize system power by finding the optimal attitude with respect to the wind, such that the magnitude of the inflow is optimal for the ideal rotor RPM. Although this is currently accomplished through a combination of collective pitch and tower yaw, Hohenemser suggested the possibility of control of tower yaw by means of rotor yaw moments generated by cyclic pitch.[5] If such an application were feasible, then a system could be designed to continuously optimize power output by means of automatic feedback control. The idea would be to use the increased control space to optimize power by controlling the system's attitude with respect to the wind and to simultaneously apply the optimal collective and cyclic pitch settings.

The primary objective of this dissertation is to investigate the effect of cyclic pitch on the optimal power coefficient. This will be done by numerically determining the parameters required to optimize the power of a wind turbine for a test case in the presence of axial and yawed inflow with the use of collective and cyclic pitch. Leading up to Hohenemser's larger idea, it would first be useful first to know if the increased control space of cyclic pitch can increase the optimal power coefficient for conditions such as yawed inflow. The model developed to perform the computation uses: 1.) a



blade-element theory to compute the system moments and forces, and 2.) a nonlinear version of the Pitt Peters dynamic inflow model to compute the induced velocities. The model is compared against a simulation that is developed and used by the National Renewable Energy Lab (NREL) to verify a reasonable output for the domain being analyzed.

A secondary objective of the research is to further investigate the effect of cyclic pitch on the optimal power coefficient when it is being used to minimize the instantaneous moments of the wind turbine at some specific yaw angle. This will be accomplished by studying trends in the power coefficient for an equivalent case where the cyclic pitch is being used to optimize the power coefficient while simultaneously keeping the system moments below a design threshold.

# Chapter 2

## Literature Review

Research relevant to this problem includes the aerodynamic theory of wind turbines, including unsteady effects. This covers research in deriving and optimizing the power coefficient, plus limited work done regarding cyclic pitch control for wind turbine applications. Extensive research on hardware modeling, blade design manufacturing improvements, sensor modeling and environmental effects is ongoing but is beyond the scope here. Previous research for optimizing the power coefficient predominantly exists for Horizontal Axis Wind Turbines (HAWTs) with some work on Vertical Axis Wind Turbines (VAWTs). At the time of this publication, little research has been found on tethered wind turbines with the exception of Peters et. al. [28] that will be covered in this review.

Models for free stream aerodynamics and collective pitch have been published for wind turbines, but no work to date has been found in modeling cyclic pitch with the intent of studying optimal power output. The organization of this literature review will fall into four sections: early works in wind turbine modeling, applied aerodynamics to wind turbines, optimization of the power coefficient and development of wind turbine codes.

### 2.1 Early Work in Wind Turbine Modeling

Early work in wind turbine theory came from logical extensions of research on propellers. Researchers focused on modeling the airflow through a disk simply to advance the understanding of screw propellers for fixed wing aircraft. Researchers such

as Rankin, Froude, Betz, Glauert, Joukowski and Prandtl made the more classic contributions to the understanding of airflow through a rotary wing system, whether it be a propeller or wind turbine.

According to Wilson and Lissaman [6], the original momentum theory for fluid flow through a turbine was derived for naval applications by Rankine [7] and Froude [8, 9]. This model was simplified assuming one dimensional, steady state axial flow and considered no rotational effects. Using a simplified one dimension model, Betz used basic fluid dynamic momentum theory and derived the ideal power coefficient, that is, the maximum percent of power that can be extracted from a steady state, axial wind flow through a disk [10]. He showed that the maximum power is extracted when the wind speed decelerates to  $2/3$  its original speed across the rotor plane and that no turbine can capture more than 59.3 percent of the kinetic energy of the wind. Frederick Lanchester, a British Scientist, had also derived this result, thus it is sometimes referred to as the Betz Lanchester limit. This momentum theory does not make any assumptions about the effects of wake behavior or unsteady flow. Yet it is classic in applying energy methods to derive the theoretical ideal values for the power coefficient.

Glauert [11, 12] and Joukowski [13] expanded on the simple momentum theory to account for wake effects including expansion and rotation. They initiated theory to begin to account for why the ideal power coefficient could not be achieved. Their work predominantly focused on propellers but did address the subject of windmills where induced flow is extracted rather than pumped. The simple momentum theory assumes perfect streamlines through the turbine disk plane whereas the rotational momentum of the actuator disk affects the wake. Glauert discussed that the rotation of the disk imparts an equal and opposite angular momentum on the wake. This loss in kinetic energy reduces the static pressure drop across the disk and reduces the extracted energy. He notes that the rotation also results in a radial pressure gradient to balance centrifugal forces. This results in yet another pressure drop in addition to the static axial drop across the disk. Joukowski derived models that estimated the power loss due to rotational effects. He also was one of the first to derive equations that relate the downstream axial and radial velocities to the velocities at the disk.

Another reason that ideal power cannot be achieved is losses at the blade tip. Prandtl [14] is well known for his work on tip losses, the energy losses due to radial wake flow around the tip of the turbine blades. Prandtl provided methods to account for tip loss, which amounts to a scale factor that shortens the radius of the blade and thereby reduces the system's effectiveness. In rotorcraft the scale factor would reduce the lift and can account for 6-9% loss of the available power. Prandtl and others used different methods to determine the scale factor, however a value commonly used is 0.97.

## **2.2 Applied Aerodynamics to Wind Turbines**

Wilson and Lissaman provided much of the early development of wind turbine theory in their NTIS report, "Applied Aerodynamics of Wind Turbines" [6]. In this work and "Applied Aerodynamics of wind power machines" the authors review many types of wind power machines and evaluate their aerodynamic characteristics. Since the early development of rotary wing aerodynamic theory, most research conducted focused on propellers, specifically as they apply to rotorcraft. Wilson and Lissaman appear to be the first to thoroughly apply the theory to windmills. They evaluate their efficiency and present advantages and disadvantages for the different configurations such as Savonius, Madarus and Darrieus rotors, Gyromills, ducted rotors, the Smith-Putnam design, circulation-controlled rotors and more. Tethered windmills were not evaluated. Additional work was spent on analyzing hub fairings, spinners and tip vanes. Regarding horizontal axis windmills, the theory reviews general momentum theory, presents the effects of wake rotation, blade element theory and also discusses vortex strip theory. All this provides the theoretical background they used for evaluating the overall efficiency of different turbine configurations.

Arguably, Wilson and Lissaman are the most-cited read early researchers in applying aerodynamic theory specifically to wind turbines. Their research expanded into experimental techniques for analyzing aerodynamic performance in wind turbines [15, 16]. And on the subject of developing wind turbine codes (Section 2.4) they are

well known for their “Prop-Code” [6], which has become a popular benchmark for Blade Element Momentum theory comparisons in most contemporary papers concerned with accurately modeling the aerodynamics and power output of wind turbines. They also extended their work in a paper in 1981 that provided a simple aerodynamic model for the turbulent windmill\ vortex ring state and for yawing moments on a wind turbine that result from blade coning [17]. Their focus of applied aerodynamics to specifically wind turbines advanced knowledge more than any other during their time.

Textbooks such as *The Wind Handbook* [18] and *Wind Energy Explained* [19] do a thorough job of presenting the categories of research and deriving the fundamental equations in aerodynamic modeling of wind turbines. They provide alternate sources and approaches to applying momentum theory, blade element theory, vortex strip theory, tip losses, the effect of collective pitch on the power coefficient, blade coning and flapping.

### **2.2.1 Dynamic Inflow and Yawed Flow**

A contemporary of Wilson and Lissaman was A. Swift who worked with Hohenemser on modeling yaw dynamics in the early 1980’s. Swift’s dissertation, “The Effects of Yawed Flow on Wind Turbine Rotors” presented an early approach to computing yawed dynamics using knowledge of steady state behavior and iterative methods via a computer algorithm [20]. He is also one of the early researchers to include a dynamic inflow model, such as the Peters Pitt model [21], into the aerodynamic modeling of wind turbines. Two limitations documented by Swift were accounting for the effects of stall and modeling performance as the rotor approached the vortex ring state [22]. Swift extended the Wilson-Lissaman model to regions with high tip speed ratios near the vortex ring state and addressed the effects of dynamic flow regimes. At issue was the fact that at higher tip speed ratios, the computed "induced flow velocity exceeds one-half of the free stream velocity, contradicting the momentum theory assumption of the model." Swift found the methods developed by

Viterna and Corrigan [23] sufficient in accounting for the effects of dynamic stall, which is largely neglected in his research.

Snel and Scheppers published a large body of theory and experimental data focused on the implementation of dynamic airflow effects in wind turbine modeling throughout the 1990s. In their JOULE 1 project, the “Joint Investigation of Dynamic Inflow Effects and Implementation of an Engineering Method” [24], the authors document much of their work and data. The paper was part of an effort to validate engineering models of dynamic inflow using wind turbine field data and wind tunnel data. Several contributors provided data in the papers and the authors compared free wake and “engineering models” to the experimental data in the Appendices of the report.

Snel and Scheppers show from both theoretical models and experimental data the importance of accounting for dynamic inflow in wind turbine models, showing the inability of BEM to account for the overshoot of various parameters during some controlled blade pitch changes. The authors divide unsteady aerodynamics on the blade into two categories: “instationary profile aerodynamics”, also called dynamic stall, and dynamic inflow. The paper states that dynamic inflow is of primary importance as the time constants are larger. They approximate the dynamic stall time constant as approximately the chord divided by the velocity at that blade section ( $c/\Omega r$ ), or approximately 0.2 seconds at blade root and 0.1 seconds at the blade tip. They approximate the dynamic inflow time constant as the rotor diameter divided by free stream wind velocity ( $D/V$ ), or on the order of 5-10 seconds, a time constant so large they call it, “quasi-steady”. Thus along with Swift, researchers consider dynamic stall a second order effect in the dynamic effects of airflow through a wind turbine.

That paper reviews the modeling successes and leaves much open for future work, citing the importance of modeling yawed airflow conditions. The authors showed a clear presence of dynamic inflow in several experimental data sets and were able to accomplish a “general” validation of their model. For yawed conditions, the authors note that dynamic inflow effects were present for wind turbines with larger loads and faster tip speed ratios.

A paper published by Suzuki [25] in 2000, presents an implementation of the Generalized Wake Theory, originally developed for rotorcraft by He and Peters[26] that is applicable to wind turbines. The paper compares BEM, a Pitt-Peters model and a Generalized Dynamic Wake model to wind turbine data measured in Denmark. Suzuki was an advisee of Dr. Craig Hansen, who published works on yawed flow in wind turbines [27]. He is also a key contributor to the wind turbine code, YAWDYN, that is documented in the codes section of this brief review (2.4).

Since Wilson and Lissaman a great deal of work has gone into learning the importance of both dynamic inflow and the need to match wind turbine data to models. The codes sections will review some of the well known codes used by government agencies and in industry. But it is clear that contemporary code developers still work to accurately model yawed flow through wind turbines.

### **2.2.2 Optimizing the Power Coefficient without Fixed Boundary Conditions**

As wind turbine designs become more complex, it cannot always be assumed that the rotor plane will have a fixed boundary condition via being attached to a tower. VAWT and various other configurations have been discussed by Wilson and Lissaman among others. A configuration of interest in this dissertation is a wind turbine with a tethered boundary condition. Previous work on this subject has been performed by Peters, Ahaus, Chan and Loyet [28].

That work uses momentum theory equations to derive the feasible design space for a tethered, yawed wind turbine. Beginning with the case of a horizontal tether and progressing to the generalized case where the tether angle is a variable, equations for the power coefficient are derived. A closed-form expression was derived for the case of a horizontal tether, but numerical iteration was required to solve the equations for the case of a general tether. The paper provides extensive plots of how the power coefficient is related to the induced flow, tether angle with respect to the wind and weight coefficient. Design charts show the power that can be expected for various

tether angles based on the system weight of the tethered wind turbine. Trend plots are also provided for the normalized induced flow (by wind speed) in the directions normal and parallel to the cable. The paper also provides results that account for the weight of a long, heavy cable and rotor efficiency showing what design limits exist for cables of various weight and length.

As expected, the higher the weight of the cable means the greater the overall weight of the system and the more thrust is required thereby reducing the power coefficient. The derived equations show that the weight per unit length also limits the feasible tether angles that are capable of extracting power from the wind. An efficiency term was implemented in the equations for the power coefficient to represent rotor and transmission losses in taking power from the wind, which reduce the power coefficient and the feasible design space of the system. The case of perfect efficiency,  $e=1$ , matches the ideal case shown in the paper.

Although an application of momentum theory alone, that work is one of the first in understanding both what physical limitations exist and what geometric orientations must exist between the angles of the wind, the cable and the rotor plane in order to optimize power extraction. The researchers conclude that with reasonable efficiencies and weight restrictions, extracting power from a tethered, yawed wind turbine is indeed feasible.

Peters and Rong extend this body of research by implementing blade element theory to compute moments and forces while using momentum theory to compute induced velocities [29]. The equations in the paper are derived to enable feasibility analysis of yawed flow. The results show the design space for where the power coefficient was optimal for various pitch settings, tip speed ratios, induced velocities and yaw angles. Although the induced velocities were computed using only momentum theory, the results did show a feasible design space demonstrating the need for continued study.



## 2.3 Optimizing the Power Coefficient in Yawed Flow

An understanding how the power coefficient changes with yawed flow is of primary importance to optimizing the performance of any wind turbine system. A familiar problem with turbine generators is that the rotor is typically designed to accommodate a specific range of RPMs based upon the expected wind speeds of the site and lift of the airfoil blades. This range of RPM defines the design space for which the power coefficient can be optimized and steady state electricity can be harnessed. Clearly if the wind speed is too light, then the rotor will not turn, and if the wind speed gets too great, then the rotor can exceed the maximum RPM and must be shut off or it will endanger the turbine itself. Yawed flow wind turbines were designed to address this constraint. These turbines are designed and manufactured to adjust the yaw angle with respect to the wind direction to control the rotor RPM and thereby optimize the power coefficient.

A large body of work was done by Hohenemser and Swift on the topic of using the wind turbine yaw angle to control the desired RPM and optimize the power coefficient. A paper by Hohenemser, Swift and Peters provided an analysis showing the feasibility of rotary sail wind systems in 1979 [30]. Hohenemser and Swift demonstrated torque control by yaw of a constant-speed two bladed wind turbine in 1983 [5]. In 1987 Hohenemser published analysis and test results for a passive cyclic pitch wind turbine [31].

In 1995 Hohenemser summarized the analysis and test results from a five year effort at Washington University in St. Louis that studied a two blade horizontal-axis wind turbine with a teetering hub [32]. It was called a passive cyclic pitch (PCP) wind turbine, which is defined as "a teeter rotor with a large delta-three angle of the teeter axis". All results in the research are largely specific to the case of teetered, two-bladed wind turbines, however much work was performed on the concept of using active yaw control and free yaw control (with a nacelle) to achieve aerodynamic rotor breaking. The active yaw control employed a mechanism that physically turned the rotor axis in the horizontal plane with respect to the tower. The free yaw could rotate freely in the

horizontal plane with respect to the tower. Comparisons are made between upwind and downwind configurations, concluding that for this specific system the downwind configuration was more stable and suitable for free yaw control. Limitations of a horizontal axis wind turbine mounted to a tower were discussed, such as the coupling between the yaw dynamics and tower bending. The authors showed these dynamics result in instability if the yawing center of gravity did not coincide very well with the tower center and if the first natural bending mode of the tower is above the minimum operating rotor rotational frequency. Thus the structural dynamics of the tower create additional complications for a rotating turbine as it yaws.

That body of work was significant in that it showed that output power could be regulated by yaw control. The analysis techniques used to evaluate the yaw dynamics were developed by Swift [20]. Hohenemser went on to suggest that both the concepts of collective and cyclic blade pitch variations could be used to regulate yaw control and thus output power.

Many contemporary wind turbines that yaw control employ a controller on the tower base to rotate the rotor plane with respect to the wind direction. Currently the World's Largest Wind Turbine (7 + Megawatts), the Enercon 126 in Emden, Germany, uses this technique; they call "side furling" [33]. In this case no collective pitch control is used; the power optimization is completely achieved by turning the rotor plane with respect to the wind. Typically the optimal wind angle for a specific wind speed is computed and the controller can rotate the tower to a desired yaw angle in order to optimize the power coefficient, and thus the output power.

Hohenemser's observation is relevant to tethered wind turbines whose boundary conditions will not necessarily be fixed. More dynamic control would be required not only to optimize the power coefficient but to provide vehicle stability.

## **2.4 Relevant Wind Turbine Codes**

There are a great number of wind turbine codes and especially amongst engineering research circles, countless small specific routines to model specific wind

turbine features. This review focuses on wind turbine codes that have matured to the point that they are used to aid in development and/or certification of wind turbine designs in industry. The evolution of these codes has been slow over the past two decades, but with the increased interest in wind energy, they have become the focus of greater study and scrutiny today.

In 2007 an international team of industry experts in wind turbine simulations participated in a benchmark exercise called “Offshore Code Collaboration Exercise” (OC3) [34]. The codes, considered the state of the art turbine simulation codes amongst wind energy experts, were evaluated against experimental data and all compared generally well in the benchmark exercises. The codes evaluated were: GH Bladed, FAST, ADAMS, HAWC, HAWC2, BHAWC and Flex5. The paper presents all the details of each software’s modeling capabilities and other characteristics of the codes. All of these codes output a full range of data relevant to wind turbine design, such as, blade loads, tip deflections, tower vibration predictions, structural dynamics and more. Each program uses a subroutine to model the rotor aerodynamics. BHAWC and Flex5 rely exclusively on Blade Element Momentum theory (BEM). The rest of the codes use both BEM and Generalized Dynamic Wake (GDW) theory to account for dynamic inflow.

NREL developed and is custodian for the WTPERF, FAST and ADAMS routines. Their website provides a great deal of detail on the use of these programs, along with preprocessing programs to set up input data and post processing programs to generate results [35]. WT Perf is a wind turbine performance tool developed by M Buhl at NREL that is based on Wilson Lissaman PROP code developed at Oregon State University [36]. The FAST and ADAMS programs are accepted as tools that can certify a wind turbine in the United States. In 2003, NREL received recognition from Germanischer Lloyd (GL), the German wind turbine certifying agency, that these codes were suitable for wind turbine design amongst international circles [37].

Both ADAMS (ADAMS2AD is the latest) and FAST use program called AeroDyn to compute the aerodynamic forces along the wind turbine blades and performance characteristics of the model. The AeroDyn program is specific to Horizontal Axis Wind Turbines. It relies on Blade-element Momentum theory and can

account for dynamic stall and dynamic inflow [38]. The software is developed and maintained by Windward Engineering company [39]. Recently NREL removed support of a similar program YawDyn that was released with AeroDyn version 12 and was developed to improve accuracy of modeling wind turbine performance in the presence of yawing motion. Although it is unclear why they dropped support for this program the primary certification programs (ADAMS and FAST) rely exclusively on AeroDyn to perform the aerodynamic computations.

# Chapter 3

## Model Development

This chapter outlines the existing theory used to develop the model for analysis. The sections define the physical system and notation in the wind and rotor frame. Equations for computing the forces and moments on the rotor plane are developed. A dynamic inflow model is presented as well as control terms that will be used to define blade twist, collective and cyclic pitch.

### 3.1 Free Body Diagram

In previous work on yawed wind through a turbine Peters and Rong [29] defined the wind frame relative to the rotor plane as shown in Figure 3.1.

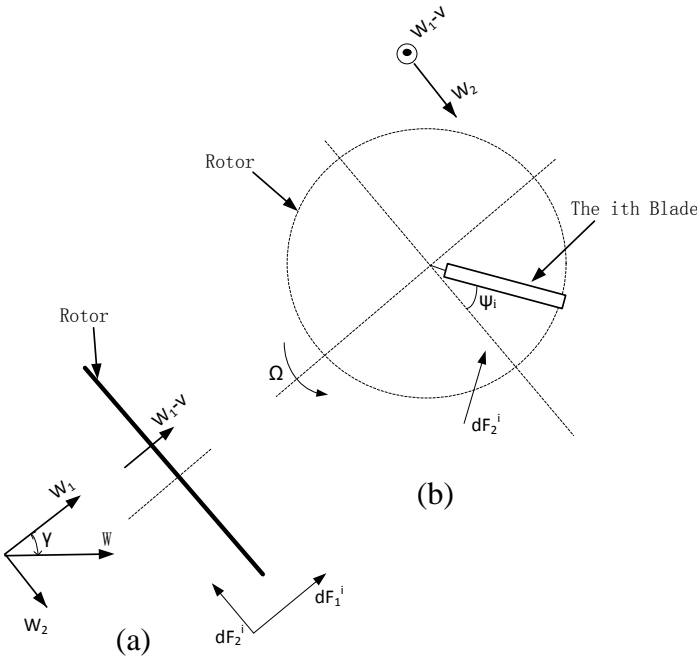


Figure 3.1 Physical system of wind flowing into the rotor plane with (a) a top view, (b) front view

In Figure 3.1,  $W$  is the magnitude of the initial wind speed flowing toward rotor plane at an angle defined by  $\gamma$  and shown in (a). The wind magnitude can be decomposed into normal and parallel components in the rotor plane as:

$$W_1 = W \cos \gamma \quad (3.1)$$

$$W_2 = W \sin \gamma \quad (3.2)$$

where  $W_1$  is the normal component and  $W_2$  is the component parallel to the rotor plane. Figure 3.1 (a) shows that the total wind on the downwind side of the rotor plane is  $W_1 - v$ , where  $v$  is the induced flow.

Figure 3.1 (b) shows the front view of the rotor plane and defines the coordinate system of the blades. The frame defines the  $0^\circ$  azimuth angle,  $\psi$ , as being parallel to  $W_2$ . Then the angle between  $W_2$  and the  $i$ th blade in the rotor plane is defined as  $\psi_i$ .  $\Omega$  is the angular velocity of the rotor,  $dF_1^i$  defines the thrust on the blade element of the  $i^{\text{th}}$  blade normal to the rotor plane and  $dF_2^i$  defines the drag on the blade element of the  $i^{\text{th}}$  blade tangential to the rotor plane. Figure 3.1 (b) shows the notional  $i$ th blade where  $b$  is the total number of blades for the specific wind turbine system. It is noted that the system analyzed here fixed at the rotor but that other boundary conditions such as tethers could be applied.

To determine the system thrust, lift, drag, moments and generated power it will be necessary to know the resultant force obtained from all the blades. This can be accomplished using blade-element concepts.

## 3.2 Blade Element Representation

Blade element theory determines the total system forces and moments on a rotor by breaking down each blade into elements. The wind speed normal and parallel,  $W_1$  and  $W_2$ , can be used to determine the lift and drag on an airfoil at any specific location along the blade. The  $i$ th blade can be broken down into elements and the

forces and moments can be computed for each element, and then summed to get the total along each blade.

The blade element representation used here will be consistent with previous work performed by Peters and Rong. Figure 3.2 shows an airfoil for one blade element in the plane of rotation.

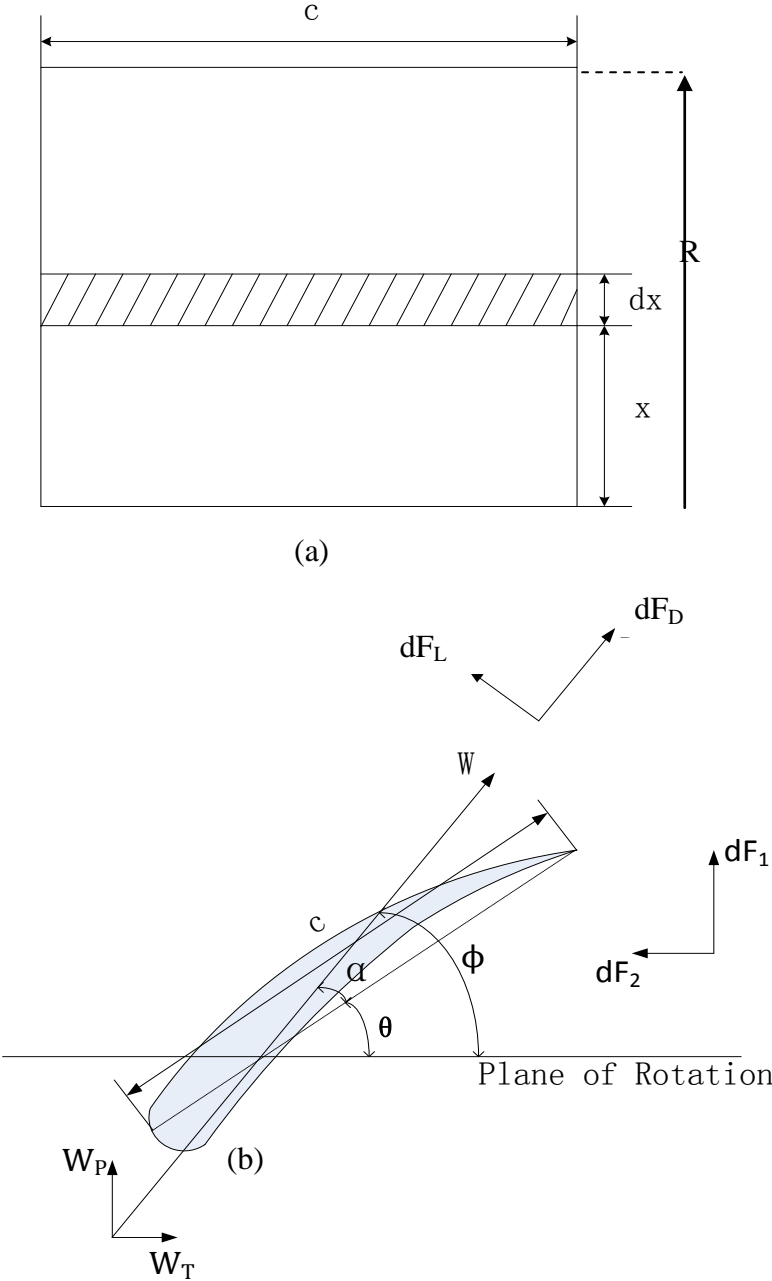


Figure 3.2 Airflow over airfoil of one blade element for (a) front view of blade, (b) top view

$W_p^i$  is the component of the wind at the  $i^{\text{th}}$  blade perpendicular to the rotor disk and  $W_T^i$  is the component of the  $i^{\text{th}}$  blade parallel to the rotor disk.  $W_T^i$  and  $W_p^i$  can be defined from the geometry in figure 3.2:

$$W_T^i = \Omega x + W_2 \sin \psi_i \quad (3.3)$$

$$W_p^i = W_1 - v \quad (3.4)$$

where the resultant wind relative wind speed at the  $i^{\text{th}}$  blade,  $W_R^i$ , is:

$$W_R^i = \sqrt{(W_T^i)^2 + (W_p^i)^2} \quad (3.5)$$

The geometry of figure 3.2 (b) also shows:

$$\cos \varphi = \frac{w_T^i}{w_R^i} \quad (3.6)$$

$$\sin \varphi = \frac{w_p^i}{w_R^i} \quad (3.7)$$

where  $\varphi$  is the angle between  $W_R^i$ , and the plane of rotation.

Figure 3.2 is the blade element representation of the blade element shown in Figure 3.1. The blade element is exposed to lift  $dF_L$  and profile drag  $dF_D$  forces which are perpendicular and parallel to  $W_R^i$  respectively. These forces can be defined for each element as:

$$dF_L = \frac{1}{2} \rho c dx (W_R^i)^2 C_L \quad (3.8)$$

$$dF_D = \frac{1}{2} \rho c dx (W_R^i)^2 C_D \quad (3.9)$$



where  $\rho$  is the air density, and the cross section of the blade element is the product of  $c$ , the chord length, and  $dx$ , the radial length of the blade element shown in 3.2 (a).  $C_D$  is the profile drag coefficient and the profile lift  $C_L$  is:

$$C_L = a[\sin(\alpha)] \quad (3.10)$$

Where “a” is the slope of the lift curve and  $\alpha$  is the angle of attack. Since the angle of attack is defined in figure 3.2 as the difference between the airflow and the blade pitch angle, it is useful to note that:

$$\sin(\varphi - \theta) = \sin\varphi\cos\theta - \cos\varphi\sin\theta \quad (3.11)$$

where  $\theta$  is the pitch angle between the chord line and plane of rotation.

The lift and drag forces can be projected into forces perpendicular and tangential to the plane of rotation as:

$$dF_1^i = dF_L\cos\phi + dF_d\sin\phi \quad (3.12)$$

$$dF_2^i = dF_L\sin\phi - dF_d\cos\phi \quad (3.13).$$

From (3.6) – (3.13) it is possible to obtain the force  $dF_1^i$  perpendicular to the plane of rotation and the drag force  $dF_2^i$  tangential to the circle of rotation. With some simplifying assumptions presented in Appendix A, the equations become:

$$dF_1^i = \frac{1}{2} \rho a c dx [-(W_T^i)^2 \theta + W_P^i W_T^i] \quad (3.14)$$

$$dF_2^i = \frac{1}{2} \rho a c dx [-(W_T^i)^2 \frac{C_d}{a} - W_P^i W_T^i \theta + (W_P^i)^2] \quad (3.15)$$

Substituting in (3.1) – (3.4) into (3.14) and (3.15) the elemental forces expressed as:

$$dF_1^i = \frac{1}{2} \rho a c dx [-\theta(\Omega^2 x^2 + W^2 \sin^2 \gamma \sin^2 \psi_i + 2\Omega x W \sin \gamma \sin \psi_i) + (\Omega x W \cos \gamma - \Omega x v + W^2 \sin \gamma \cos \gamma \sin \psi_i - v W \sin \gamma \sin \psi_i)] \quad (3.16)$$

$$dF_2^i = \frac{1}{2} \rho a c dx [-\frac{c_d}{a}(\Omega^2 x^2 + W^2 \sin^2 \gamma \sin^2 \psi_i + 2\Omega x W \sin \gamma \sin \psi_i) - \theta(\Omega x W \cos \gamma - \Omega x v + W^2 \sin \gamma \cos \gamma \sin \psi_i - v W \sin \gamma \sin \psi_i) + (W^2 \cos^2 \gamma + v^2 - 2v W \cos \gamma)] \quad (3.17)$$

which can be computed and summed to find the forces for the  $i^{\text{th}}$  blade. The system forces and moments on the entire rotor can then be obtained with the following relationships:

$$T = \sum_{i=1}^b \int_0^R dF_1^i \quad (3.18)$$

$$F_D = \sum_{i=1}^b \int_0^R dF_2^i \quad (3.19)$$

$$M = -\sum_{i=1}^b \int_0^R x dF_1^i \cos \psi_i \quad (3.20)$$

$$L = -\sum_{i=1}^b \int_0^R x dF_1^i \sin \psi_i \quad (3.21)$$

$$P = \sum_{i=1}^b \int_0^R \Omega x dF_2^i \quad (3.22)$$

where  $b$  is the number of blades,  $R$  is the rotor radius,  $T$  is the instantaneous thrust,  $F_D$  the instantaneous drag force,  $M$  the instantaneous pitch moment,  $L$  the instantaneous roll moment and  $P$  is the instantaneous power. Using this blade element representation it is possible to compute the instantaneous forces, moments and extracted power for the system.

### 3.3 Dynamic Inflow Model

In the blade element representation above, the induced flow is assumed to be constant as is assumed in momentum theory. But even under steady state conditions,

the rotor can induce unsteady effects resulting in the need for dynamic inflow modeling. The subject of dynamic inflow and relevance to rotary wing systems is discussed extensively by Gaonkar and Peters [40].

For the purposes of this research the Pitt Peters dynamic inflow model will be used due to its computational simplicity. The initial Pitt Peters model was a linearized version useful for evaluating perturbations to the system due to quasi-unsteady effects. Peters and HaQuang [41] derived a nonlinear version of the Pitt and Peters dynamic inflow model, which is a more useable format for this problem in that it can be dimensionalized and solved using time-marching methods in a simulation.

The inflow distribution  $v(x, \psi)$  is a function of both the radial coordinate  $x$  and azimuth position  $\psi$  and is defined as:

$$v(x, \psi) = v_o + v_s \frac{x}{R} \sin \psi + v_c \frac{x}{R} \cos \psi \quad (3.23)$$

where  $v_o$ ,  $v_s$ , and  $v_c$  are the uniform, lateral and longitudinal variations in flow through the rotor plane respectively. These values will be time varying and can be computed with the first order differential equation:

$$[M] \begin{Bmatrix} \frac{\dot{v}_o}{\Omega R} \\ \frac{\dot{v}_s}{\Omega R} \\ \frac{\dot{v}_c}{\Omega R} \end{Bmatrix} + [L]_{nl}^{-1} \begin{Bmatrix} \frac{v_o}{\Omega R} \\ \frac{v_s}{\Omega R} \\ \frac{v_c}{\Omega R} \end{Bmatrix} = \begin{Bmatrix} C_T \\ -C_{LL} \\ -C_M \end{Bmatrix} \quad (3.24)$$

where  $[M]$ , the apparent mass terms that represent a time delay due to unsteady flow, is :

$$[M] = \begin{bmatrix} \frac{8}{3\pi} & 0 & 0 \\ 0 & \frac{16}{45\pi} & 0 \\ 0 & 0 & \frac{16}{45\pi} \end{bmatrix} \quad (3.25)$$

and  $[L]_{nl}$  is the nonlinear version of the inflow gain matrix:

$$[L]_{nl} = [L][V]^{-1} \quad (3.26)$$

In this form, the equation is non-dimensional using  $C_T$ ,  $C_M$  and  $C_L$ , the instantaneous thrust pitch and roll coefficients. The above equation is in helicopter form, being normalized on  $\Omega R$ . For the purposes of this research the nonlinear Pitt Peters model can be expressed as shown in (3.27), the dimensional form to reduce computational steps.

$$[M] \begin{Bmatrix} \dot{v}_o \\ \dot{v}_s \\ \dot{v}_c \end{Bmatrix} + [L]_{nl}^{-1} \begin{Bmatrix} v_o \\ v_s \\ v_c \end{Bmatrix} = \begin{Bmatrix} \frac{T}{\rho\pi R^2} \\ \frac{L}{\rho\pi R^3} \\ \frac{M}{\rho\pi R^3} \end{Bmatrix} \quad (3.27)$$

The matrix  $[L]_{nl}$  is defined in (3.26) where  $[L]$  is:

$$[L] = \begin{bmatrix} \frac{1}{2} & 0 & -\frac{15\pi}{64} \frac{\sqrt{1-\sin\alpha_d}}{\sqrt{1+\sin\alpha_d}} \\ 0 & \frac{4}{1+\sin\alpha_d} & 0 \\ \frac{15\pi}{64} \frac{\sqrt{1-\sin\alpha_d}}{\sqrt{1+\sin\alpha_d}} & 0 & \frac{4\sin\alpha_d}{1+\sin\alpha_d} \end{bmatrix} \quad (3.28)$$

$\alpha_d$  is the wake angle with respect to the rotor plane shown in (3.29),

$$\alpha_d = \tan^{-1} \left[ \frac{|W\cos\gamma - v_o|}{W\sin\gamma} \right] \quad (3.29)$$

and the matrix  $[V]$  is:

$$[V] = \begin{bmatrix} V_T & 0 & 0 \\ 0 & V & 0 \\ 0 & 0 & V \end{bmatrix} \quad (3.30)$$

where  $V_T$  is the resultant of the total flow through the disk and  $V$  is a parameter that varies with the cyclic disturbances through the rotor plane. Both can be obtained from momentum theory:

$$V_T = W_2^2 + (W_1 - v_o)^2 \quad (3.31)$$

$$V = \frac{W_2^2 + (W_1 - v_o)(W_1 - 2v_o)}{\sqrt{W_2^2 + (W_1 - v_o)^2}} \quad (3.32)$$

Substitution into (3.1), (3.2), yields  $V_T$  and  $V$  as:

$$V_T = W^2 + v_o^2 - 2Wv_o \cos \gamma \quad (3.33)$$

$$V = \frac{W^2 + 2v_o^2 - 3Wv_o \cos \gamma}{\sqrt{W^2 + v_o^2 - 2Wv_o \cos \gamma}} \quad (3.34)$$

### 3.4 Control Terms

For most wind turbines, the pitch angle of the blade will be fixed as each blade is swept around the rotor plane. However, for this problem, this assumption is not the case. It has been shown that collective pitch can be controlled to optimize the extracted power from the wind. This research will also examine if cyclic pitch can further optimize power extraction through balancing the pressure of the airflow through the rotor plane.

Implementing cyclic pitch will mean that the blade pitch angle is a function of the azimuth position  $\psi$ . Typically there is blade twist from the hub to the blade tip so the pitch angle will also be a function of the radial position. Thus the blade pitch angle with control terms can be expressed as:

$$\theta(x, \psi) = \theta_o + \theta_s \sin(\psi_i) + \theta_c \cos(\psi_i) \quad (3.35)$$

where  $\theta_o$  is the collective pitch angle,  $\theta_s$  is the longitudinal pitch angle and  $\theta_c$  is the lateral pitch angle.

# Chapter 4

## Model Comparison to the WT\_PERF Simulation

Chapter 3 outlined the theory that will be used to study how the power coefficient is optimized in yawed flow. It defined a free body diagram, the blade element representation for computing power, forces and moments, the dynamic inflow model used to compute induced velocity as well as representation of the control terms that can be used to study the effects of collective and cyclic pitch. Closed form solutions can be found for simplified cases but due to the large number of variables, but solving for the power coefficient quickly becomes an iterative process. Furthermore, the blade element and dynamic inflow models are coupled in that each time step the forces and moments change as do the induced velocities with blade radius and azimuth. Thus to study trends over a larger domain, a non-linear time based simulation will be implemented.

As two of the primary objectives of this research are to learn how the power coefficient changes with yawed flow and to study the effects of cyclic pitch, the code used has been generated in MATLAB's Simulink software to allow user friendly control over the varying parameters. A number of industry codes exist that model wind turbine performance, but typically include models for tower effects, vibration, complex wind patterns such as turbulence and shear which are not required for this research at this time. And based upon initial review of the codes listed in the literature review, none of them explicitly model cyclic pitch (although some allow the pitch for each blade to be varied independently). For this reason it was decided to use Simulink where such control terms are easily implemented.

To build confidence in the simulation results of this model, benchmark cases are compared to code that has been developed and is currently maintained by the National Renewable Energy Lab (NREL). As mentioned, NREL's FAST and ADAMS codes enjoy the most international recognition as they were certified by Germanischer Lloyd (GL) (the German wind turbine certifying agency) as suitable for wind turbine design [37]. The codes use a subroutine called AeroDyn to model the turbine's aerodynamic performance. AeroDyn itself is not a standalone program and cannot be executed without interfacing with a system level dynamics software such as FAST or ADAMS.

NREL does maintain a code that focuses specifically on wind turbine aerodynamic performance called WT\_PERF. For comparable cases, WT\_PERF has been described as "almost identical to AeroDyn" and has been shown to match AeroDyn very well as is described on the "WT\_PERF Verification Page" [42]. WT\_PERF is a standalone program which makes it easier to use as a benchmark for comparison. WT\_PERF uses blade element theory and is basically an implementation of the Wilson Lissaman PROP code. It contains models for hub loss, tip loss, swirl, skew wake, rotor shaft tilt or preconeing, all of which can be turned off for research comparisons. The code allows the user to change the yaw angle of the free stream wind and vary the collective pitch (but not cyclic pitch). WT\_PERF does not use a dynamic inflow model however cases can be generated for which the dynamic inflow model behaves like the momentum theory like that used in the Wilson Lissaman PROP code. For these reasons, WT\_PERF is used for benchmark comparisons to add confidence to the simulation results.

This chapter will describe the model setup, specifics about the benchmark cases being run and comparison results between the Simulink non-linear simulation being developed and WT\_PERF simulation.

## 4.1 Model Implementation

The Simulink simulation being developed for this research is called WT\_3DOF, a short name for this simple 3 Degree of Freedom ( $C_T$ ,  $C_M$ ,  $C_{LL}$ ) Wind Turbine aerodynamic model. The Matlab environment makes it possible to initialize parameters, run the simulation, and post-process the results. Although the current WT\_3DOF simulation is implemented in a simple way, it is set up to be expanded on in the future with more advanced wind models, rigid body dynamics, control inputs etc. For the scope of understanding and plotting the aerodynamic behavior of this plant, the model should be sufficient.

WT\_3DOF runs in dimensional time at a variable step size that is determined by MATLAB depending on the system dynamics. All subroutines within the simulation, namely the blade element and the dynamic inflow routines, are set up dimensionally to run with time (as opposed to converging on solutions in non-dimensional form.)

The simulation currently is set up to evaluate the power coefficient in yawed flow and the feasibility of using cyclic pitch to optimize performance. As with many feasibility studies, it must be proven that there is a feasible design space in the best of circumstances before the necessity of investing effort in investing additional fidelity to the model. With that being said, there are many real world features not modeled such as rigid body dynamics of the boundary conditions or rotor, dynamic stall of the airfoil, wind turbulence or shear, blade coning, shaft tilt and hub losses. Tip losses can be accounted for in the simulation by adding a scale factor such as 0.97 to the radial length of the blade. Another current limitation is that the simulation is only set up to run in the windmill state and so the design space being evaluated will avoid the propeller, vortex ring or propeller brake states (i.e. the results are only valid when the normalized induced velocity remains between 0 and 1).

All the simulation values are relative to the rotor tip path plane. Peters and HaQuang [41] have shown a convenient way to transform wind magnitudes and directions from a real world wind frame to the rotor tip plane. For this simplified simulation,  $W$  and  $\gamma$  are always relative to the rotor tip plane. The sign conventions for the simulation are shown in Figure 4.1.



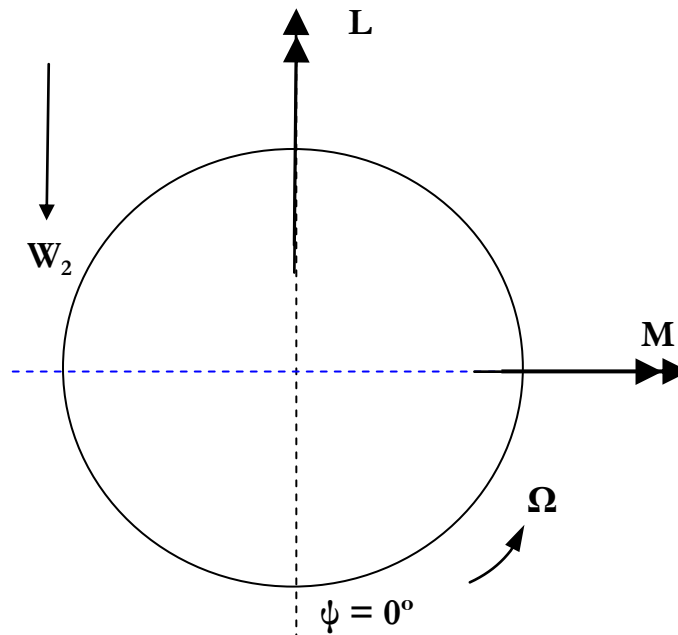


Figure 4.1 Sign Conventions for WT\_3DOF

For this simulation, thrust should always be positive. Azimuth angle is assumed to be zero in the direction of  $W_2$  as defined in chapter 3. Facing forward toward an azimuth position of 180 degrees, the roll Moment is positive with advancing blade down on the right side and pitch moment is positive with nose up. The sign conventions for the side to side cyclic induced velocity,  $v_s$ , and the fore to aft cyclic induced velocity,  $v_c$  are the same: positive with leading edge down.

Table 4.1 shows what inputs are currently required to run the WT\_3DOF simulation.

Table 4.1 Input Variables required to run WT\_3DOF

Variable Name	Variable	Units
Time	t	sec
Rotor Speed	$\Omega$	rad/sec
Wind Magitude	W	ft/s or m/s
Wind Direction relative to rotor disk	$\gamma$ (gamma)	rad
Air Density	$\rho$ (rho)	slug/ft <sup>3</sup> or kg/m <sup>3</sup>
Rotor Radius	R	ft or m
Chord	c	ft or m
Slope of CL(alpha)	a	1/rad
Blade Pitch	$\theta_0$	rad
Cyclic Pitch	$\theta_s$ & $\theta_c$	rad
Blade Twist	$\theta_t$	rad
Initial Blade Positions	$az_1, az_2, \dots, az_b$ (b=number of blades)	deg
Blade Section Array	$x_1, x_2, \dots, x_n$ (n= number of blade elements)	ft or m

Note that the initial blade positions define the number of blades and should be equally spaced throughout the 360 degree rotor plane. For example two blades could have  $az_1=0^\circ$  &  $az_2=180^\circ$ , three blades could have  $az_1=0^\circ$ ,  $az_2=120^\circ$  and  $az_3=240^\circ$ . In its current form, the simulation reads the initial values from the MATLAB workspace through a script but as its expanded the variables could become real-time inputs to a single block. The Blade Section Array defines the number of blade elements that the blade is broken into as well as the element sizes and centroid locations. The algorithm was adapted from the WT\_Perf simulation to make sure that the differences in the blade element computations did not create differences between WT\_3DOF and WT\_Perf.

Table 4.2 shows the simulation outputs.

Table 4.2 Simulation outputs from WT\_3DOF

Variable Name	Variable	Units
Power	P	W
Power Coefficient	cp	-
Thrust	T	lb or N
Pitch Moment	M	lb-ft or N-m
Roll Moment	L	lb-ft or N-m
axial induced velocity	vo	ft/s or m/s
side to side cyclic induced velocity	vs	ft/s or m/s
for to aft cyclic induced velocity	vc	ft/s or m/s

The current implementation makes specific assumptions on the lift and drag coefficients as described in chapter 3. The lift coefficient was defined in (3.10) and substituted for  $a \cdot \sin(\alpha)$ . The drag coefficient is assumed to be a constant and currently does not vary with  $\alpha$ . These assumptions are built into the blade element equations that compute the local power, thrust, roll pitch moments along the blades. The simulation could be reworked to read in a lift and drag coefficient for a specific airfoil from a lookup table, but for the parametric work at this phase, the assumptions should suffice for this feasibility study. Figures of the system blocks can be found in Appendix B

## 4.2 Case Study Description

In order to gain confidence in the simulation results, a case study was put together that could be run in both the WT\_3DOF and WT\_Perf simulations. WT\_Perf is set up to allow for parametric analysis. All of the WT\_3DOF results are compared to WT\_Perf version 3.10. Many of its features, such as hub losses, tip losses, skew wake corrections, blade coning and shaft tilt can be turned off for research comparison purposes. NREL has published a short user's manual to execute WT\_Perf that is available on their website and describes in detail how to set up an input file to evaluate the aerodynamic performance of a wind turbine [36].

Figure 4.2 shows a sample input file used to compare WT\_3DOF to WT\_Perf.

```

----- WT_Perf Input File -----
WT_Perf Test01 input file.  Concept Airfoil (dimen, English, Space, PROP-PC).
Compatible with WT_Perf v3.00f
----- Input Configuration -----
False Echo: Echo input parameters to "<rootname>.ech"?
True DimenInp: Turbine parameters are dimensional?
False Metric: Turbine parameters are Metric (MKS vs FPS)?
----- Model Configuration -----
1 NumSect: Number of circumferential sectors.
5000 MaxIter: Max number of iterations for induction factor.
1.0e-6 ATol: Error tolerance for induction iteration.
1.0e-6 SWTol: Error tolerance for skewed-wake iteration.
----- Algorithm Configuration -----
False TipLoss: Use the Prandtl tip-loss model?
False HubLoss: Use the Prandtl hub-loss model?
False Swirl: Include Swirl effects?
False SkewWake: Apply skewed-wake correction?
False AdvBrake: Use the advanced brake-state model?
False IndProp: Use PROP-PC instead of PROPX induction algorithm?
False AIDrag: Use the drag term in the axial induction calculation?
False TIDrag: Use the drag term in the tangential induction calculation?
----- Turbine Data -----
3 NumBlade: Number of blades.
16.5 RotorRad: Rotor radius [length].
3.2 HubRad: Hub radius [length or div by radius].
0.0 FreCone: Frecone angle, positive downwind [deg].
0.0 Tilt: Shaft tilt [deg].
0.0 Yaw: Yaw error [deg].
48 HubHt: Hub height [length or div by radius].
16 NumSeg: Number of blade segments (entire rotor radius).
    RElm  Twist  Chord  AFfile  PrntElem
3.713  0.000  1.5032  1  False
4.537  0.000  1.5032  1  False
5.3625  0.000  1.5032  1  False
6.1875  0.000  1.5032  1  False
7.0125  0.000  1.5032  1  False
7.8375  0.000  1.5032  1  False
8.6625  0.000  1.5032  1  False
9.4875  0.000  1.5032  1  False
10.3125  0.000  1.5032  1  False
11.1625  0.000  1.5032  1  False
11.9875  0.000  1.5032  1  False
12.8125  0.000  1.5032  1  False
13.6375  0.000  1.5032  1  False
14.4625  0.000  1.5032  1  False
15.3125  0.000  1.5032  1  False
16.1375  0.000  1.5032  1  False
----- Aerodynamic Data -----
0.0019749 Rho: Air density [mass/volume].
0.0001625 KinVisc: Kinematic air viscosity
0.0 ShearExp: Wind shear exponent (1/7 law = 0.143).
False UseCm: Are Cm data included in the airfoil tables?
1 NumAF: Number of airfoil files.
"simplified airfoil.dat" AF_File: List of NumAF airfoil files.
----- I/O Settings -----
True TabDel: Make output tab-delimited (fixed-width otherwise).
True KFact: Output dimensional parameters in K (e.g., kN instead on N)
True WriteBED: Write out blade element data to "<rootname>.bed"?
False InputTSR: Input speeds as TSRs?
"fps" SpdUnits: Wind-speed units (mps, fps, mph).
----- Combined-Case Analysis -----
0 NumCases: Number of cases to run. Enter zero for parametric analysis.
WS or TSR RotSpd Pitch Remove following block of lines if NumCases is zero.
----- Parametric Analysis (Ignored if NumCases > 0) -----
3 ParRow: Row parameter (1-rpm, 2-pitch, 3-tsr/speed).
2 ParCol: Column parameter (1-rpm, 2-pitch, 3-tsr/speed).
1 ParTab: Table parameter (1-rpm, 2-pitch, 3-tsr/speed).
True OutPwr: Request output of rotor power?
True OutCp: Request output of Cp?
False OutTrq: Request output of shaft torque?
False OutFlp: Request output of flap bending moment?
True OutThr: Request output of rotor thrust?
-5, 5, 1 PitSt, PitEnd, PitDel: First, last, delta blade pitch (deg).
70, 70, 0 OmgSt, OmgEnd, OmgDel: First, last, delta rotor speed (rpm).
12, 50, 1 SpdSt, SpdEnd, SpdDel: First, last, delta speeds.

```

Figure 4.2 Sample WT\_Perf input file used for case study

The input file is set up to be consistent with the output of WT\_Perf. The input and output variables are dimensional, tip loss, hub loss, swirl, skew wake, advanced braking are all disabled. The turbine data section of the input file defines the number of blades, rotor radius, hub radius (required by WT\_Perf), cone angle, shaft tilt, nacelle yaw, hub height and number of blade elements. The array at the end of this section defines the radial element locations of each blade element, the twist angle and chord length for each blade element section. This data array of blade element locations, twist angles and chord lengths can be loaded into WT\_Perf to maintain consistency.

The aerodynamic data section defines the air density, the airfoil data file. The airfoil file, defined as `AF_File`, provides `WT_Perf` the lookup table to find the lift and drag coefficients as a function of angle of attack. Values are provided for angles of attack from -180 to 180 degrees. There is an option to look up a pitch moment coefficient but this feature is disabled for this comparison. The syntax for the airfoil file is identical to the one used by `AeroDyn`. `WT_Perf` does not model dynamic stall. To make the airfoil data consistent between `WT_3DOF` and the `WT_Perf` input configuration, an airfoil was created that can be executed by `WT_Perf`. `WT_3DOF` assumes  $CL = a \cdot \sin(\alpha)$  and a fixed value for `CD`. Thus files were created for angles of attack from -180 to 180 degrees where `CL` is computed as in (3.10), `CD` is a static value independent of angle of attack that can be varied (i.e. 0.00, 0.02, 0.04, etc), and `CM` is defined as zero.

The remainder of the input file shown in Figure 4.2 defines the format of the output files as well as the variables to be studied in the Parametric Analysis. The Parametric Analysis section defines what simulation outputs are to be studied as well as what range of variation is desired for each parameter. In 4.2, pitch angles of -5 to 5 degrees are specified in increments of 1 degree. Rotor speed is fixed for this study at 70 RPM and the wind speed is varied from 12 to 50 in increments of 1 meter per second.

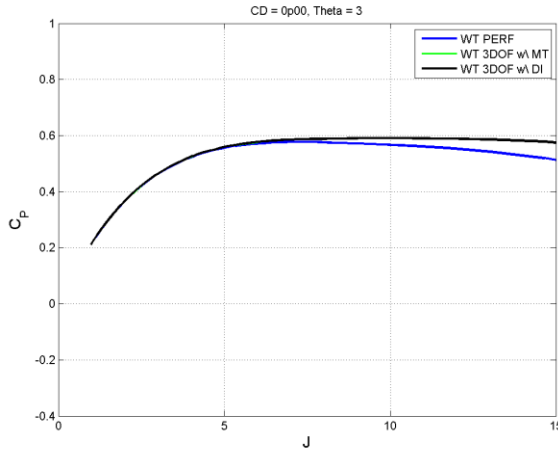
This provides the means to obtain data sweeps of power, the power coefficient and thrust as a function of tip speed or wind speed for a variety of pitch settings. The equivalent case was then run in the `WT_3DOF` simulation being developed and compared to `WT_Perf` to increase confidence that the results are reasonable.

## 4.3 Comparison of Results

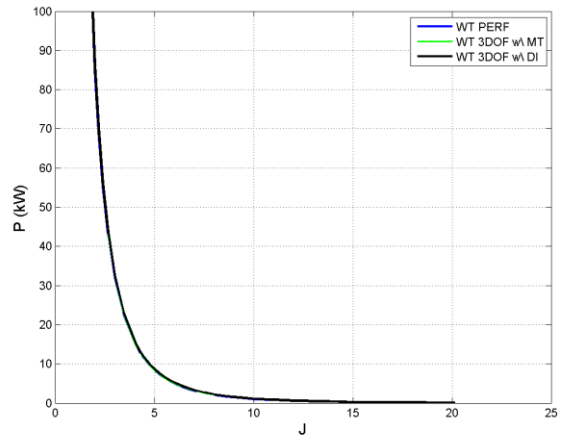
This section presents the comparison of the simulations, `WT_Perf` and `WT_6DOF` for a basic parameter analysis. Although the simulation codes are different the objective is to verify that the `WT_Perf` code is generating reasonable results for the power output and power coefficient. For that reason special attention will be paid to those outputs.

Because this section is interested in benchmarking, the comparisons chosen are those for which WT\_Perf (which does not include a dynamic inflow model) are expected to match. A progression was put together to help make the comparison between the simulations. For each case shown, the WT\_3DOF was run with two different methods for computing the induced velocities. The first method uses momentum theory which is consistent with the WT\_Perf implementation. In the following plots, this is called out as WT\_3DOF with momentum theory or "WT\_3DOF w/MT". This result is expected to show nearly exact match with WT\_Perf for wind turbine systems in the windmill state (i.e. normalized induced velocity between 0 and 0.5-0.6). The second method implements the nonlinear Peters Pitt dynamic inflow model outlined in Chapter 3. This is called out as WT\_3DOF with dynamic inflow theory, or "WT\_3DOF w/ DI" in the plots. For yawed flow, it is not necessarily expected that the results should always match WT\_Perf closely. (In fact WT\_Perf has additional code to account for swirl in yawed flow.) For cases such as purely axial flow, the dynamic inflow model is expected to converge to momentum theory and thus show a good match for those cases. When the flow becomes yawed or cyclic pitch is input into the system, the match would of course break down. The dynamic inflow model would model the collective and cyclic variation in the induced velocities and the result in power, thrust, roll and pitch moments would differ.

The following figures show comparisons of the power coefficient and power output for a variety of settings on the drag coefficient and pitch magnitudes.

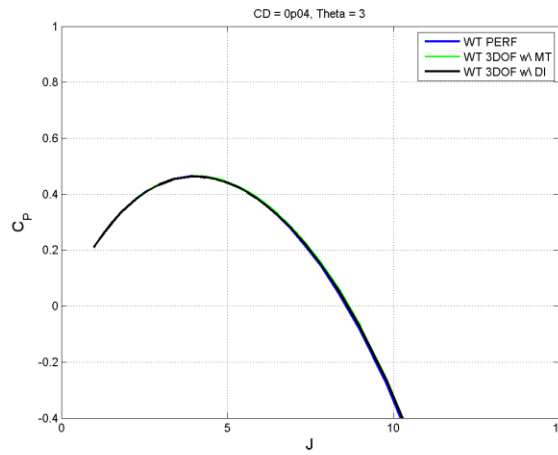


(a)

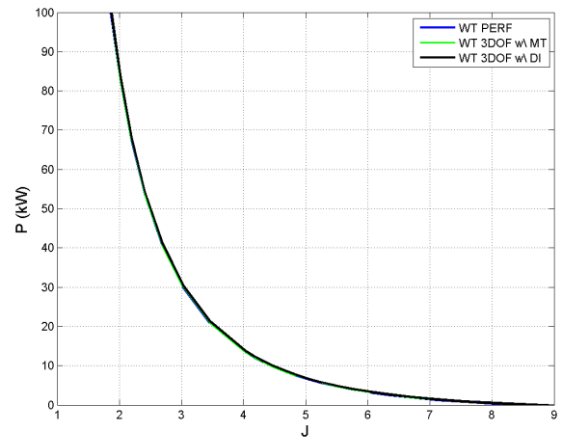


(b)

Figure 4.3 Comparisons of (a)  $C_p$  and (b) Power as a function of tip speed for  $C_D=0.00$ ,  $\theta_0=3$

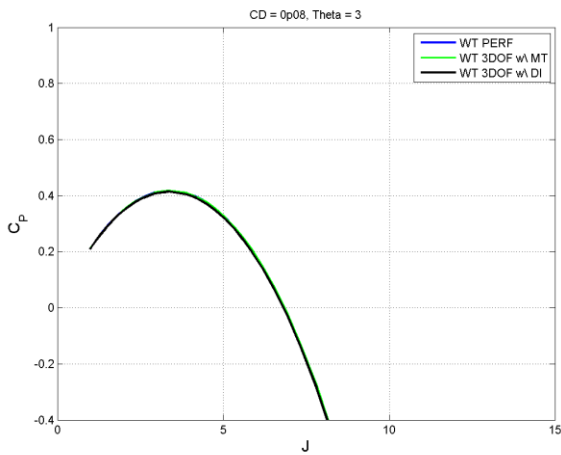


(a)

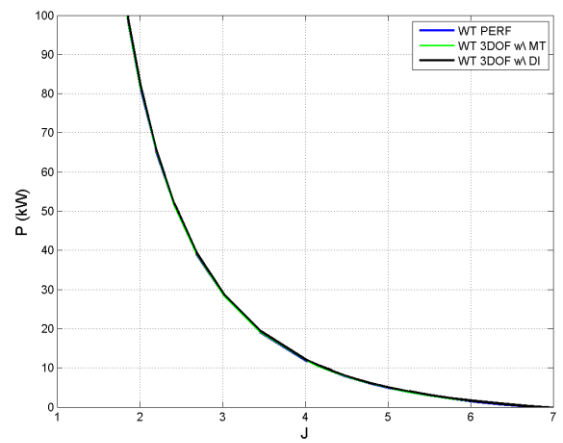


(b)

Figure 4.4 Comparisons of (a)  $C_p$  and (b) Power as a function of tip speed for  $C_D=0.04$ ,  $\theta_0=3$



(a)



(b)

Figure 4.5 Comparisons of (a)  $C_p$  and (b) Power as a function of tip speed for  $C_D=0.08$ ,  $\theta_0=3$

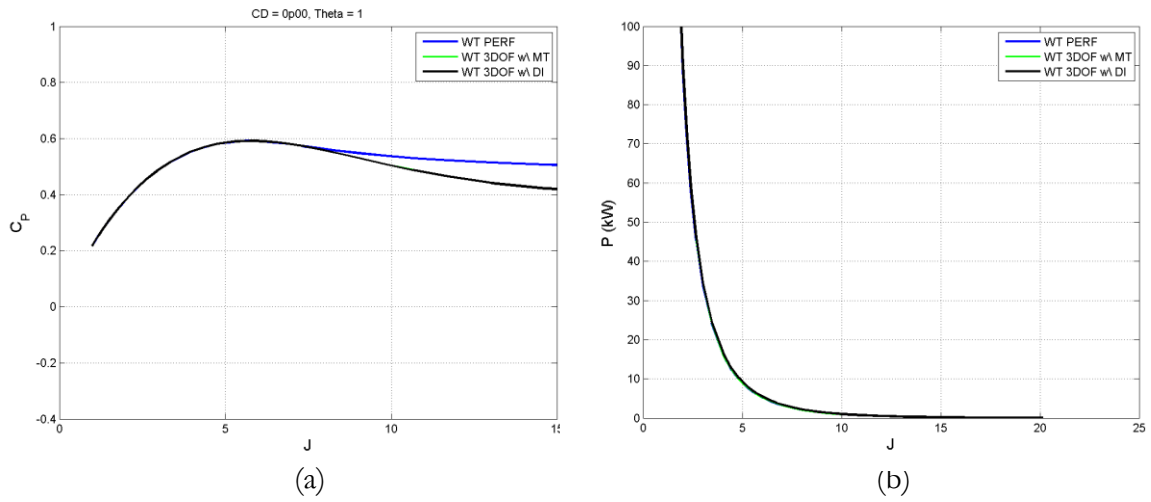


Figure 4.6 Comparisons of (a)  $C_p$  and (b) Power as a function of tip speed for  $C_D=0.00$ ,  $\theta_0=1$

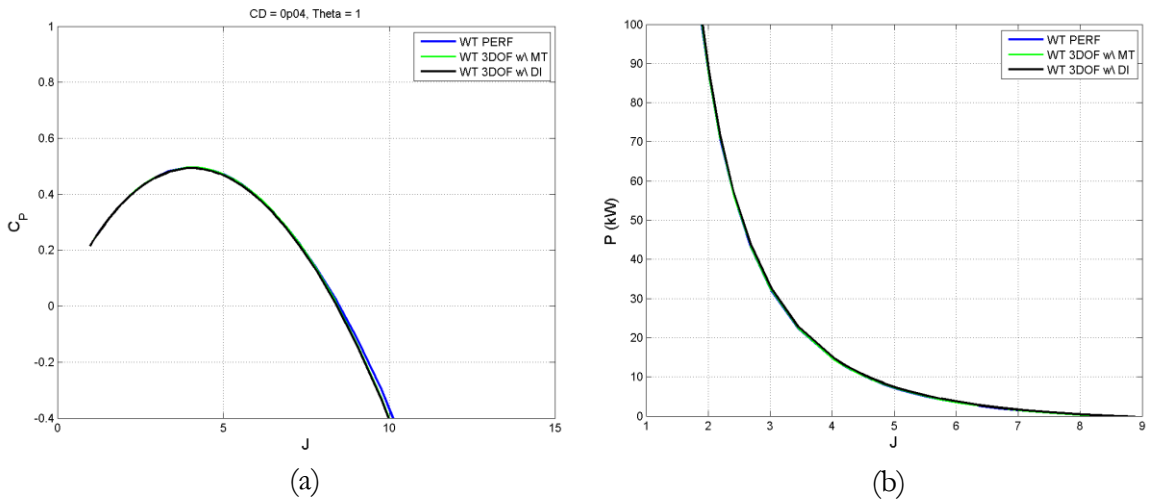


Figure 4.7 Comparisons of (a)  $C_p$  and (b) Power as a function of tip speed for  $C_D=0.04$ ,  $\theta_0=1$

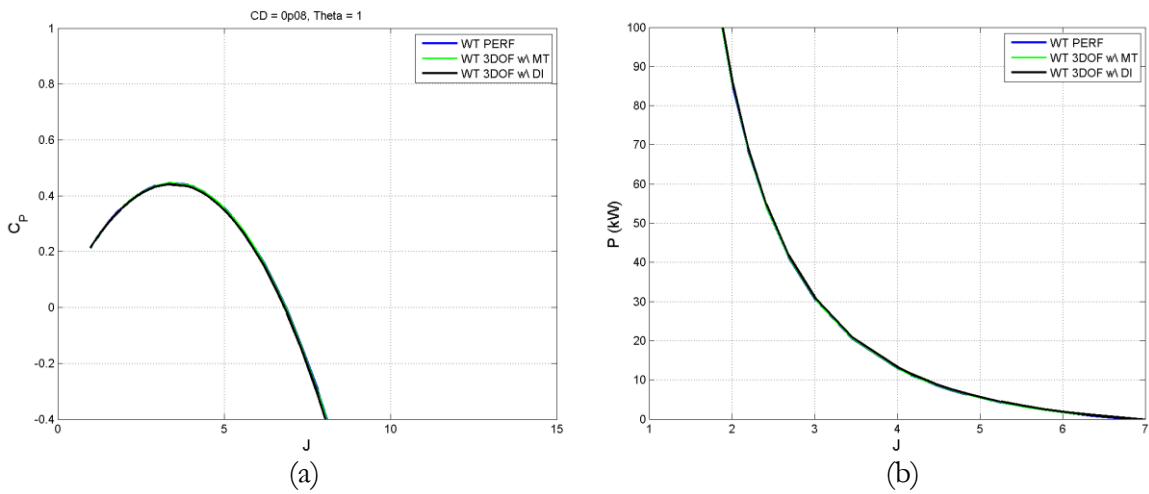
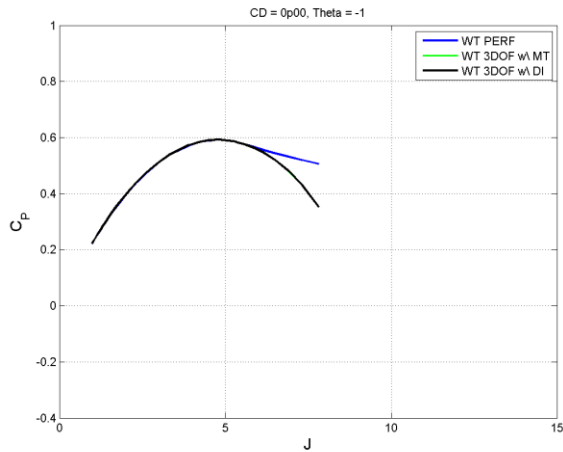
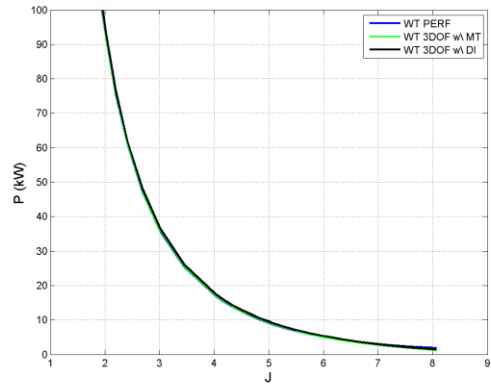


Figure 4.8 Comparisons of (a)  $C_p$  and (b) Power as a function of tip speed for  $C_D=0.08$ ,  $\theta_0=1$



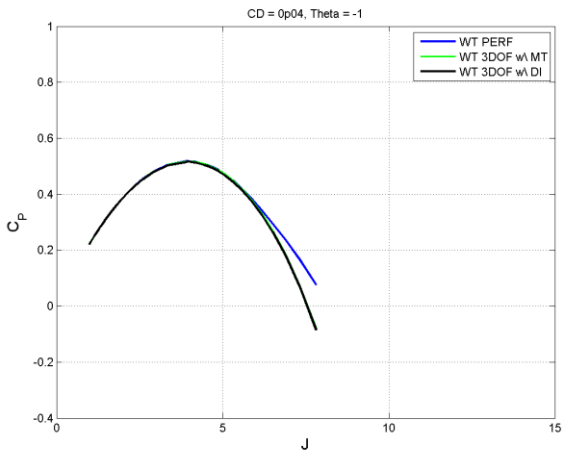


(a)

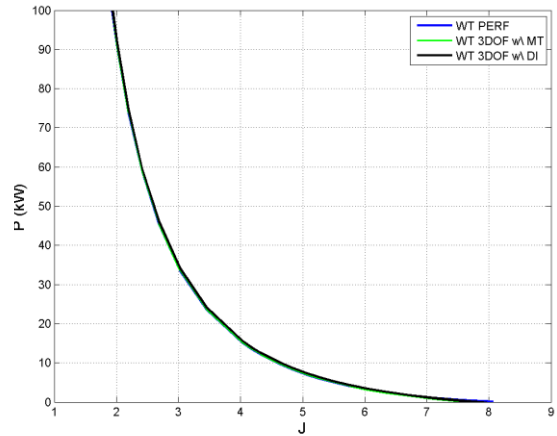


(b)

Figure 4.9 Comparisons of (a)  $C_p$  and (b) Power as a function of tip speed for  $C_D=0.00$ ,  $\theta_0=-1$

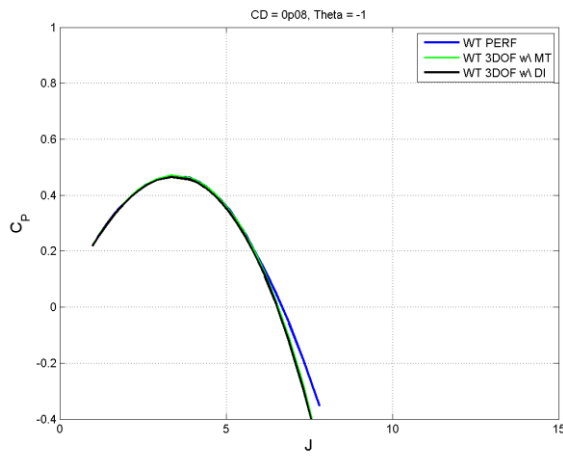


(a)

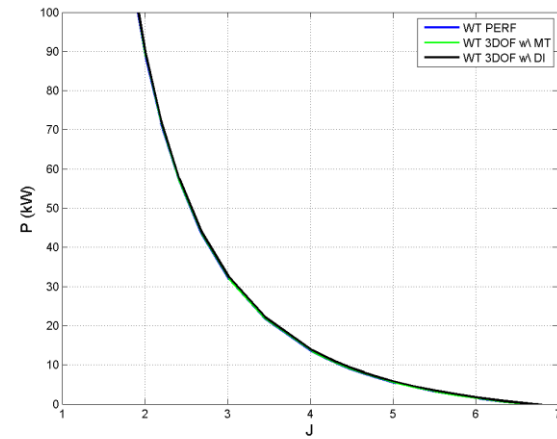


(b)

Figure 4.10 Comparisons of (a)  $C_p$  and (b) Power as a function of tip speed for  $C_D=0.04$ ,  $\theta_0=-1$



(a)



(b)

Figure 4.11 Comparisons of (a)  $C_p$  and (b) Power as a function of tip speed for  $C_D=0.08$ ,  $\theta_0=-1$

Figures 4.3, 4.4 and 4.5 show the results for a pitch setting of 3 degrees, for a drag coefficient of 0.00, 0.04 and 0.08 respectively. Figures 4.6-4.8 show the results for a pitch setting of 1 degree with the same drag coefficients. Figures 4.9-4.11 show the results for a pitch setting of -1 degree and the same progression of values for the drag coefficient.

In general a close match is observed between the simulations. Areas where the match degrades are when the power output becomes very small and when the drag coefficient is also small. The power output decreases with tip speed, that is, as the wind magnitude decreases. This test case assumes a fixed value for rotor speed so as the wind speed decreases the simulation naturally expects power to maintain the rotor speed in the presence of light wind and enters the propeller state, a region for which the comparisons here are not valid. A zero drag coefficient was chosen as a setting for the purposes of parametric study, however in realistic cases the drag coefficient will not be zero.

The research to follow will focus on how the collective and cyclic pitch influence the aerodynamic performance of wind turbines. Although WT\_Perf does not model cyclic pitch, it does collective. Thus a comparison to pitch as a parameter is prudent. Figure 4.12-15 show the power coefficient as a function of pitch for four different tip speeds, 2, 4, 5 and 7 for the case shown in Figure 4.11 (a), a drag coefficient of 0.08. The low tip speed shows behavior in the high wind speed region, two points near the optimal  $C_p$  and one in the negative power region.

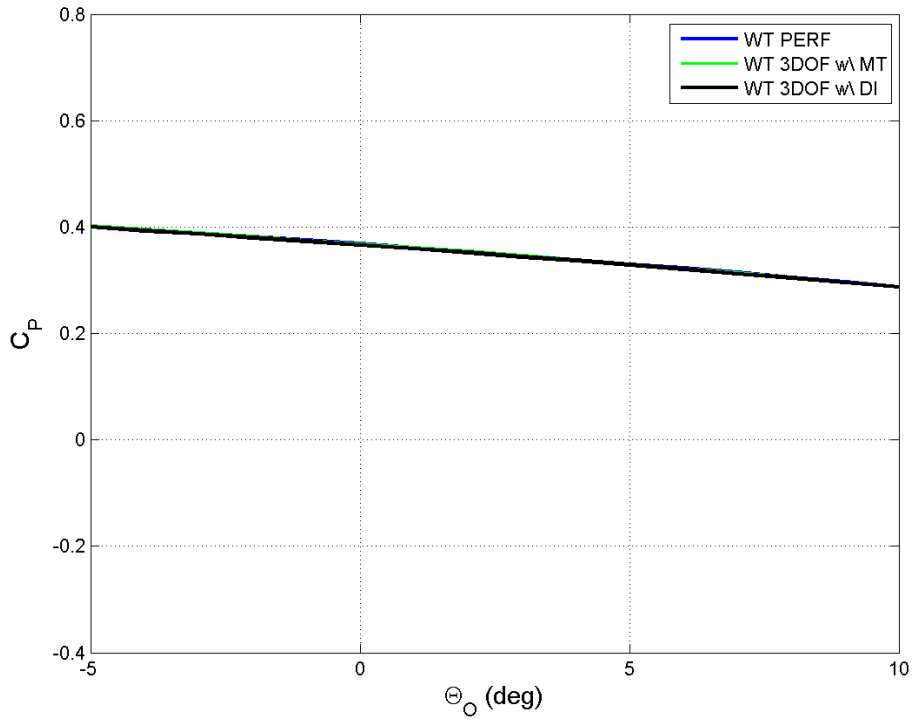


Figure 4.12 Comparisons of  $C_P$  as a function of theta for tip speed  $J = 2$  and  $C_D=0.08$

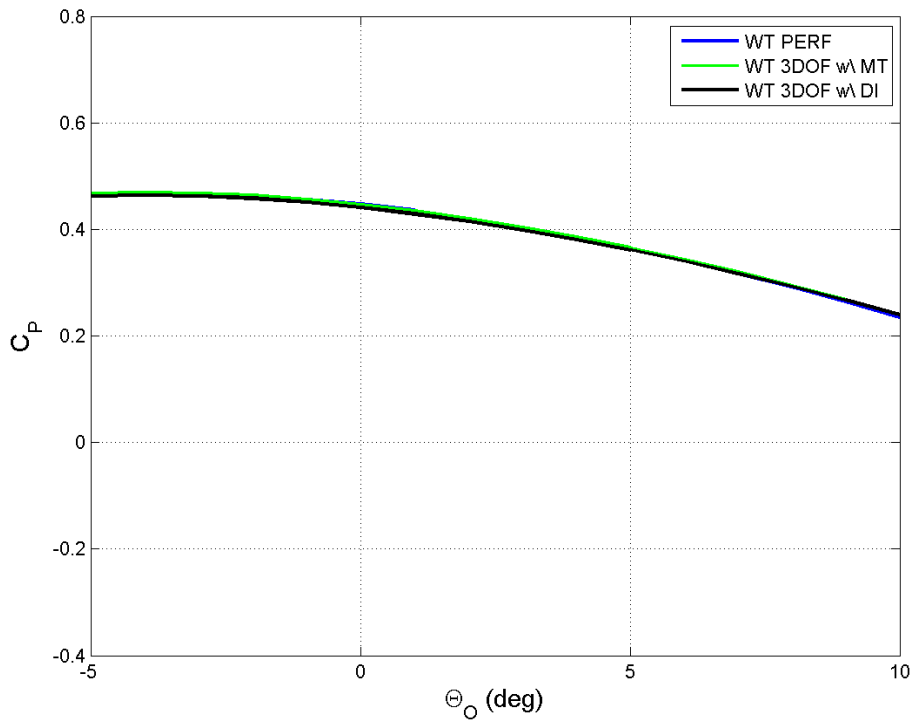


Figure 4.13 Comparisons of  $C_P$  as a function of theta for tip speed  $J = 4$  and  $C_D=0.08$

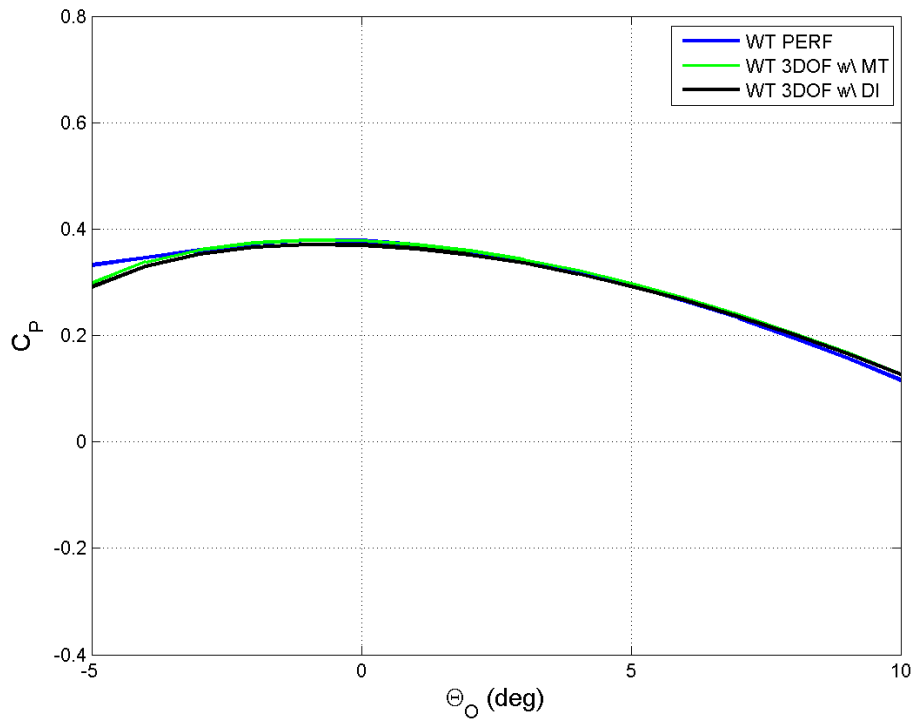


Figure 4.14 Comparisons of  $C_P$  as a function of theta for tip speed  $J = 5$  and  $C_D=0.08$

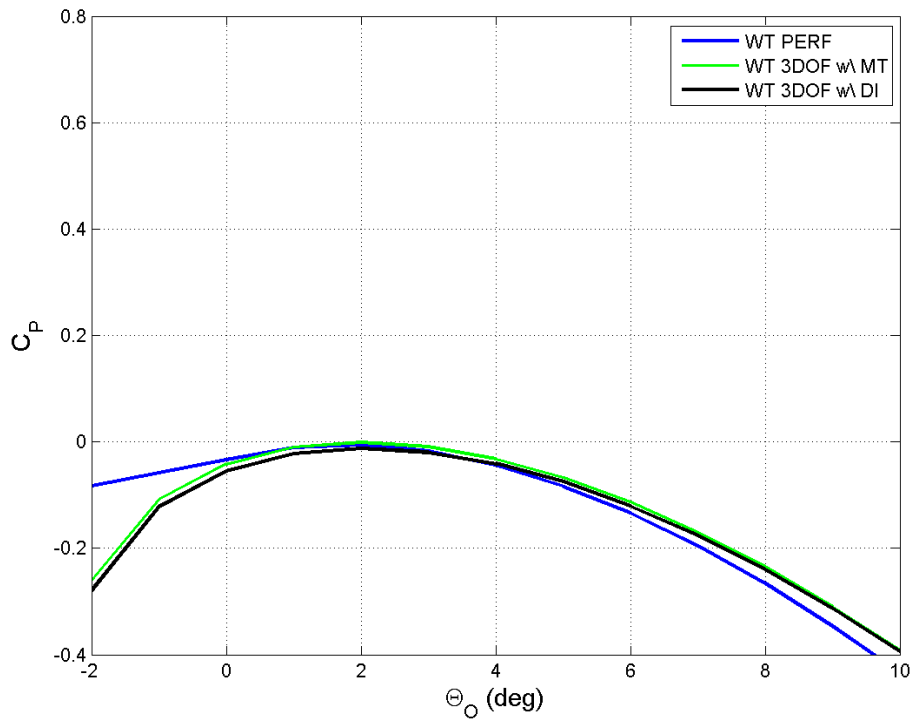


Figure 4.15 Comparisons of  $C_P$  as a function of theta for tip speed  $J = 7$  and  $C_D=0.08$

Figure 4.12 shows a very good match in high wind conditions between the simulations for all theta. Figures 4.13 and 4.14 compare the performance near the optimal values of CP and show a good match for positive pitch. For negative pitch, the match between momentum theory and dynamic inflow is close. WT\_Perf shows more optimistic numbers as theta becomes very negative. One reason for the discrepancy is that the normalized induced velocity is exceeding 0.5 which is on the verge the turbulent windmill state for which momentum theory and dynamic inflow are not valid; and there are additional code differences to handle this transition in WT\_Perf. For the purposes of this research, WT\_3DOF is slightly pessimistic and can still be used to identify where the power coefficient is above zero. Figure 4.15 shows a comparison for a negative power region. It shows further degradation in match as is expected for the propeller state; however the match is still decent and sufficient as a benchmark check case for this feasibility analysis.

# Chapter 5

## WT\_3DOF Simulation Results of $C_p$ for Varying Collective and Cyclic Pitch

The simulation developed in chapters 3 and 4 will be the code used to find the design space of power coefficient for winds at different yaw angles and using collective and cyclic pitch. Before putting an optimizer around the code, this chapter provides aerodynamics plots of the systems behavior. The section will consist of two parts: (1) parameter sweeps and (2) surface plots of the control space. The objective of doing (1) is to make sure the results make sense and to observe where the design space shows potential for optimizing the power output. The objective of (2) is to evaluate examples of the surface of  $C_p$  as the control terms are varied. This will present how  $C_p$  varies with both  $\theta_s$  and  $\theta_c$  and will give insight into the risks of local minimums and maximums preventing an optimization routine from finding the true optimal settings.

### 5.1 Parameter Sweeps of the Power Coefficient

Previous work has shown the design space of  $C_p$  for a variety of parameters using momentum theory to compute the axial induction and assuming a zero hub radius [29]. The results presented will show similar plots to outline the design space using the nonlinear dynamic inflow model. The progression shows how  $C_p$  changes with tip speed, induced velocity then collective pitch, cyclic pitch and gamma.

Figures 5.1-5.3 show the power coefficient as a function of tip speed. The optimum power varies with drag and pitch settings as is shown and depending upon these parameters, the optimal power coefficient occurs somewhere between 2-7. Figures 5.4-5.6 show the power coefficient as a function of the normalized induced velocity,  $w$ , for 3 pitch settings. For an ideal rotor in axial flow, the optimal induced

flow is expected to be  $1/3$ , however the plots show that this is not always the optimum as the drag increases and pitch settings are varied. As the collective pitch is increased to 4 degrees, the behavior of the induced flow becomes more complex showing the possibility of 2 different power coefficients for one induced flow when the drag is very small. However as drag is increased the performance degrades more gracefully.

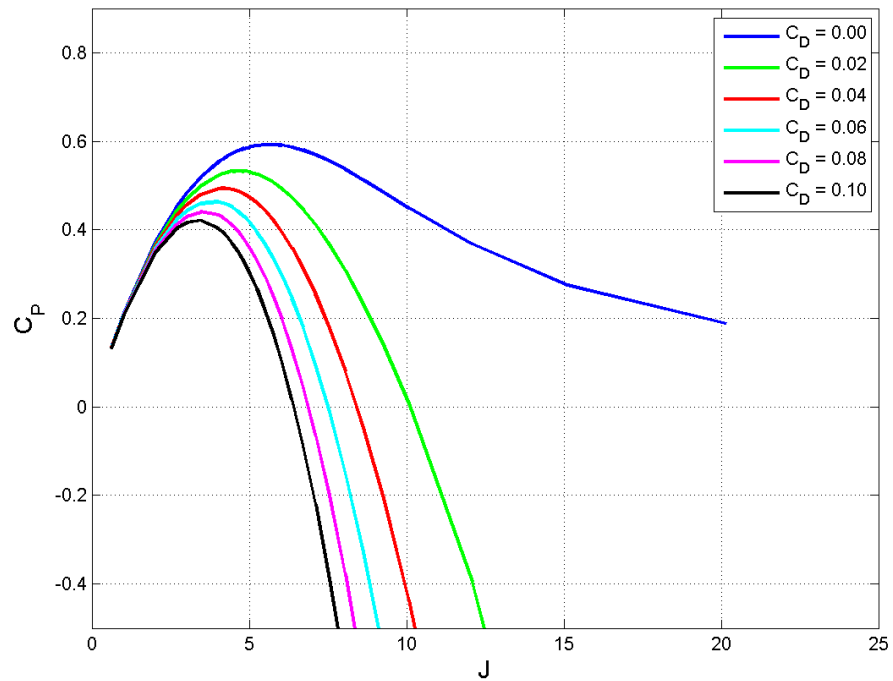


Figure 5.1  $C_P$  as a function of tip speed,  $\gamma=0^\circ$ ,  $\theta_0=0^\circ$ ,  $\theta_s=0^\circ$ ,  $\theta_c = 0^\circ$

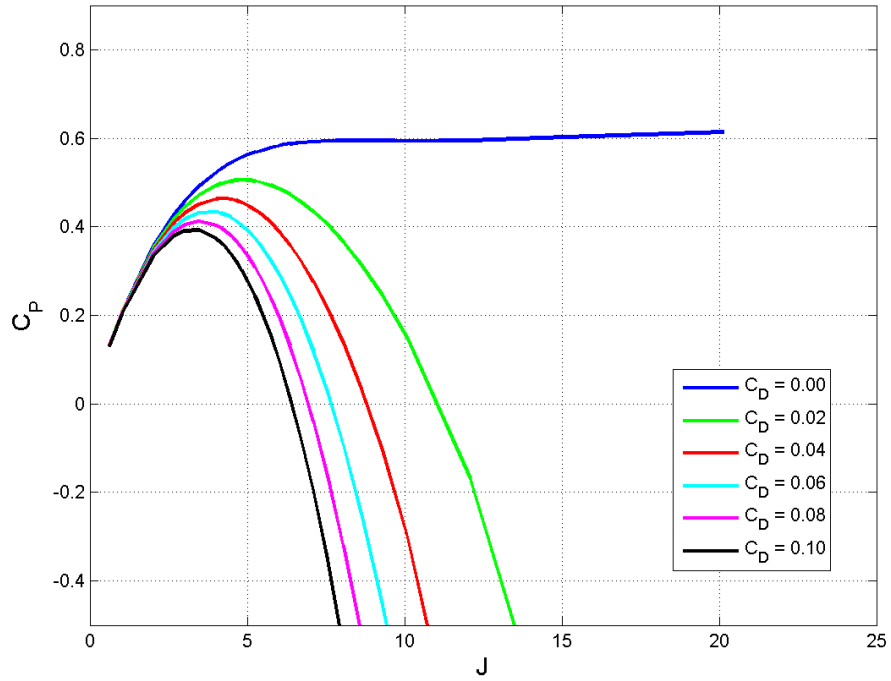


Figure 5.2  $C_P$  as a function of tip speed,  $\gamma=0^\circ$ ,  $\theta_0=2^\circ$ ,  $\theta_s=0^\circ$ ,  $\theta_c = 0^\circ$

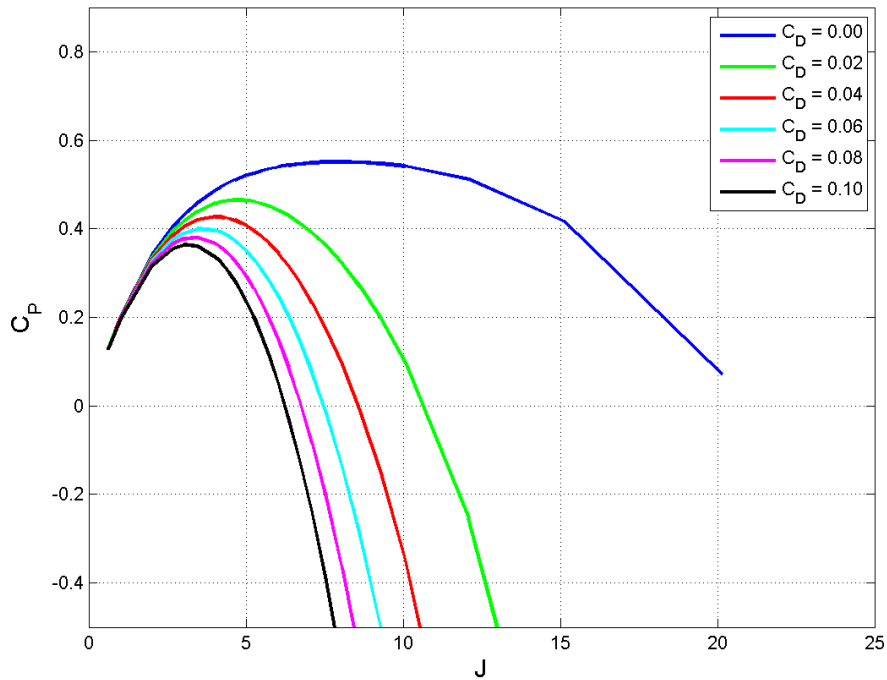


Figure 5.3  $C_P$  as a function of tip speed,  $\gamma=0^\circ$ ,  $\theta_0=4^\circ$ ,  $\theta_s=0^\circ$ ,  $\theta_c = 0^\circ$



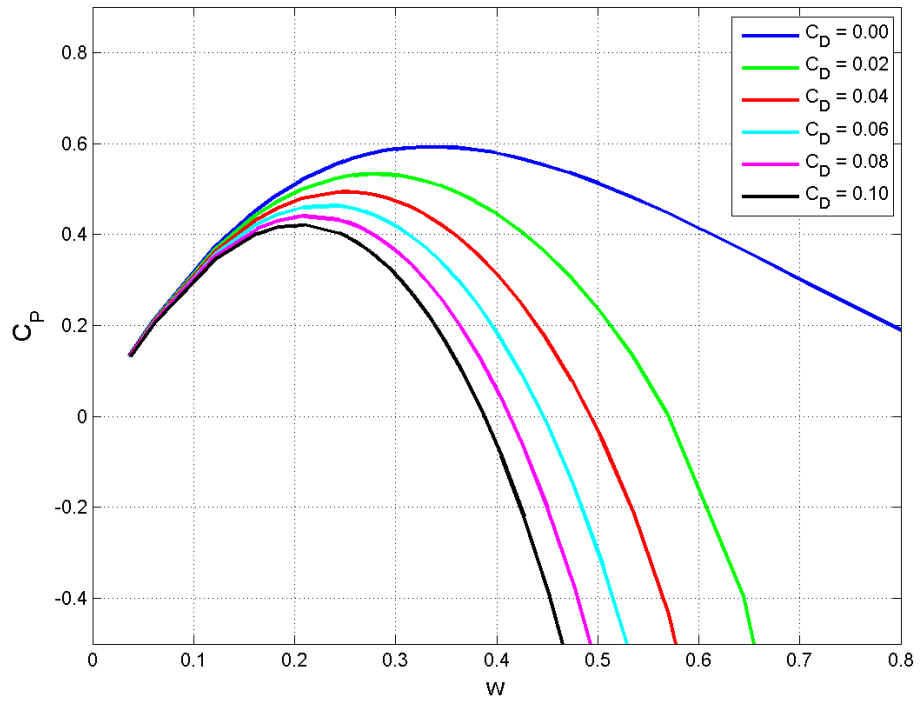


Figure 5.4  $C_P$  as a function of  $w$ ,  $\gamma=0^\circ$ ,  $\theta_0=0^\circ$ ,  $\theta_s=0^\circ$ ,  $\theta_c = 0^\circ$

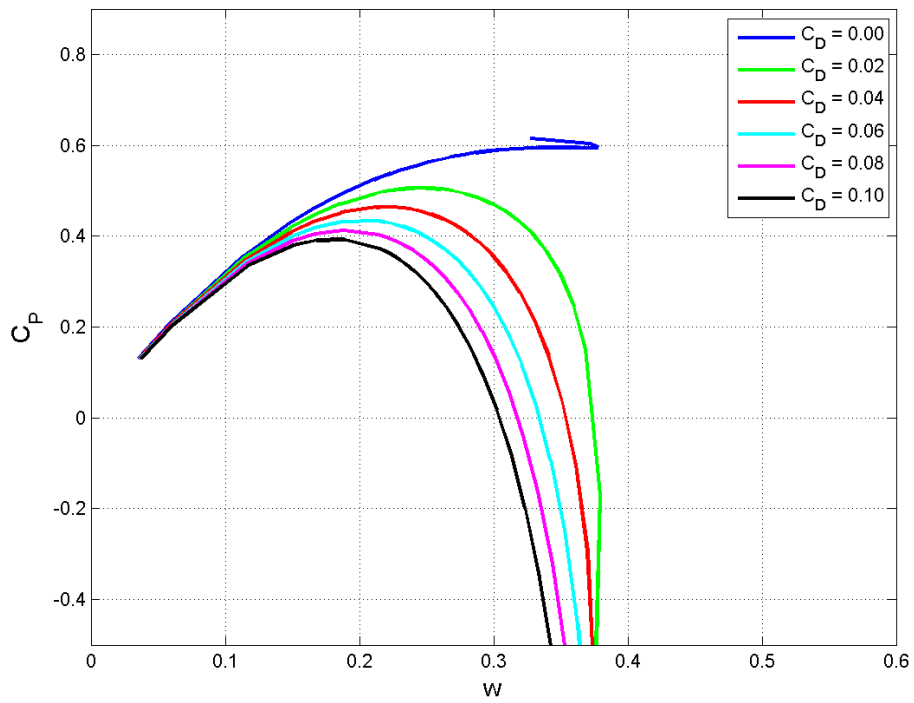
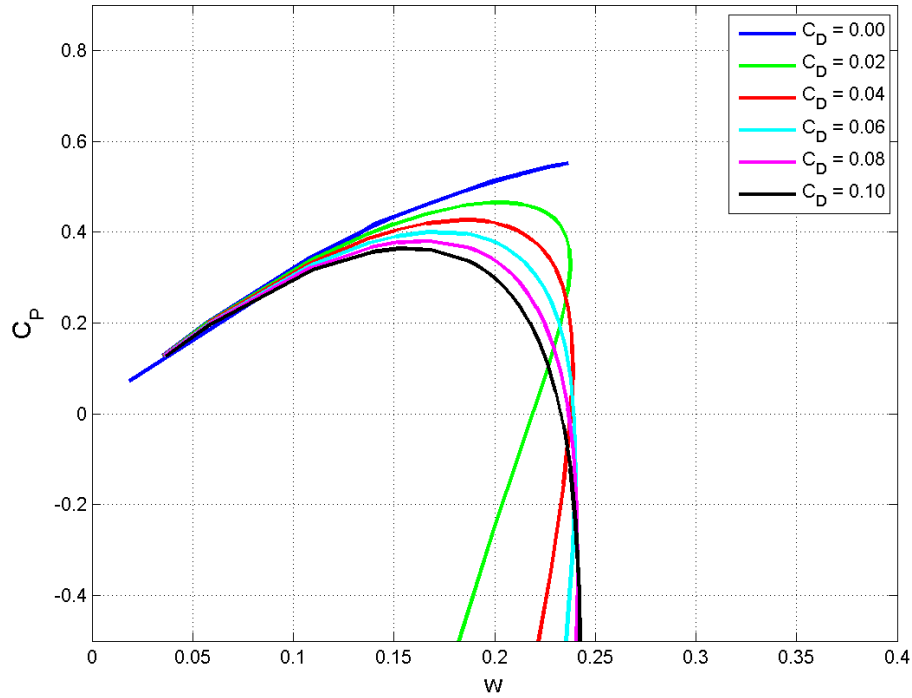
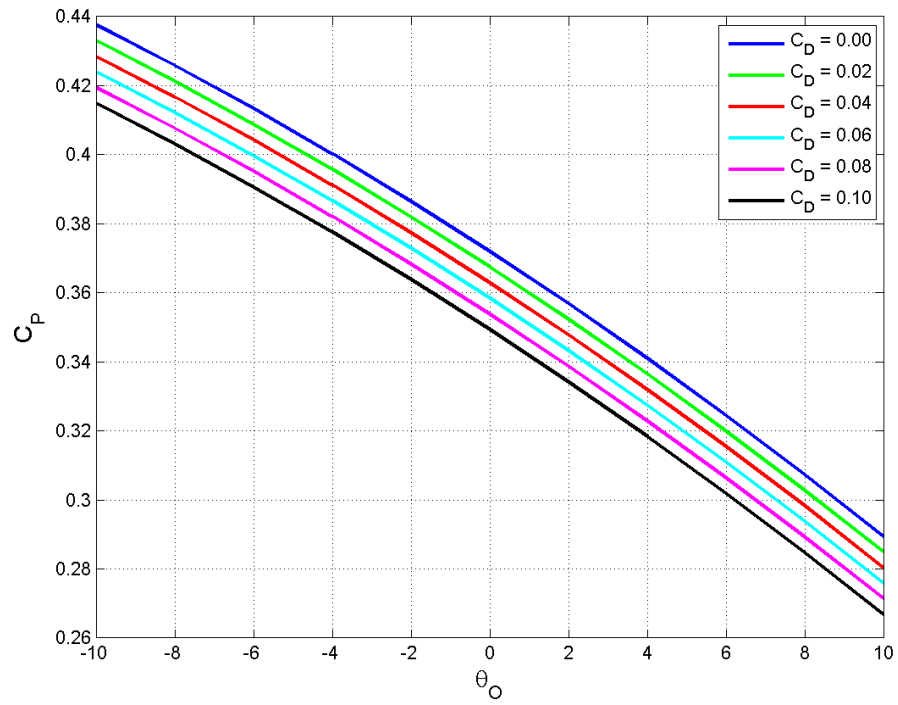


Figure 5.5  $C_P$  as a function of  $w$ ,  $\gamma=0^\circ$ ,  $\theta_0=2^\circ$ ,  $\theta_s=0^\circ$ ,  $\theta_c = 0^\circ$



**Figure 5.6** CP as a function of w,  $\gamma=0^\circ$ ,  $\theta_o=4^\circ$ ,  $\theta_s=0^\circ$ ,  $\theta_c = 0^\circ$

Figures 5.7 through 5.9 show the power coefficient as a function of the collective pitch for tip speeds of 2, 4, and 6 respectively. The results illustrate that the power coefficient can be improved by variations in collective pitch and that the trends vary with tip speed. In the case of a low tip speed, a negative collective pitch increases the power coefficient, yet as the tip speed increases the trend changes such that positive pitch settings may be required. Figures 5.10-5.12 show the power coefficient as a function of the side to side cyclic pitch for tip speeds of 2, 4 and 6 respectively. Figures 5.13-5.15 show the power coefficient as a function of the fore to aft cyclic pitch for tip speeds of 2, 4 and 6 respectively. In all cases, the flow is axial—that is gamma is zero—so the optimal cyclic pitch settings occur at zero regardless of the tip speed.



**Figure 5.7** CP as a function of  $\theta_O$ ,  $J=2$ ,  $\gamma=0^\circ$ ,  $\theta_s=0^\circ$ ,  $\theta_c=0^\circ$

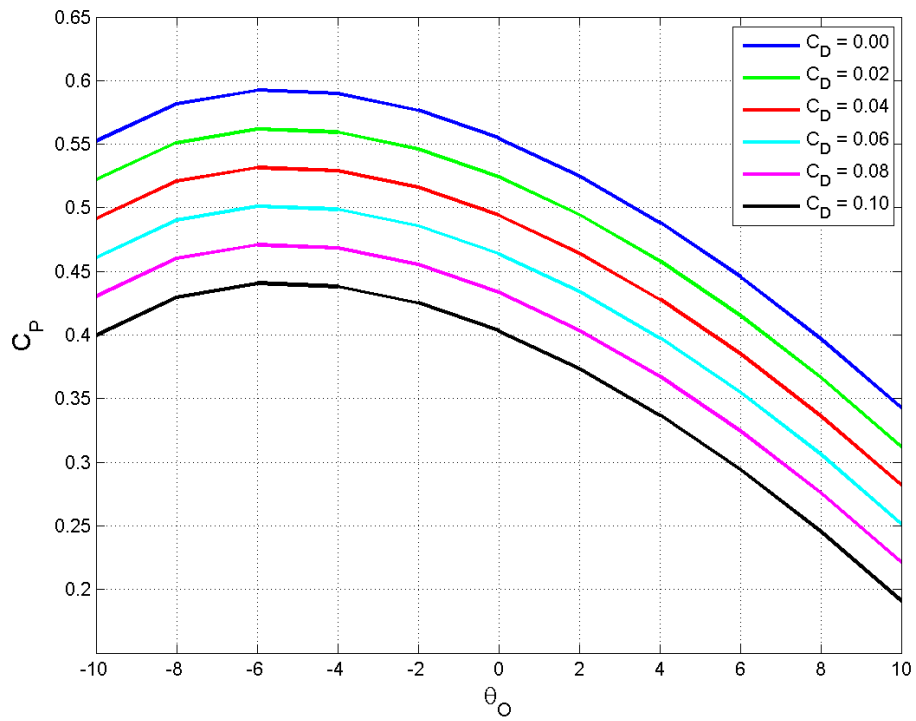


**Figure 5.8** CP as a function of  $\theta_O$ ,  $J=4$ ,  $\gamma=0^\circ$ ,  $\theta_s=0^\circ$ ,  $\theta_c=0^\circ$

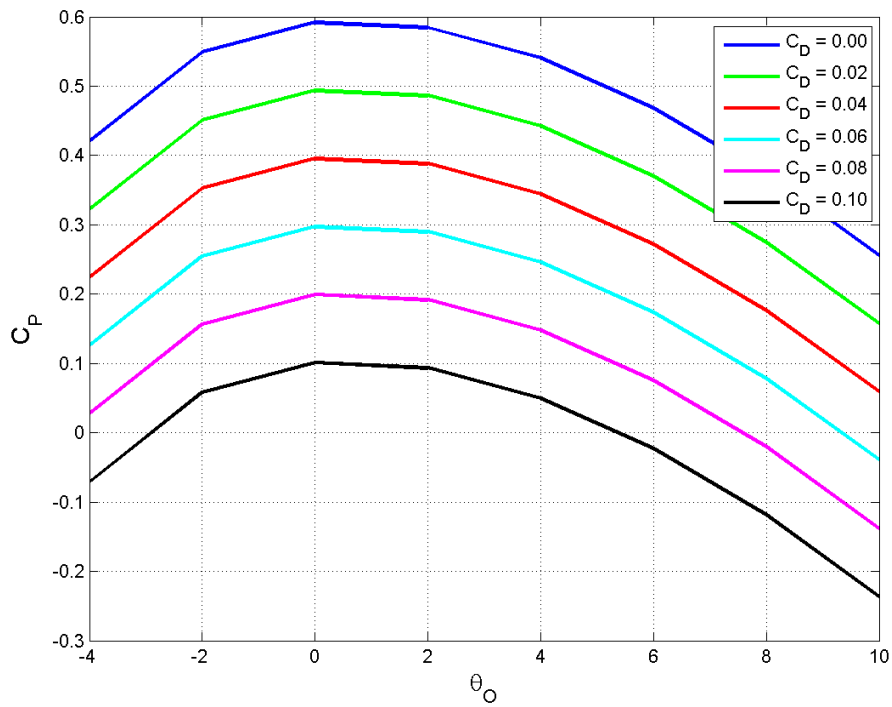


Figure 5.9 CP as a function of  $\theta_o$ ,  $J=6$ ,  $\gamma=0^\circ$ ,  $\theta_s=0^\circ$ ,  $\theta_c=0^\circ$

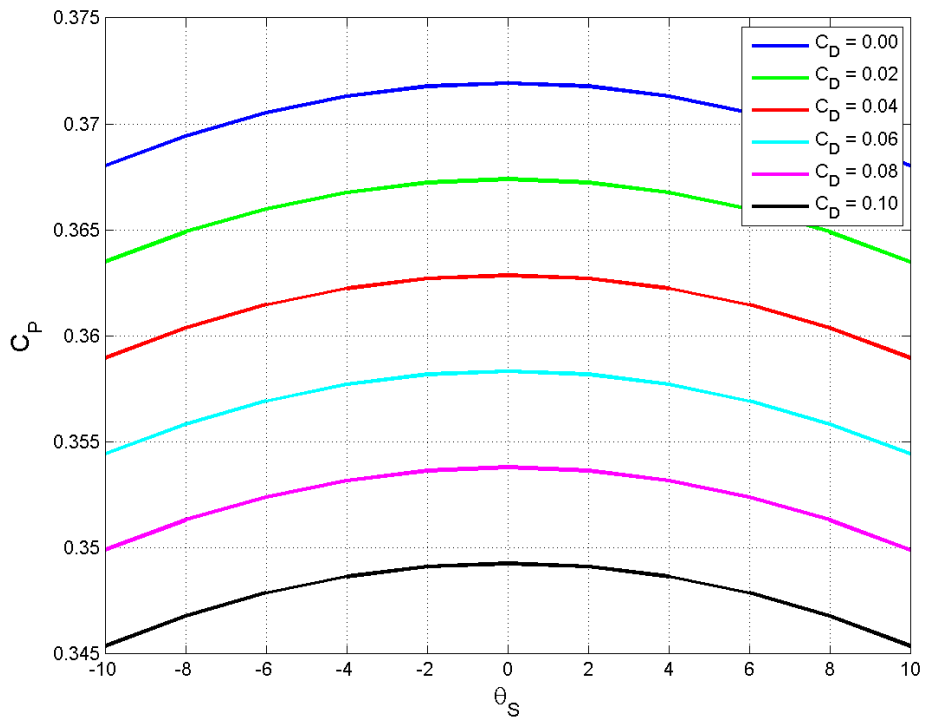


Figure 5.10 CP as a function of  $\theta_s$ ,  $J=2$ ,  $\gamma=0^\circ$ ,  $\theta_o=0^\circ$ ,  $\theta_c=0^\circ$

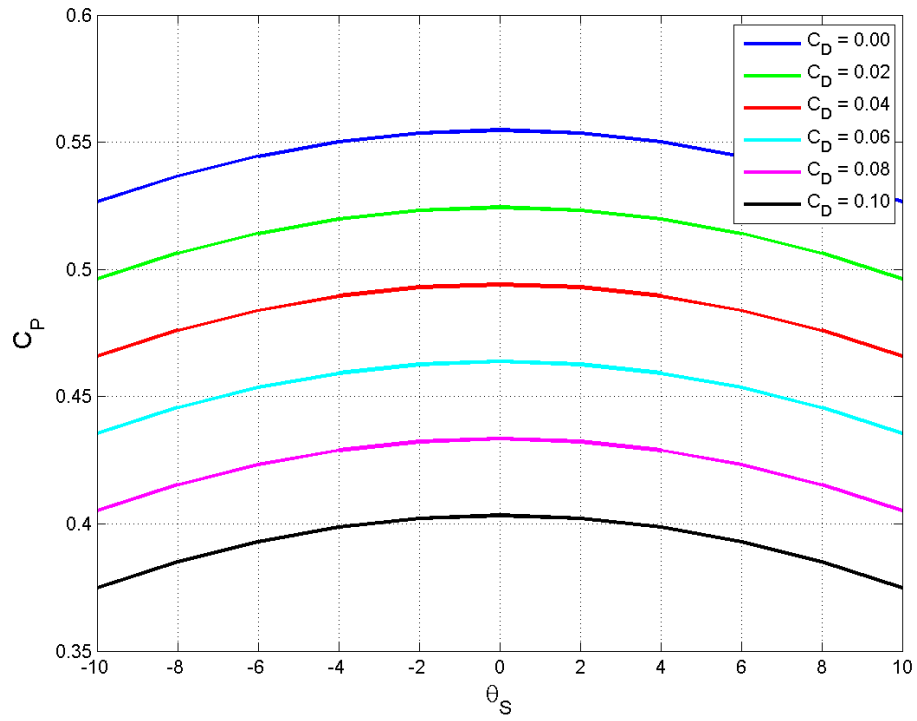


Figure 5.11  $C_P$  as a function of  $\theta_s$ ,  $J=4$ ,  $\gamma=0^\circ$ ,  $\theta_0=0^\circ$ ,  $\theta_c = 0^\circ$

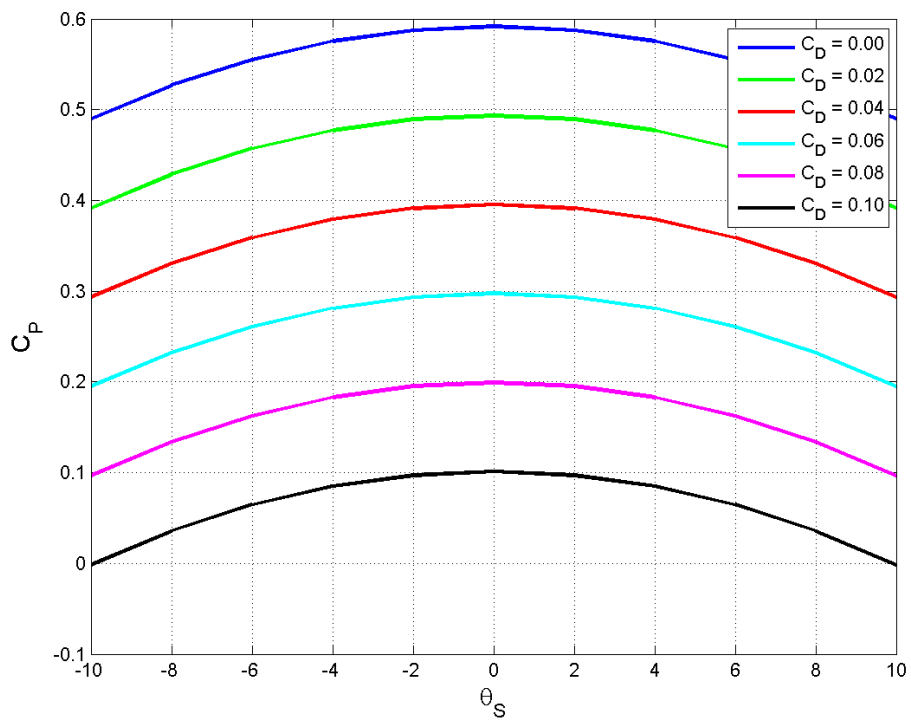


Figure 5.12  $C_P$  as a function of  $\theta_s$ ,  $J=6$ ,  $\gamma=0^\circ$ ,  $\theta_0=0^\circ$ ,  $\theta_c = 0^\circ$

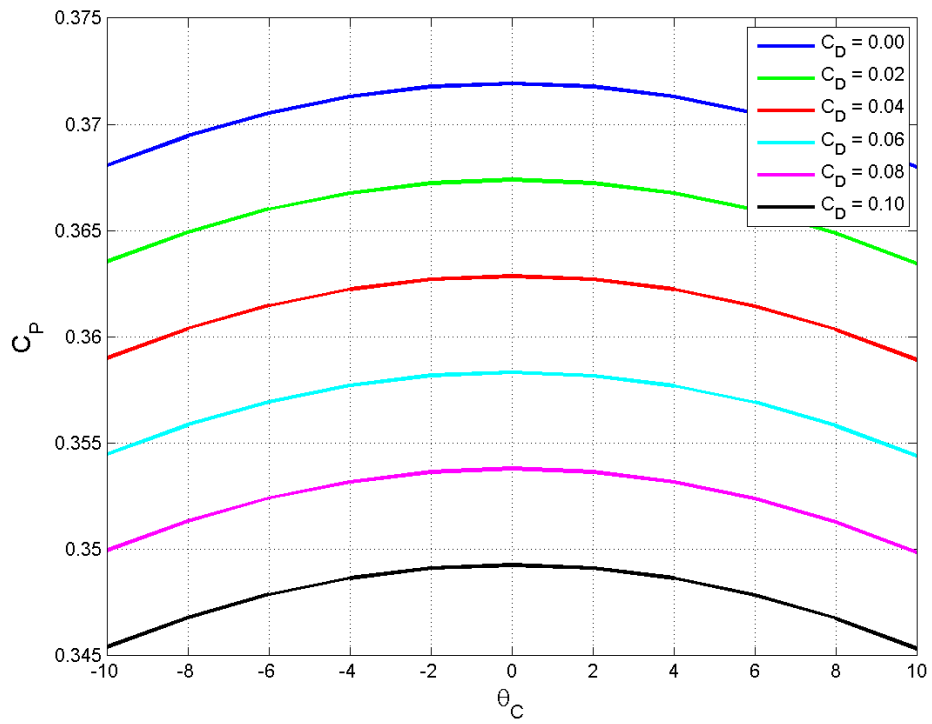


Figure 5.13 CP as a function of  $\theta_c$ ,  $J=2$ ,  $\gamma=0^\circ$ ,  $\theta_o=0^\circ$ ,  $\theta_s = 0^\circ$

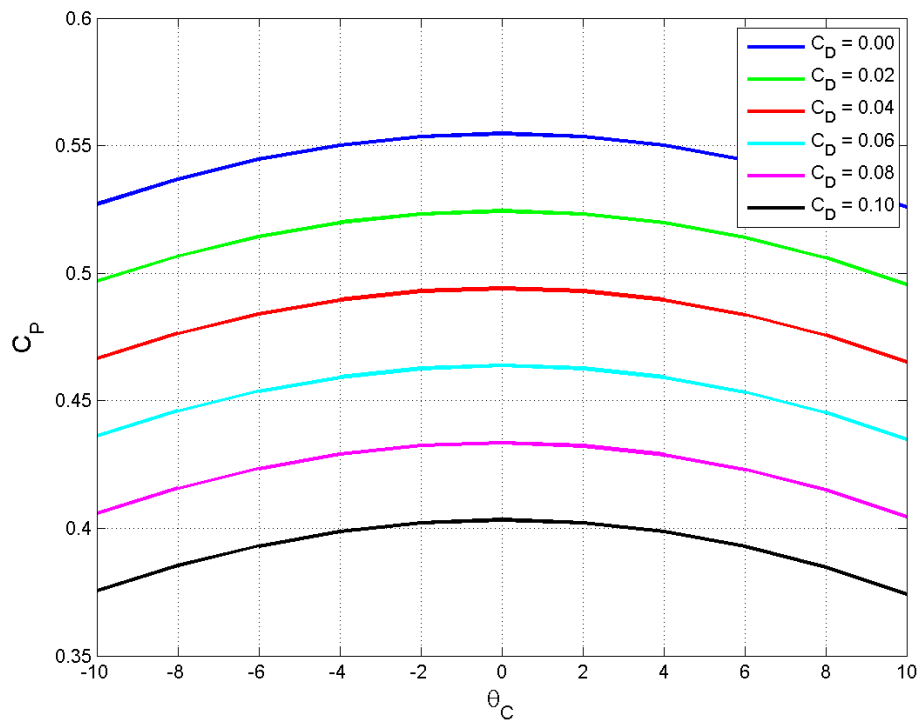
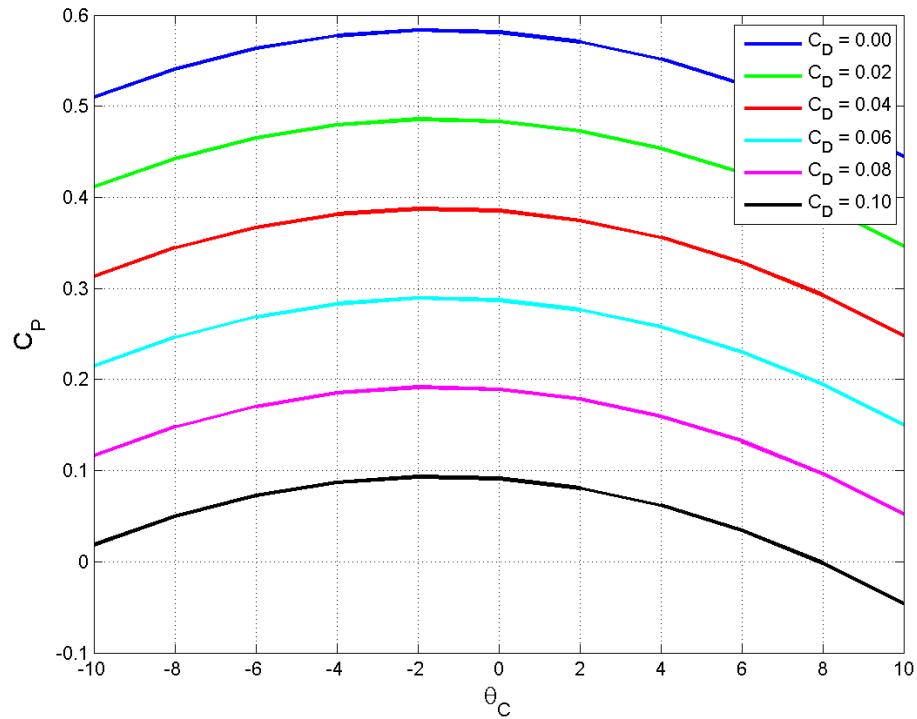


Figure 5.14 CP as a function of  $\theta_c$ ,  $J=4$ ,  $\gamma=0^\circ$ ,  $\theta_o=0^\circ$ ,  $\theta_s = 0^\circ$



**Figure 5.15**  $C_P$  as a function of  $\theta_C$ ,  $J=6$ ,  $\gamma=0^\circ$ ,  $\theta_0=0^\circ$ ,  $\theta_s = 0^\circ$

Figures 5.16-5.18 show the power coefficient as a function of the side to side cyclic pitch for tip speeds of 2, 4 and 6 respectively with yawed flow of 60 degrees. Figures 5.19-5.21 show the power coefficient as a function of the fore to aft cyclic pitch for tip speeds of 2, 4 and 6 respectively with yawed flow of 60 degrees. Although the magnitudes are small for the cases shown, it is observed that varying the cyclic pitch can increase the power coefficient in the presence of yawed flow. As for the case of collective pitch in axial flow, the cyclic pitch settings that optimize the power vary with tip speed.

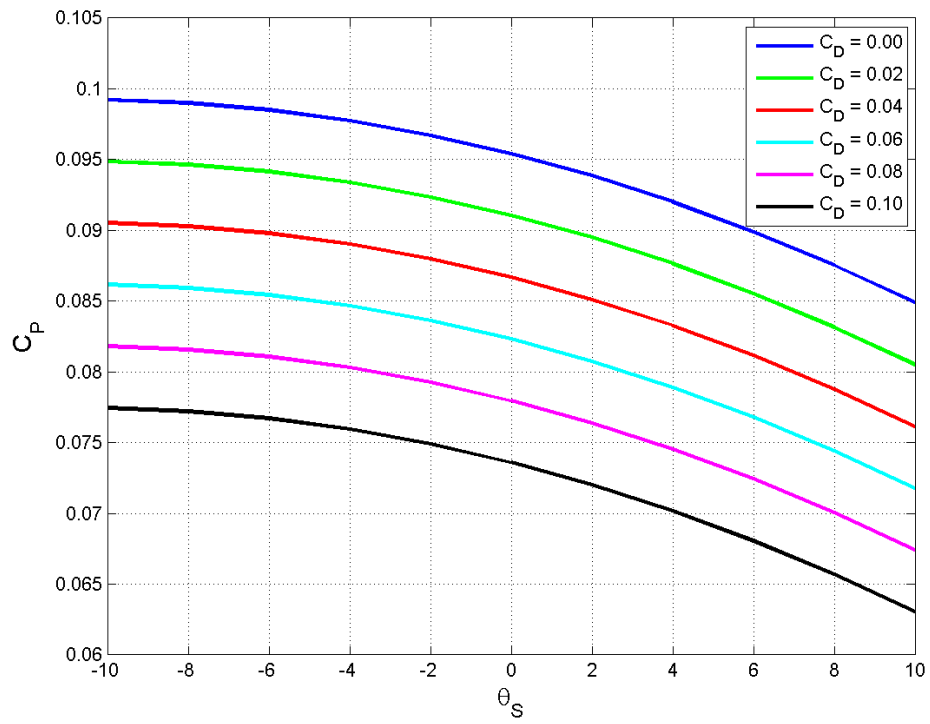


Figure 5.16 CP as a function of  $\theta_s$ ,  $J=6$ ,  $\gamma=60^\circ$ ,  $\theta_0=0^\circ$ ,  $\theta_c = 0^\circ$

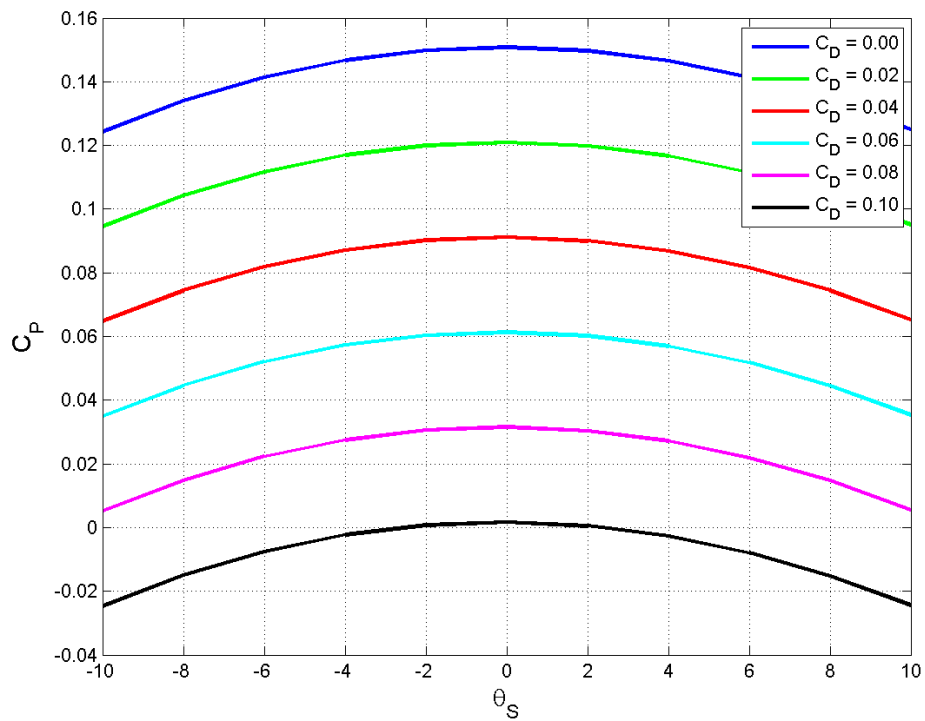


Figure 5.17 CP as a function of  $\theta_s$ ,  $J=4$ ,  $\gamma=0^\circ$ ,  $\theta_0=0^\circ$ ,  $\theta_c = 0^\circ$



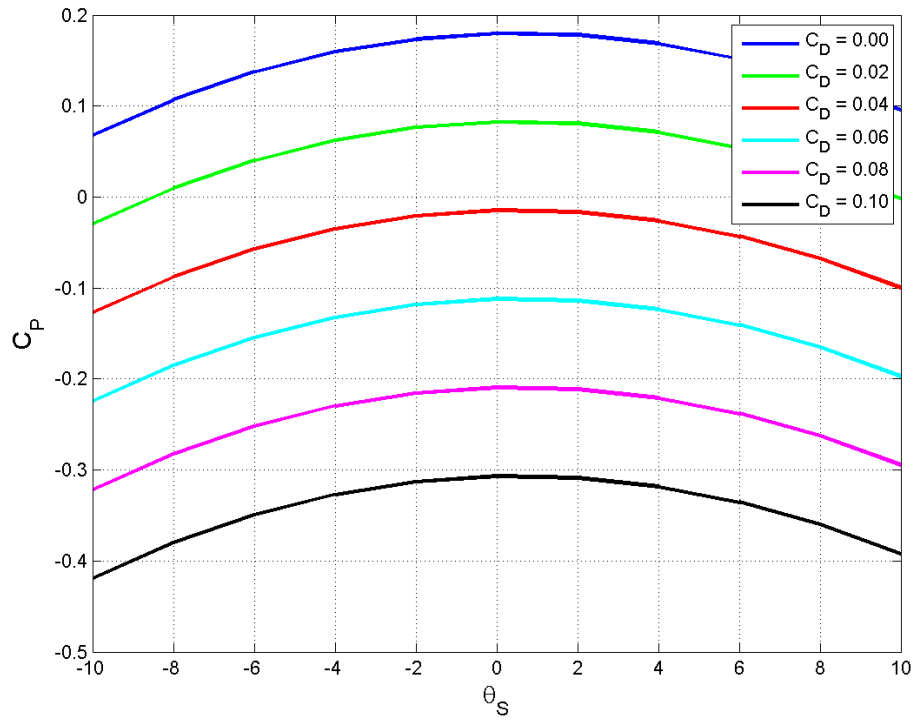


Figure 5.18  $C_p$  as a function of  $\theta_s$ ,  $J=6$ ,  $\gamma=0^\circ$ ,  $\theta_0=0^\circ$ ,  $\theta_c = 0^\circ$

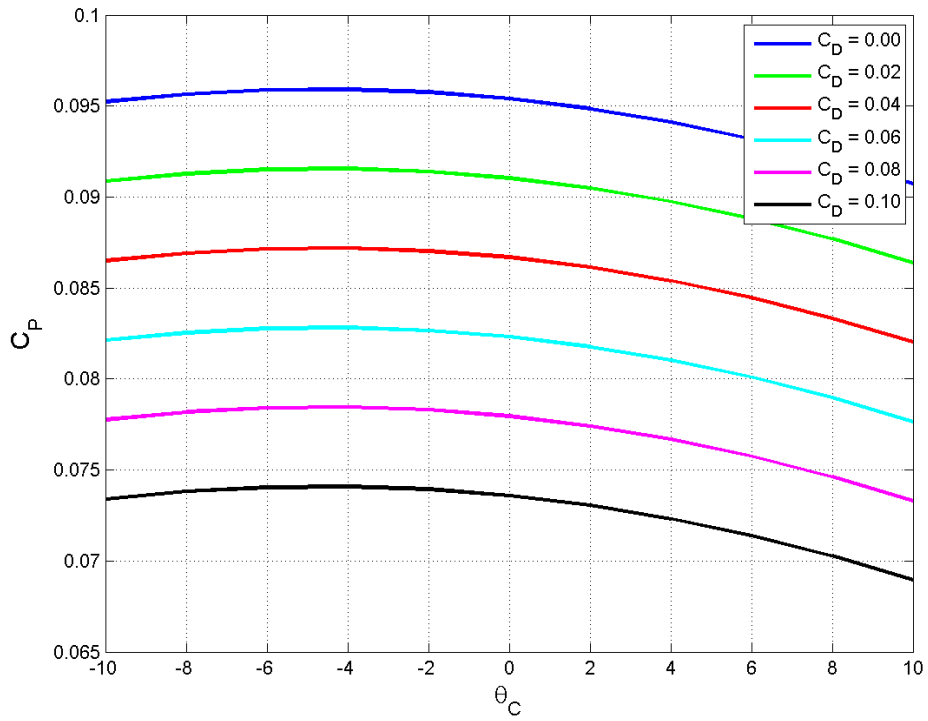


Figure 5.19  $C_p$  as a function of  $\theta_c$ ,  $J=2$ ,  $\gamma=60^\circ$ ,  $\theta_0=0^\circ$ ,  $\theta_s = 0^\circ$

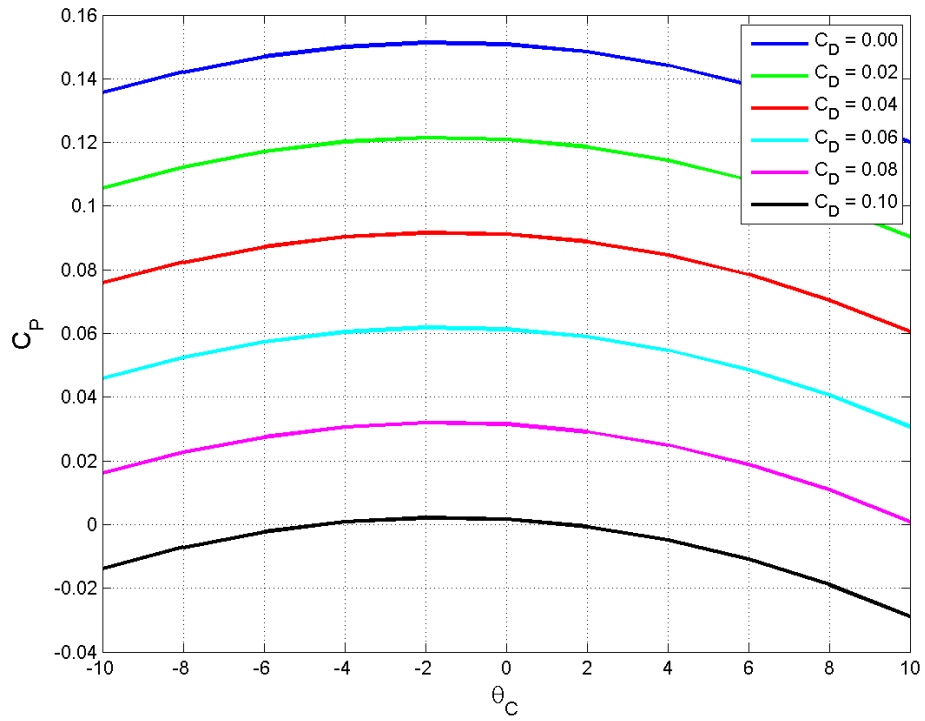


Figure 5.20 CP as a function of  $\theta_C$ ,  $J=4$ ,  $\gamma=60^\circ$ ,  $\theta_O=0^\circ$ ,  $\theta_S = 0^\circ$

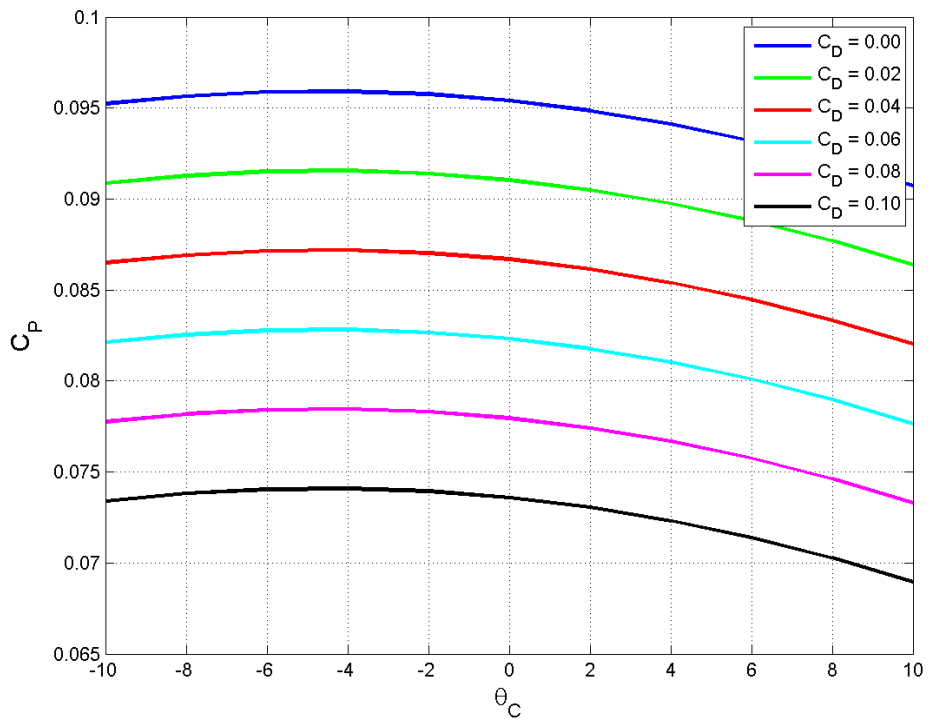


Figure 5.21 CP as a function of  $\theta_C$ ,  $J=6$ ,  $\gamma=60^\circ$ ,  $\theta_O=0^\circ$ ,  $\theta_S = 0^\circ$

Figures 5.22-5.24 show the power coefficient as a function of gamma (the yawed inflow angle of the free stream wind) for tip speeds of 2, 4, and 6, respectively. These plots show that the power coefficient will decrease with yaw angle. The figures also show that the range of feasible yaw angles for which power can be extracted is a function of tip speed.

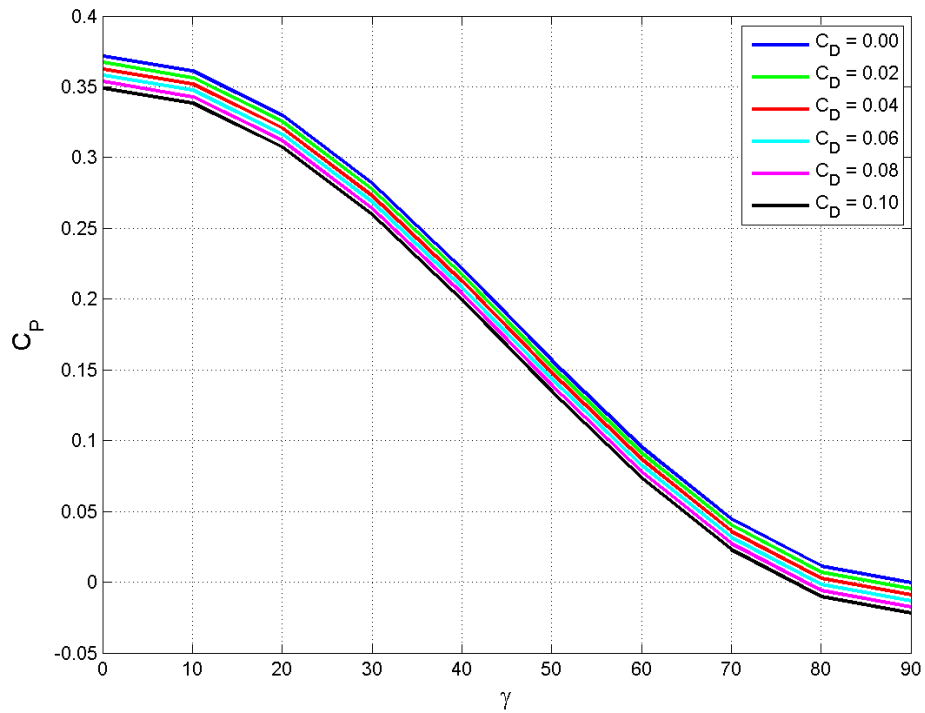


Figure 5.22 CP as a function of  $\gamma$ ,  $J=2$ ,  $\theta_o=0^\circ$ ,  $\theta_s=0^\circ$ ,  $\theta_c=0^\circ$

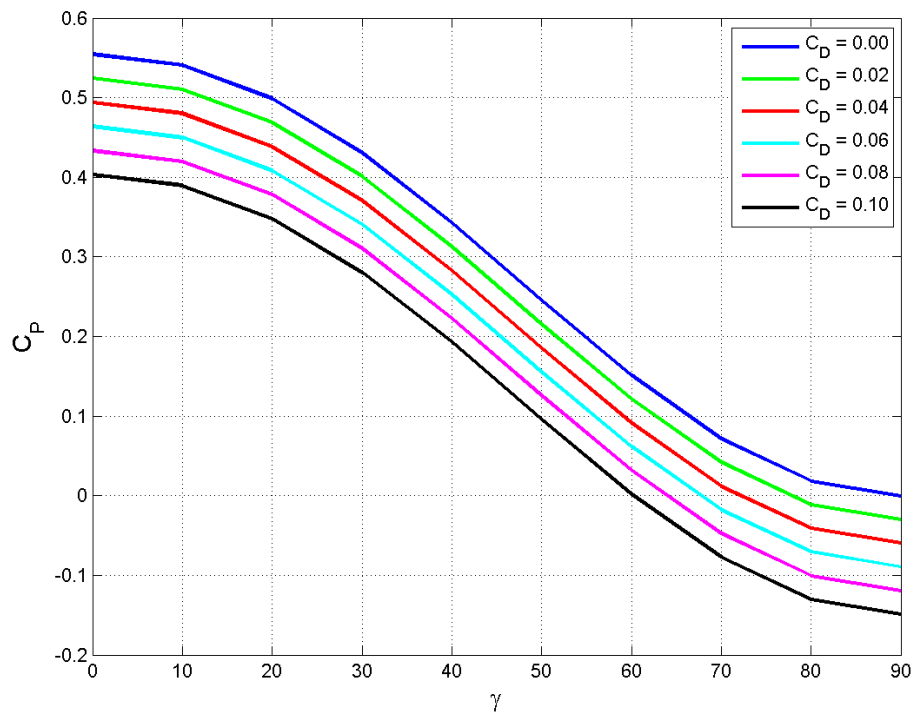


Figure 5.23 CP as a function of  $\gamma$ ,  $J=4$ ,  $\theta_0=0^\circ$ ,  $\theta_s=0^\circ$ ,  $\theta_c=0^\circ$

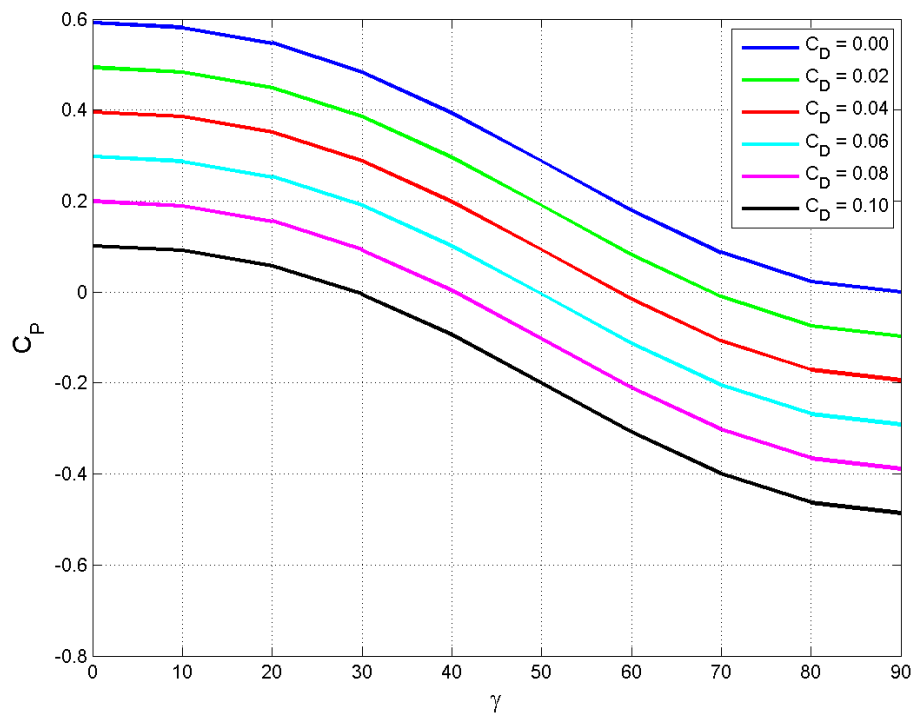
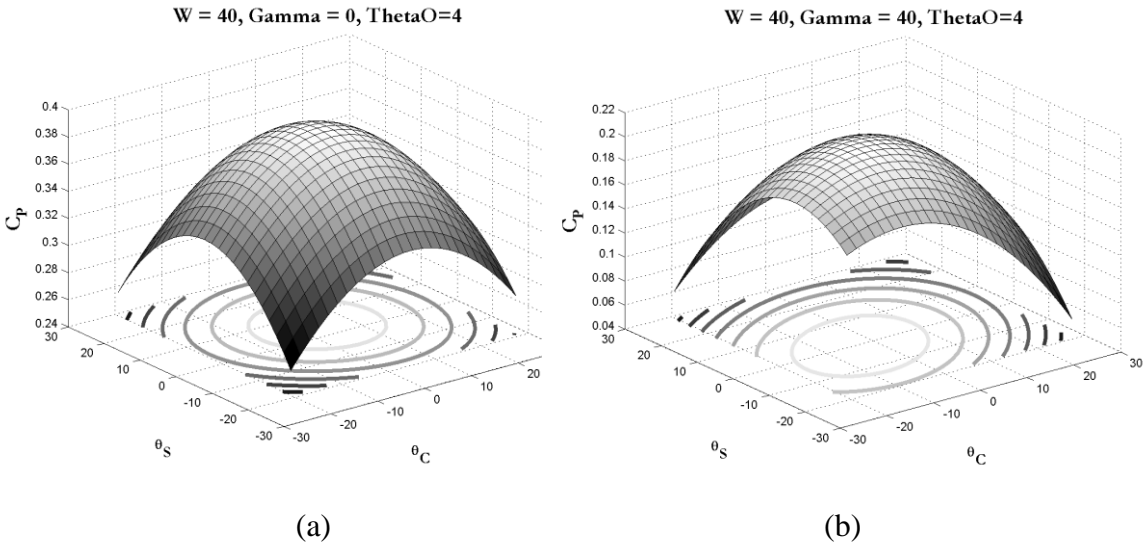


Figure 5.24 CP as a function of  $\gamma$ ,  $J=6$ ,  $\theta_0=0^\circ$ ,  $\theta_s=0^\circ$ ,  $\theta_c=0^\circ$

# 5.2 Surface Plots of the Control Space

Optimization problems typically have challenges working well over very complex dynamically changing surfaces or design spaces. Surfaces that fluctuate can result in an optimizer finding a local minimum or maximum as opposed to the global value. For this reason it is worthwhile to make some surface plots of the control space that will be optimized to gain some insight into how the power coefficient will change with control increments being added to the system. Since there are three control terms in the optimization,  $\theta_o$ ,  $\theta_s$ , and  $\theta_c$ , it makes sense to look at some surface plots of the power coefficient varying two of the terms at a time. The following surface plots will show an example for axial flow and for a yawed flow case and a couple different tip speeds for evaluation.

Figures 5.25-5.30 shows the two dimensional surface plot of the power coefficient as a function of  $\theta_s$ , and  $\theta_c$ . The plots are intended to give insight into the behavior of the power coefficient as a viable parameter in a cost function.



**Figure 5.25** CP as a function of  $\theta_s, \theta_c$  with  $J=3, \theta_o = 4^\circ$ , for (a)  $\gamma = 0^\circ$  (b)  $\gamma = 40^\circ$

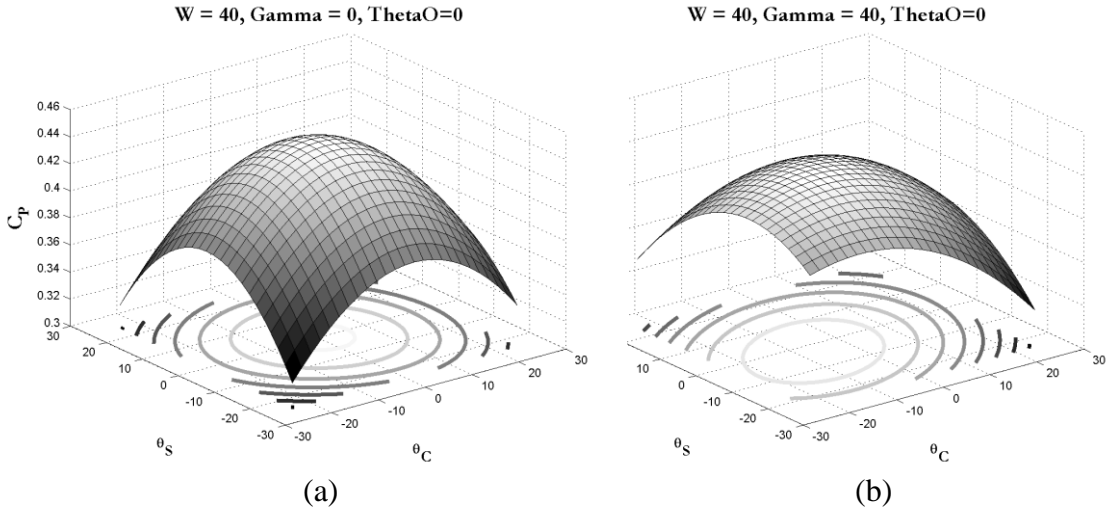


**Figure 5.26** CP as a function of  $\theta_S, \theta_C$  with  $J=3, \theta_O = 0^\circ$ , for (a)  $\gamma = 0^\circ$  (b)  $\gamma = 40^\circ$

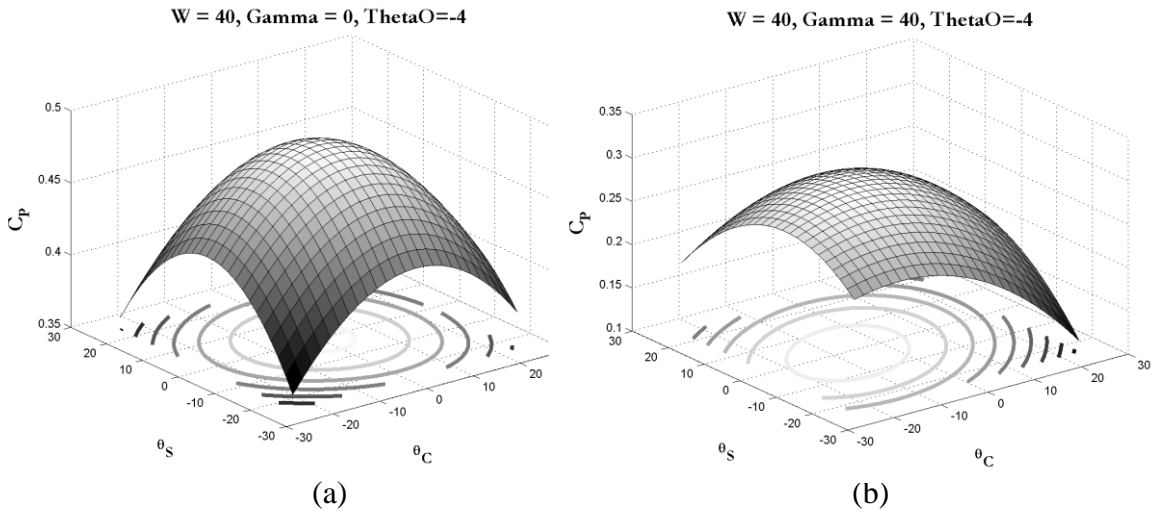


**Figure 5.27** CP as a function of  $\theta_S, \theta_C$  with  $J=3, \theta_O = -4^\circ$ , for (a)  $\gamma = 0^\circ$ , (b)  $\gamma = 40^\circ$

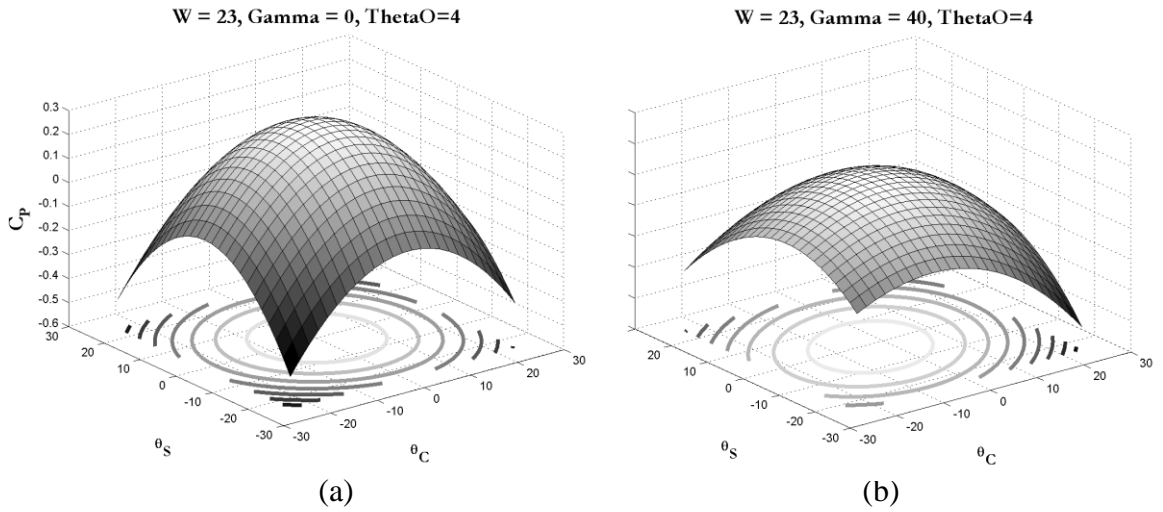


**Figure 5.28** CP as a function of  $\theta_S, \theta_C$  with  $J=5, \theta_O = 4^\circ$ , for (a)  $\gamma = 0^\circ$ , (b)  $\gamma = 40^\circ$

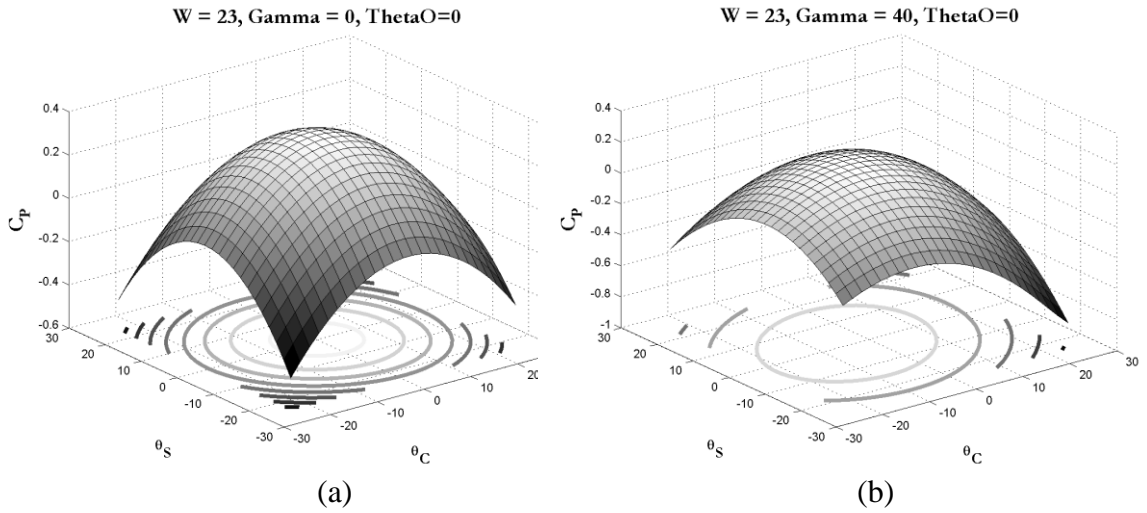


**Figure 5.29** CP as a function of  $\theta_s, \theta_c$  with  $J=5, \theta_O = 0^\circ$ , for (a)  $\gamma = 0^\circ$ , (b)  $\gamma = 40^\circ$

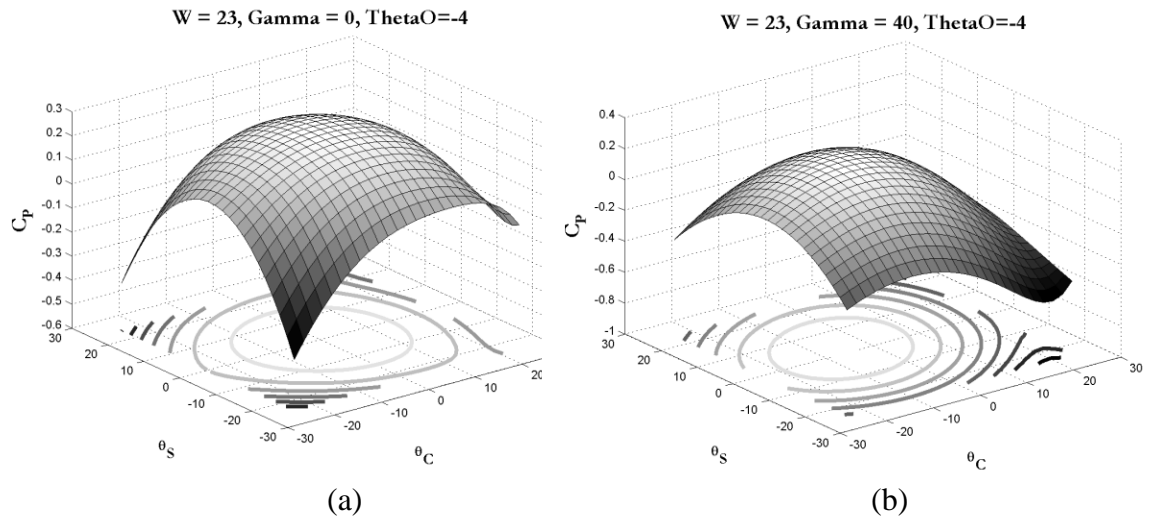
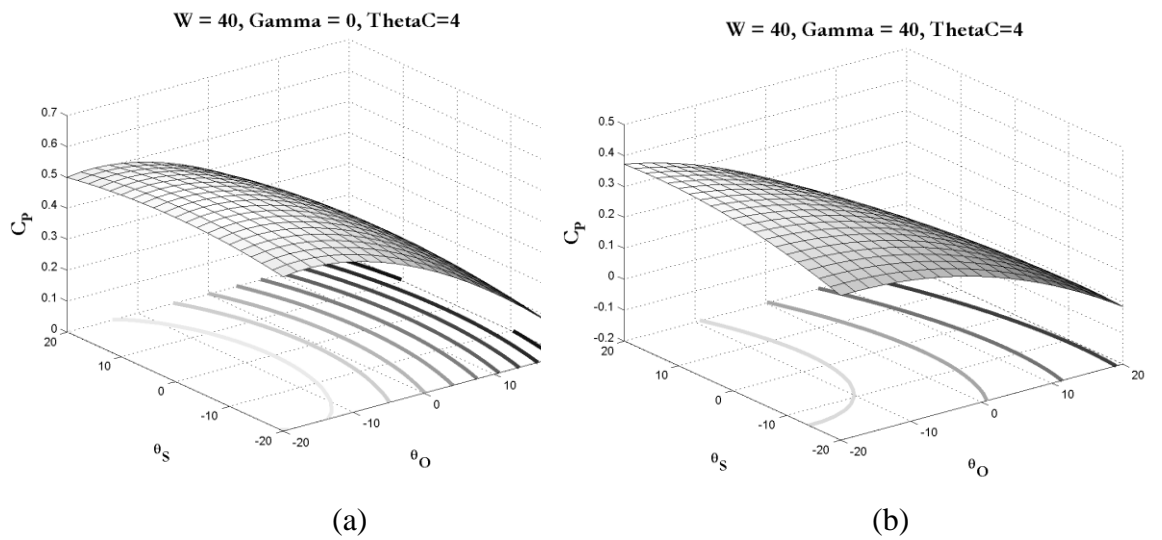


**Figure 5.30** CP as a function of  $\theta_s, \theta_c$  with  $J=5, \theta_O = -4^\circ$ , for (a)  $\gamma = 0^\circ$ , (b)  $\gamma = 40^\circ$

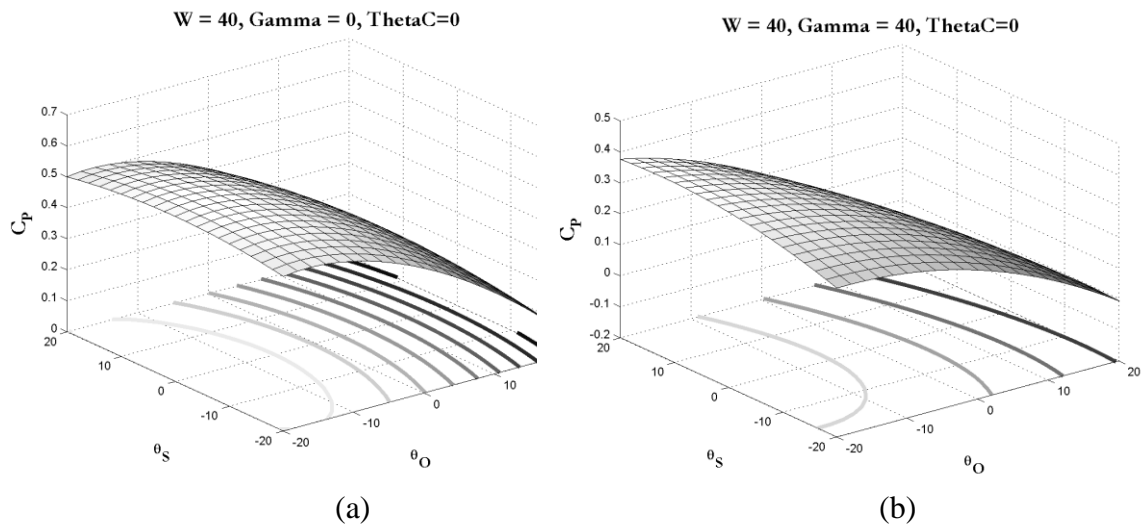
Figures 5.25-5.30 show that the value of the power coefficient changes smoothly as  $\theta_s$  and  $\theta_c$  are varied. Furthermore, plots show the general trend that there are not numerous local minimums or maximums, especially in the windmill state of positive power for which this model will be evaluating. In addition to inspecting the surface, contours are projected into the X-Y plane. They show another general trend regarding the location of the global maximum. In the presence of yawed flow, the global maximum can occur at a non zero value for the side to side cyclic pitch term,  $\theta_s$ , or the fore to aft cyclic pitch term,  $\theta_c$ , indicating that the optimum power coefficient is

achieved with non-zero cyclic pitch terms. Thus for the given collective pitch settings, these grids show a reasonable design space in which to optimize cyclic pitch.

It is also insightful to see how collective and cyclic pitch interacts. To do this, we can plot grids showing the variation of the power coefficient with collective and each cyclic pitch term. Figures 5.31-5.33 show the power coefficient as a function of collective and side to side cyclic pitch  $\theta_s$ .

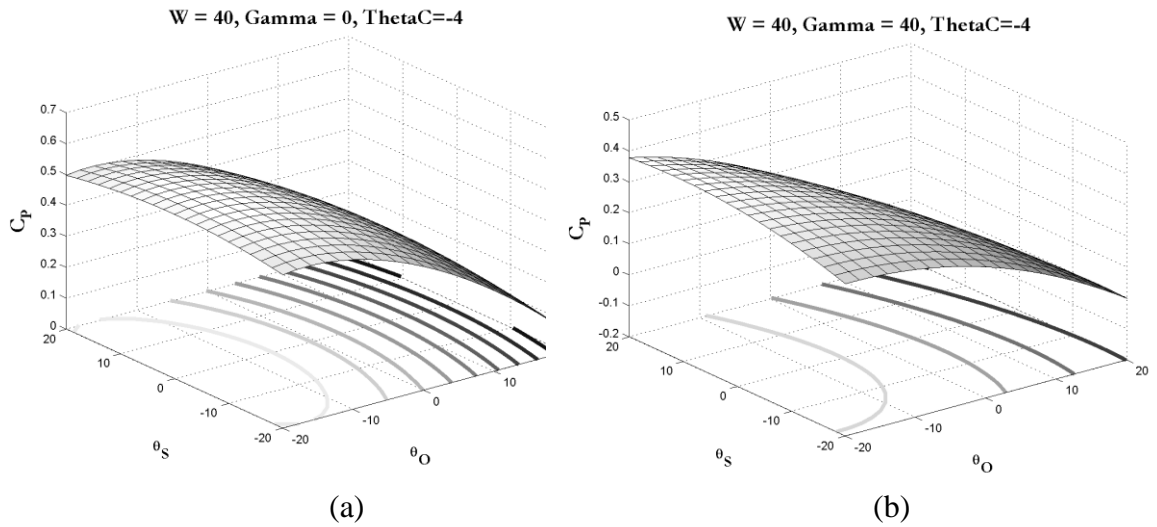


**Figure 5.31** CP as a function of  $\theta_O$ ,  $\theta_s$  with  $J=3$ ,  $\theta_C = 4^\circ$ , for (a)  $\gamma = 0^\circ$ , (b)  $\gamma = 40^\circ$



**Figure 5.32** CP as a function of  $\theta_O$ ,  $\theta_s$  with  $J=3$ ,  $\theta_O = 0^\circ$ , for (a)  $\gamma = 0^\circ$ , (b)  $\gamma = 40^\circ$

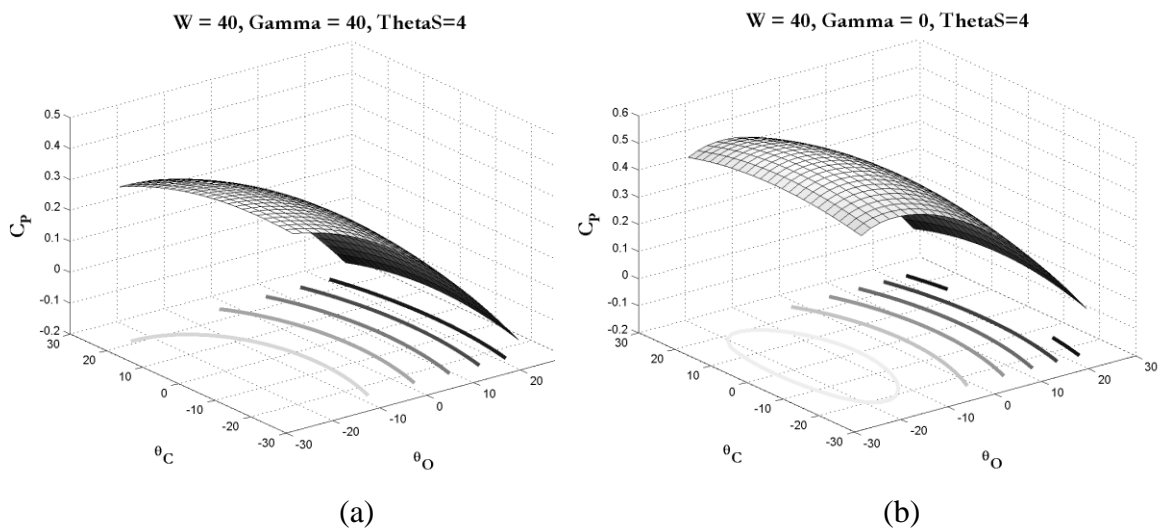




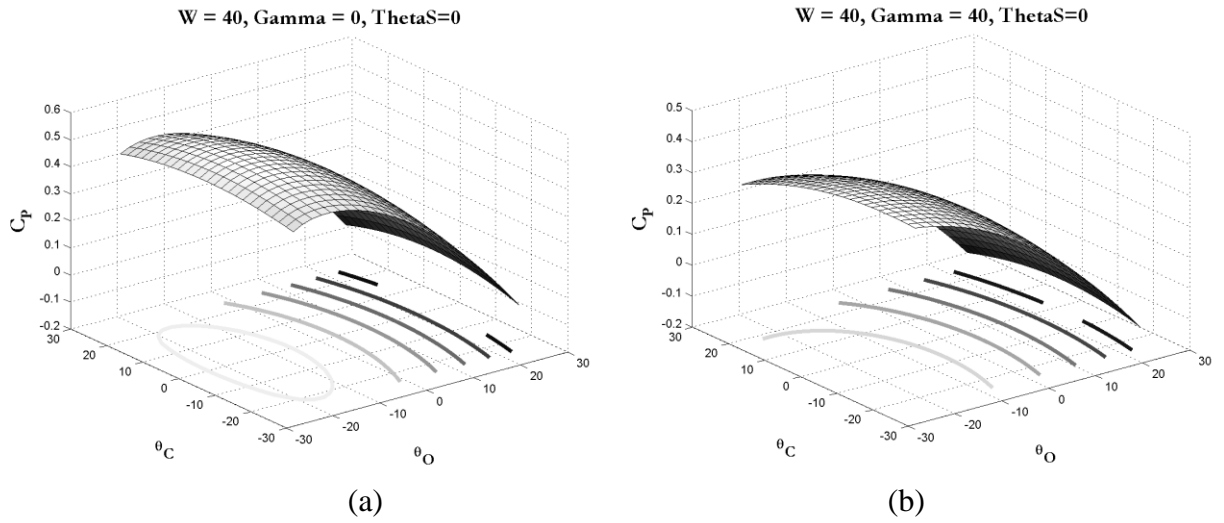
**Figure 5.33**  $C_p$  as a function of  $\theta_O$ ,  $\theta_S$  with  $J=3$ ,  $\theta_C = -4^\circ$ , for (a)  $\gamma = 0^\circ$ , (b)  $\gamma = 40^\circ$

Figure 5.31-33 show smooth change in the windmill state for the power coefficient as  $\theta_O$  and  $\theta_S$  are varied. The plots show that even though the collective pitch term is dominant that the optimal power coefficient in yawed flows is for non-zero cyclic pitch.

Figures 5.34-5.36 show the power coefficient as a function of collective and fore to aft cyclic pitch  $\theta_C$ .



**Figure 5.34**  $C_p$  as a function of  $\theta_O$ ,  $\theta_C$  with  $J=3$ ,  $\theta_S = 4^\circ$ , for (a)  $\gamma = 0^\circ$ , (b)  $\gamma = 40^\circ$



**Figure 5.35** CP as a function of  $\theta_O$ ,  $\theta_C$  with  $J=3$ ,  $\theta_S = 0^\circ$ , for (a)  $\gamma = 0^\circ$ , (b)  $\gamma = 40^\circ$

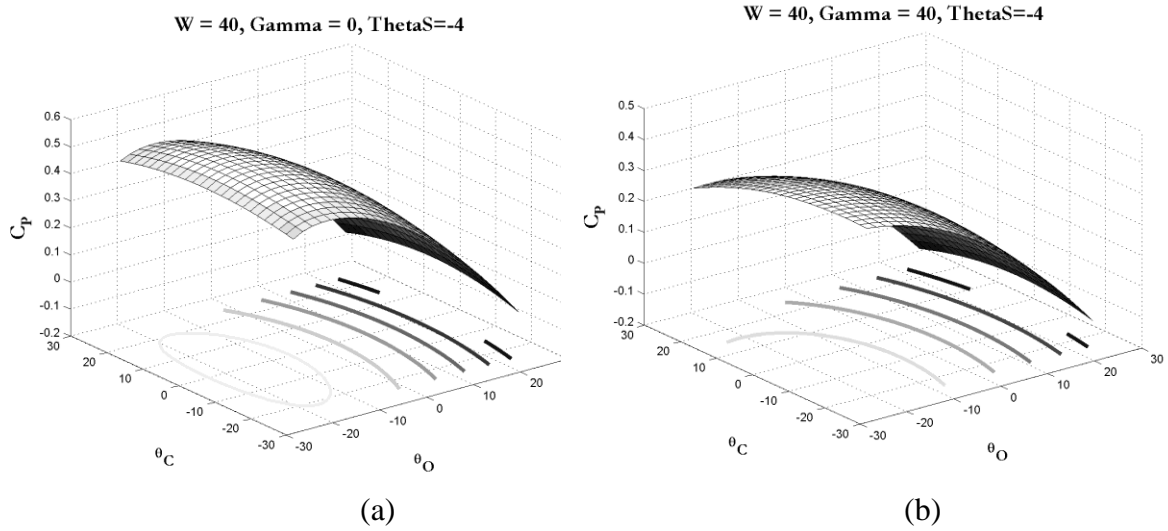


**Figure 5.36** CP as a function of  $\theta_O$ ,  $\theta_C$  with  $J=3$ ,  $\theta_S = -4^\circ$ , for (a)  $\gamma = 0^\circ$ , (b)  $\gamma = 40^\circ$

Figures 5.34-5.36 also show smooth change in the windmill state for the power coefficient when  $\theta_S$  and  $\theta_C$  are varied. These examples also suggest that varying  $\theta_C$  may increase the optimum power for the system.

The surface plots shown have presented some examples that focus predominantly on the windmill state, which is the domain for which this model is valid and the research is interested. An area that may give the optimization process some

challenges will be transition states, specifically, the transition from the propeller to windmill state. Figure 5.37 shows an example of the transition from the propeller to the windmill state.

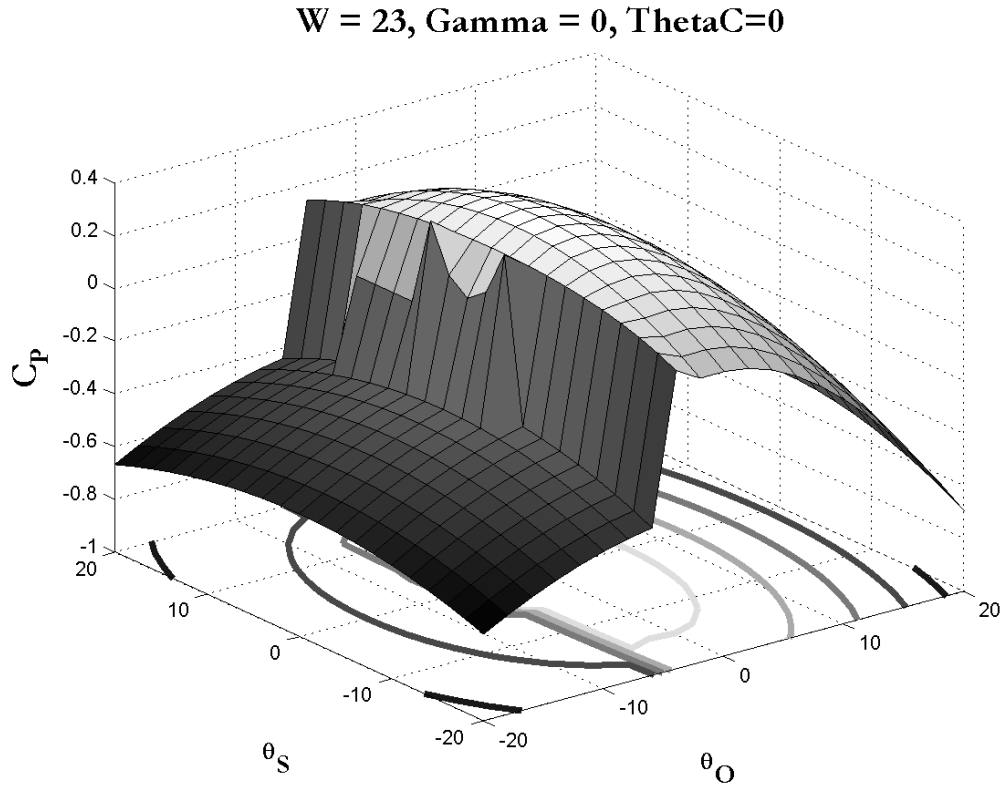


**Figure 5.37**  $C_P$  as a function of  $\theta_O$  and  $\theta_S$  with  $J=5$ ,  $\theta_C = 0^\circ$ , for  $\gamma = 0^\circ$

Figure 5.37 shows an abrupt change in the power coefficient as the collective pitch is varied. As the pitch is decreased, and depending on the operating conditions such as wind speed, RPM or yaw inflow angle, the total lift along the blades will switch sign. For twisted blades it is possible that this transition may change more gracefully, but this study uses fixed theta. Although the transition can result in transient results this behavior should not prevent an off-the-shelf optimizer from finding an optimal solution so long as the final results are watched closely when small values for the power coefficient are being analyzed.

# Chapter 6

## Results for Optimal Power Coefficient with Varying Controls

In this chapter an optimizing routine will finally be wrapped around the WT\_3DOF simulation to study the behavior of the optimal power coefficient as a wind turbines control space is opened. The section will consist of two parts, discussion with checkout of the optimizer being used and the optimization results. The results section will show a progression of increasing the control space by comparing a fixed pitch case, a case where only collective pitch is optimized and a case where both collective and cyclic pitch are optimized. Previous research and test data have shown that varying collective pitch with wind speed can improve power optimization so this progression should help provide an appreciation of any improvements plausible by extending the results for cyclic pitch.

### 6.1 Optimization Set up and Check out

Optimization problems take the general form of:

$$\begin{aligned} & \text{minimize } f_0(x) \\ & \text{subject to } f_i(x) \leq b_i, i = 1, 2, \dots, m \end{aligned} \tag{6.1}$$

where  $x = (x_1, x_2, \dots, x_n)$  is the vector of variables,  $f_0$  is the objective function to be minimized and  $f_i$  is the constraint function with boundaries  $b_i$  [43]. The optimal solution is the vector  $x$  that minimizes the objective function subject to the constraint

function and boundary values. In our case the variables being optimized are the control terms,  $\theta_o$ ,  $\theta_s$  and  $\theta_c$ . The objective function will be the minimizing the resulting power coefficient (multiplied by -1) as computed by the WT\_3DOF simulation.

For this phase of research, the problem will be set up without a constraint function with corresponding boundary values. Constraints such as blade rotation limits or dynamic stall may be added to the optimization problem for a given wind turbine or blade; but at this point is the research objective is to find the optimal solution without constraint.

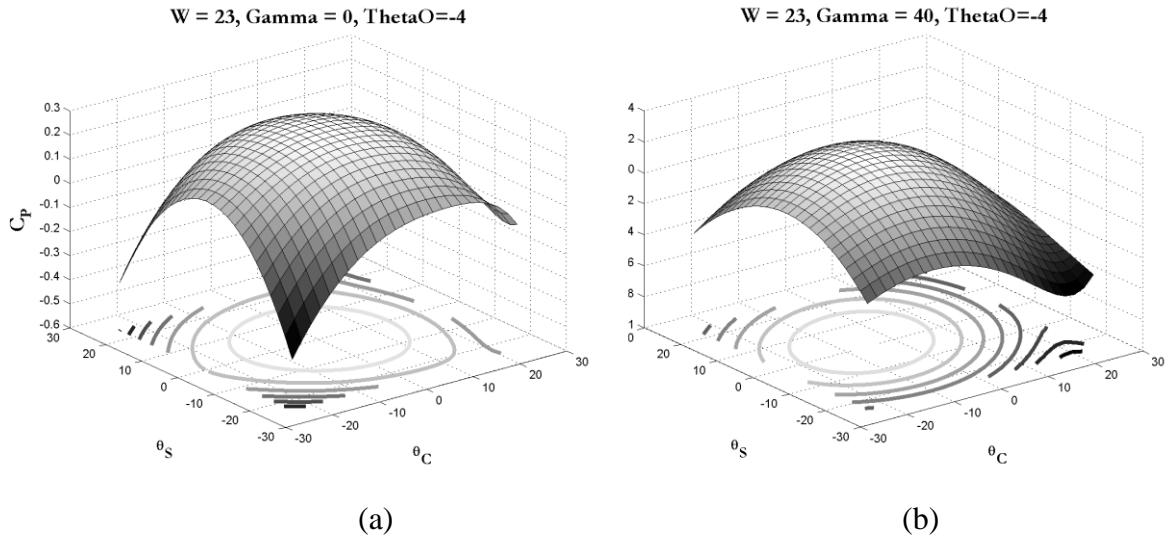
As noted in chapter 5, a common challenge in optimization problems is finding global minimums where the value of the cost function is highly nonlinear. Optimizers can get stuck in local minimums and not find the global result. However the plots in chapter 5 show that the general change in the power coefficient is quite smooth as the control terms are varied. For such surfaces, techniques such as gradient search have success. These results support the use of using commercially available tools such as the MATLAB optimization toolbox set. For systems with many local minimums, such simple tools may not be appropriate, however for this defined system and feasibility study, the MATLAB optimizer is sufficient. (The specific function being used is *fminunc* for which a complete description can be found in the MATLAB documentation.)

Chapter 5 also shows that there are some limited areas where the behavior of the power coefficient can jump erratically, namely, when transitioning between the propeller and windmill state. This jump is observed to only be along one dimension of the optimal variables, the collective pitch  $\theta_o$ . The gradient search approach is still well suited to handle the transition, however the results will be monitored for any erratic results where the power coefficient can be unrealistic due to division by a small number.

Before running the optimization program for the larger domain being studied, some test cases were conducted to verify the optimizer provided reasonable results. The test case was set up with the same parameter values used during the benchmark exercise with the NREL WT\_PERF simulation. For this set of values, test cases were run to evaluate two of the control terms at a time and compared to the surface plots that were presented in chapter 5. Testing two parameters at a time provides some ability to visually inspect the results. The first test case presented here will evaluate the

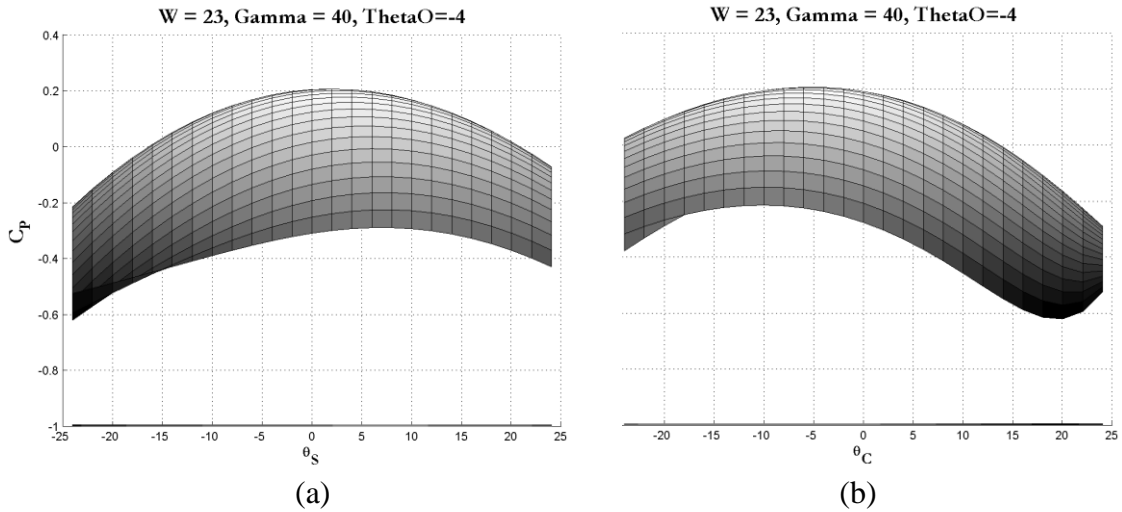
cyclic pitch results for a fixed collective value for axial and yawed flow. The second case presented here will evaluate the results for varying collective and side to side cyclic pitch for a fixed value of fore to aft cyclic pitch.

Figure 6.1 shows the power coefficient as a function of  $\theta_s$  and  $\theta_c$  for fixed values of collective pitch, tip speed and yawed angle of the inflow.



**Figure 6.1** CP as a function of  $\theta_s$  and  $\theta_c$  with  $J=5$ ,  $C_D = 0.08$ ,  $\theta_0 = -4^\circ$ , for (a)  $\gamma = 0^\circ$ , and (b)  $\gamma = 40^\circ$

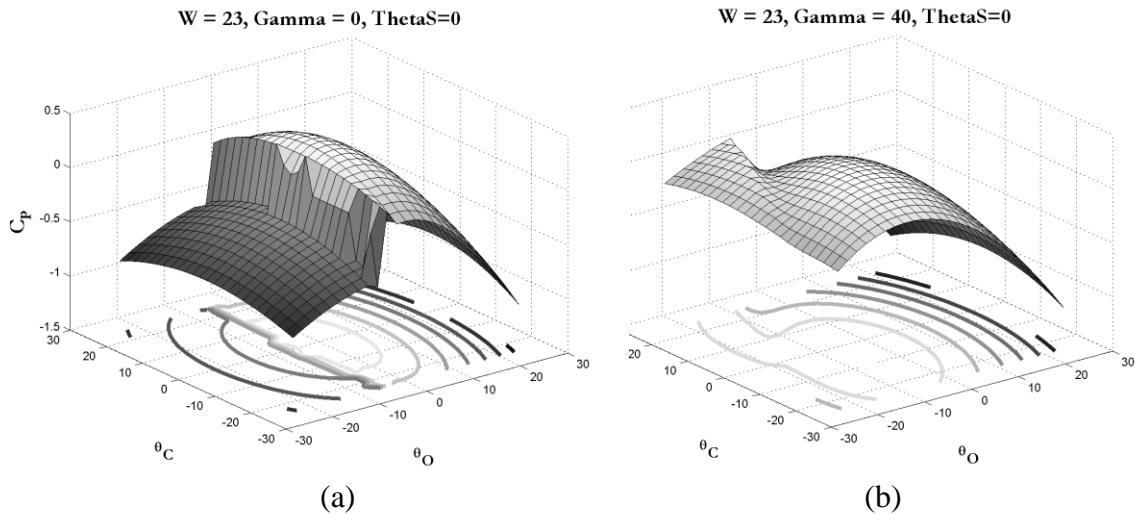
For each case shown in Figure 6.1 (a) and (b), the optimization was performed fixing the variable  $\theta_0 = -4$  deg.. For case (a), the optimizer reported the optimal solution of  $\theta_s = 0$  deg and  $\theta_c = 0$  deg for a maximum value of  $C_p = 0.273$ . For case (b) optimal solution found was  $\theta_s = 1.9$  deg and  $\theta_c = -5.2$  for a maximum value of  $C_p = 0.205$ . Figure 6.2 shows a two dimensional plot of the power coefficient as a function of (a)  $\theta_s$  and (b)  $\theta_c$  for the test case shown in Figure 6.1(b).



**Figure 6.2** CP as a function of (a)  $\theta_s$ , (b)  $\theta_c$  with  $J=5$ ,  $C_D = 0.08$ ,  $\theta_0 = -4^\circ$ ,  $\gamma = 40^\circ$

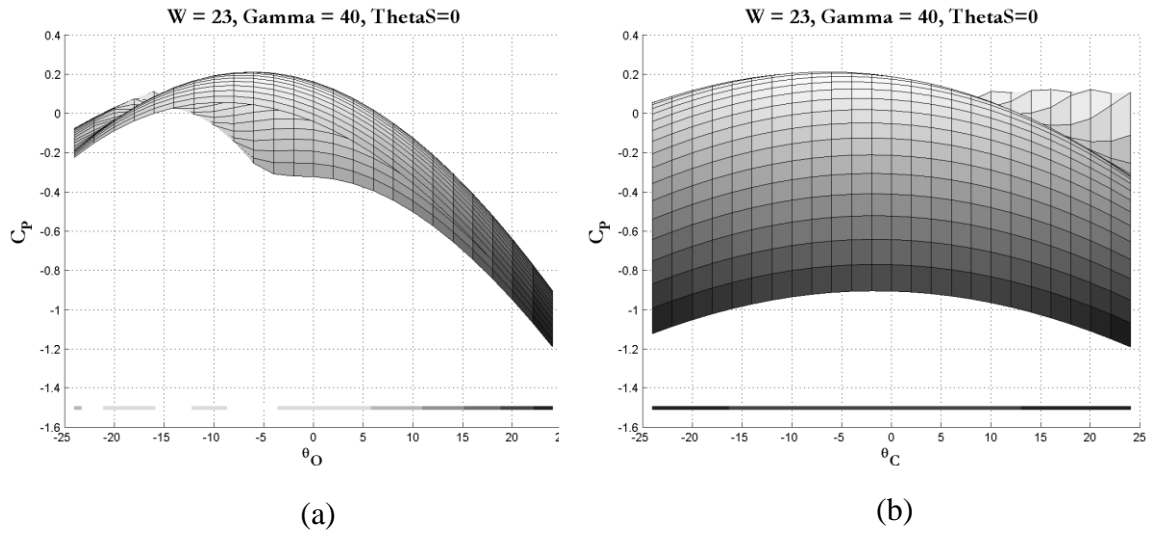
Figure 6.2 is intended to provide some graphical confirmation of a sample test case run to check out the optimization routine. Over 15 cases were evaluated with varying values of collective pitch, wind speed, and yaw angle (gamma)—all verifying the optimal solution was found for each grid case.

Figure 6.3 shows the power coefficient as a function of  $\theta_0$  and  $\theta_c$  for fixed values of side to side cyclic pitch, tip speed and yawed angle of the inflow. This case is one in which the transition region from propeller to windmill state causes some fluctuation in the value of the power coefficient as the control terms are varied.



**Figure 6.3** CP as a function of  $\theta_0$  and  $\theta_c$  with  $J=5$ ,  $C_D = 0.08$ ,  $\theta_s = 0^\circ$ , for (a)  $\gamma = 0^\circ$ , and (b)  $\gamma = 40^\circ$

For each case shown in Figure 6.3 (a) and (b), the optimization was performed fixing the variable  $\theta_s = 0$ . For case (a), the optimizer reported the optimal solution of  $\theta_o = -0.2$  deg and  $\theta_c = 0$  deg for a maximum value of  $C_p = 0.343$ . For case (b) optimal solution found was  $\theta_s = -6.2$  deg and  $\theta_c = -6.4$  for a maximum value of  $C_p = 0.209$ . Figure 6.4 shows a two dimensional plot of the power coefficient as a function of (a)  $\theta_o$  and (b)  $\theta_c$  for the test case shown in Figure 6.3(b).



**Figure 6.4**  $C_p$  as a function of (a)  $\theta_o$ , (b)  $\theta_c$  with  $J=5$ ,  $C_D = 0.08$ ,  $\theta_o = 0^\circ$ ,  $\gamma = 40^\circ$

Figure 6.4 is intended to provide some graphical confirmation of a sample test case run to check out the optimization routine. Over 15 cases were evaluated varying collective pitch, and both side to side and fore to aft cyclic pitch with wind speed and yaw angle ( $\gamma$ ), all verifying the optimal solution was found for each grid case. Thus the test cases have shown that for this system being evaluated, the MATLAB optimization tool is sufficient.



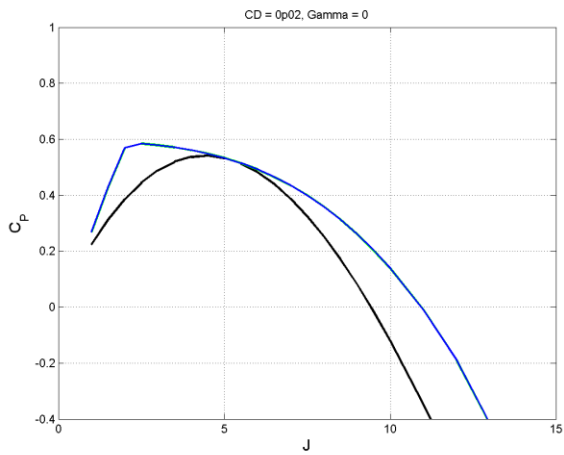
## 6.2 Optimization Results

With the optimization routine chosen and some checkout performed with test cases, the optimization routine was run and data recorded on the optimal power coefficient and corresponding optimal solution (i.e. the optimal  $\theta_O$ ,  $\theta_S$  and  $\theta_C$ ). The results can be evaluated with parameter sweeps of tip speed, yaw angle ( $\gamma$ ) and drag coefficient. As discussed in the introduction, the results section will show a progression of increasing the control space by comparing a fixed pitch case ( $\theta_O = 0$ ), a case where only collective pitch is optimized and a case where both collective and cyclic pitch are optimized.

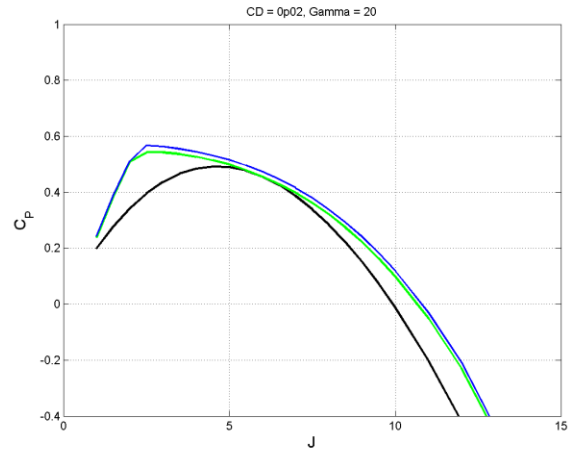
The value of  $\theta_O = 0$  for the fixed theta case was arbitrarily chosen, thus in any condition it may or may not be optimal. For the second case, optimizing the collective pitch only, the same optimization routine discussed in Section 6.1 was used with fixed values of  $\theta_S = 0$  and  $\theta_C = 0$ . Optimizing  $\theta_O$  alone has been studied and proven useful in increasing power output for axial flow with variable wind speeds. Systems that use feedback control to adjust collective pitch to the optimal solution for the real-time wind speed produce more power than conventional systems with a fixed pitch angle. The third case will vary both collective and cyclic pitch without limitation on the magnitude of the optimal solution.

It is not expected that opening up the cyclic pitch control space will help in axial flow, but rather in yawed flow. The theoretical hypothesis is that the power coefficient will be improved by maintaining a smooth, balanced flow of air across the disk plane. The results should answer the question of whether cyclic pitch can improve the smoothness of flow (fewer gradients) through the disk in yawed flow.

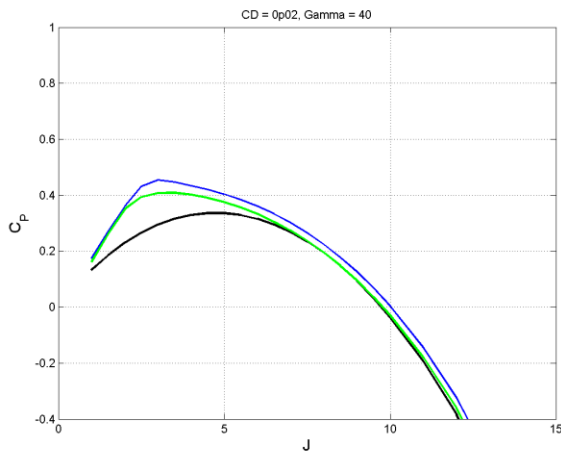
Figures 6.5 – 6.7 shows the optimal power coefficient as a function of tip speed for drag coefficients of 0.02, 0.04 and 0.08 respectively. The black line is the fixed theta case, the green line shows the results for collective pitch optimization and the blue line shows the results for both collective and cyclic pitch optimization.



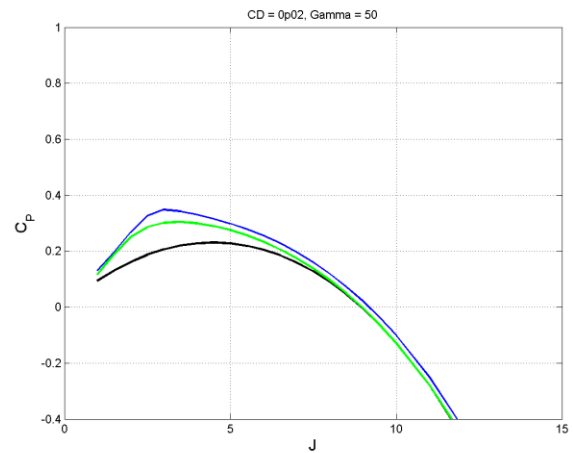
(a)



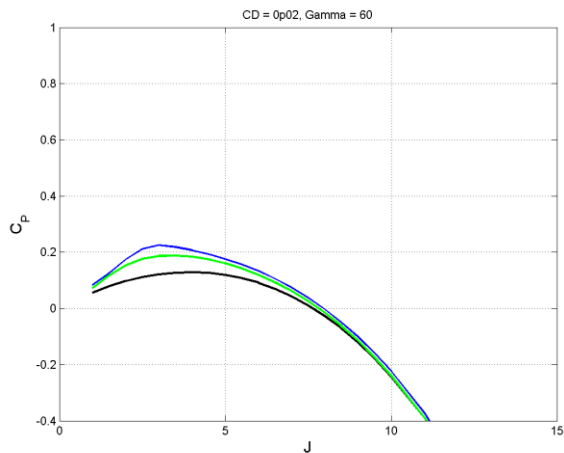
(b)



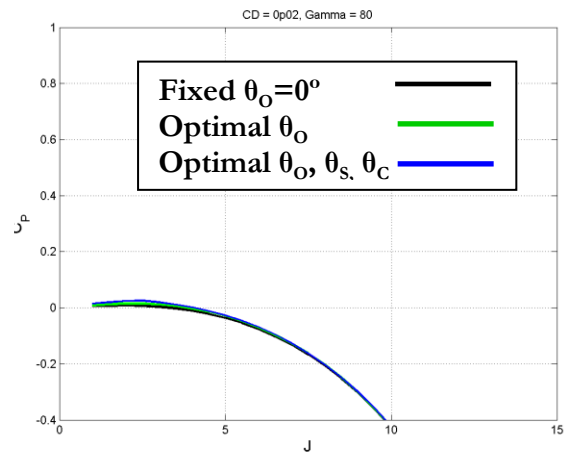
(c)



(d)



(e)



(f)

**Figure 6.5 Optimal CP as a function of tip speed, J, for  $C_D = 0.02$ , and (a)  $\gamma = 0^\circ$ , (b)  $\gamma = 20^\circ$ , (c)  $\gamma = 40^\circ$ , (d)  $\gamma = 50^\circ$ , (e)  $\gamma = 60^\circ$ , (f)  $\gamma = 80^\circ$**

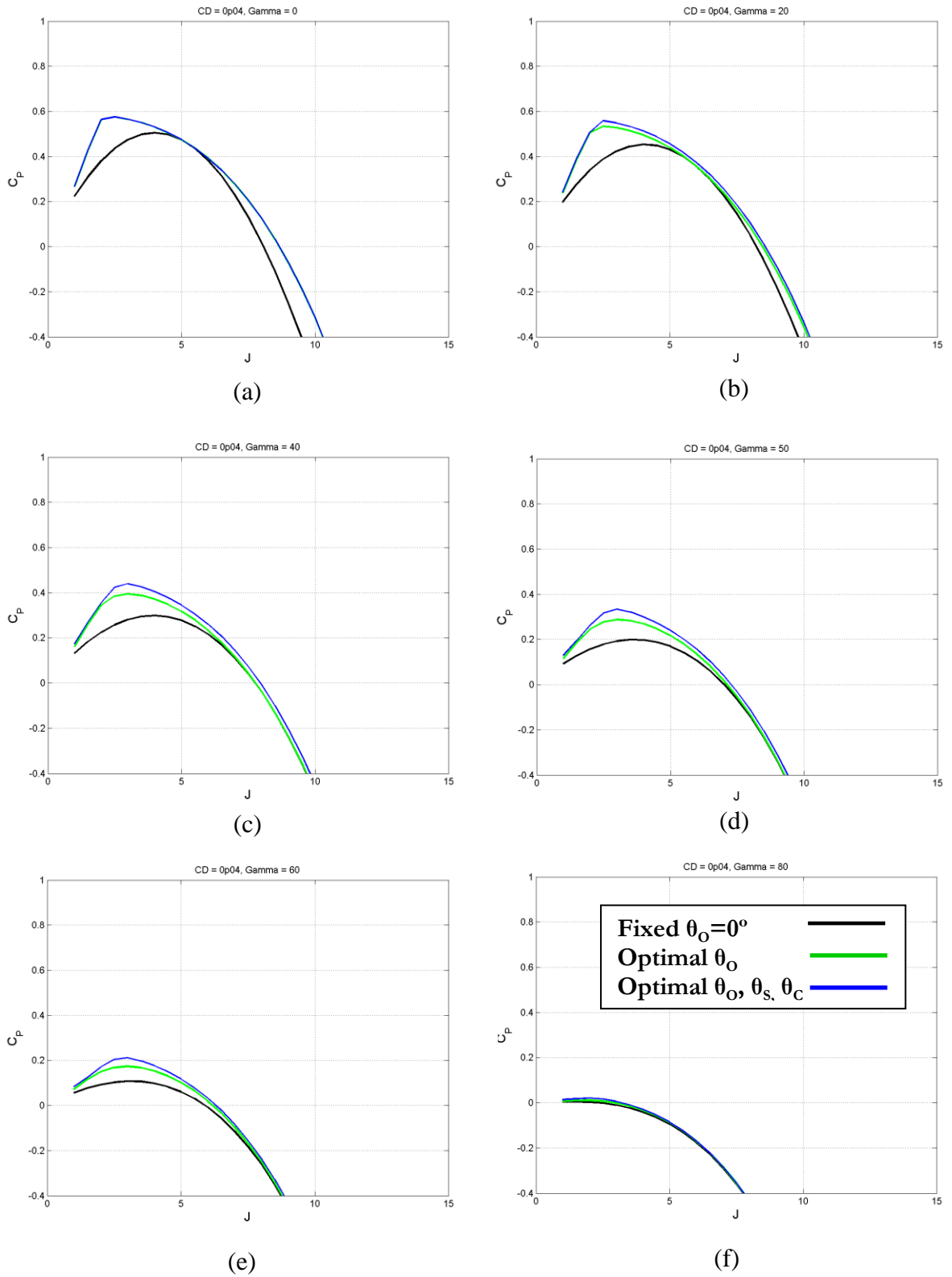


**Figure 6.6 Optimal  $C_P$  as a function of tip speed,  $J$ , for  $C_D = 0.04$ , and (a)  $\gamma = 0^\circ$ , (b)  $\gamma = 20^\circ$ , (c)  $\gamma = 40^\circ$ , (d)  $\gamma = 50^\circ$ , (e)  $\gamma = 60^\circ$ , (f)  $\gamma = 80^\circ$**

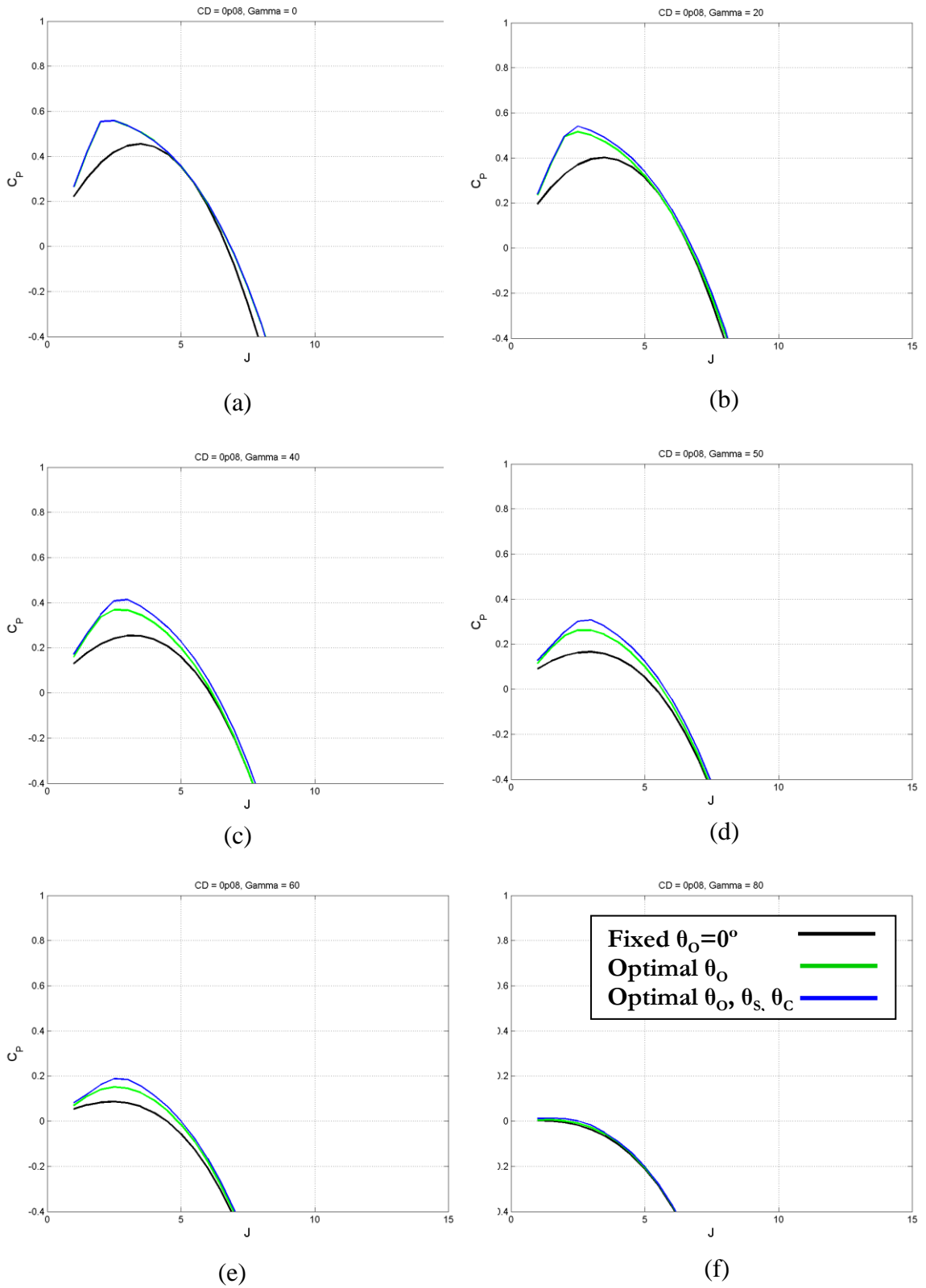


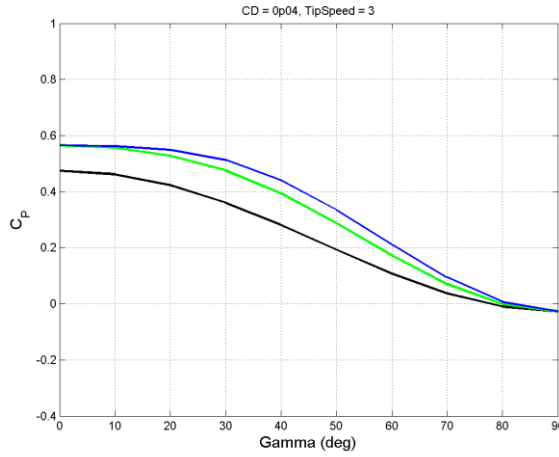
**Figure 6.7** Optimal  $C_P$  as a function of tip speed,  $J$ , for  $C_D = 0.08$ , and  
 (a)  $\gamma = 0^\circ$ , (b)  $\gamma = 20^\circ$ , (c)  $\gamma = 40^\circ$ , (d)  $\gamma = 50^\circ$ , (e)  $\gamma = 60^\circ$ , (f)  $\gamma = 80^\circ$

The results indicate that inclusion of the cyclic pitch terms in the optimization routine does result in an increased optimal power coefficient. Figures 6.5 – 6.7(a) show the expected results for axial flow in which the optimization results match for varying collective only and varying all control terms. Figures 6.5 – 6.7 (f) show that as the yaw angle increases to a near perpendicular orientation to the wind, that the optimal power coefficient decreases to zero and no increase in control space can help in that condition.

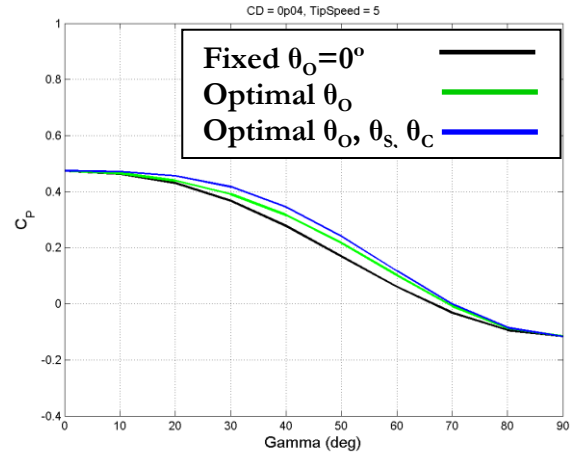
In Figures 6.5 – 6.7 plots (b) through (e) show the relative improvement in the optimal power coefficient for varying degrees of yaw angle. The increase in the optimal power coefficient due to the implementation of cyclic pitch peaks at around a 15-20 % improvement over collective pitch alone. The relative improvements for using cyclic pitch diminish for low tip speeds (less than 3), when the RPM is small relative to the wind.

It should be noted that the relative improvement of using optimal control values is significant in both magnitude and domain compared to the fixed theta case. Peak improvements in the optimal power coefficient for the collective only or cyclic and collective cases, double the value compared to the fixed pitch case. In terms of domain, improvements can be observed for a wider variety of both tip speeds and yaw angles with respect to the wind. So the improvements are observed not only seen in peak performance conditions, but in much wider variety of operating conditions.

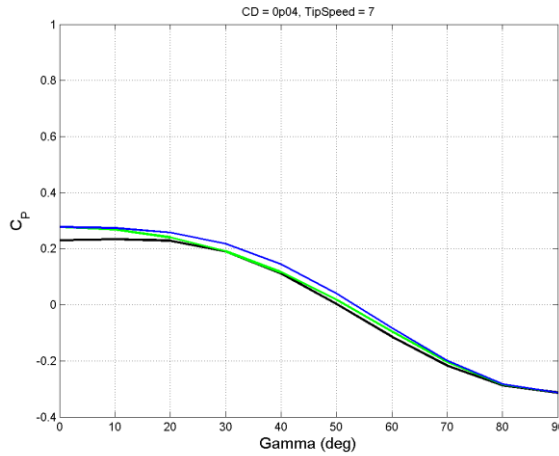
Figure 6.8 shows the optimal power coefficient as a function of yaw angle ( $\gamma$ ) for various tip speeds for a drag coefficient of 0.04. Figure 6.9 shows the optimal power coefficient as a function of yaw angle ( $\gamma$ ) for various tip speeds for a drag coefficient of 0.08.



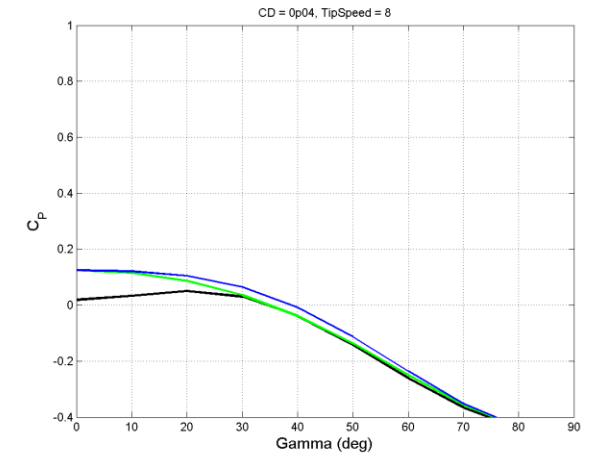
(a)



(b)



(c)



(d)

**Figure 6.8 Optimal CP as a function of Yaw Angle,  $\gamma$ , for  $C_D = 0.04$ , and (a)  $J = 3$ , (b)  $J = 5$ , (c)  $J = 7$  and (d)  $J = 8$**

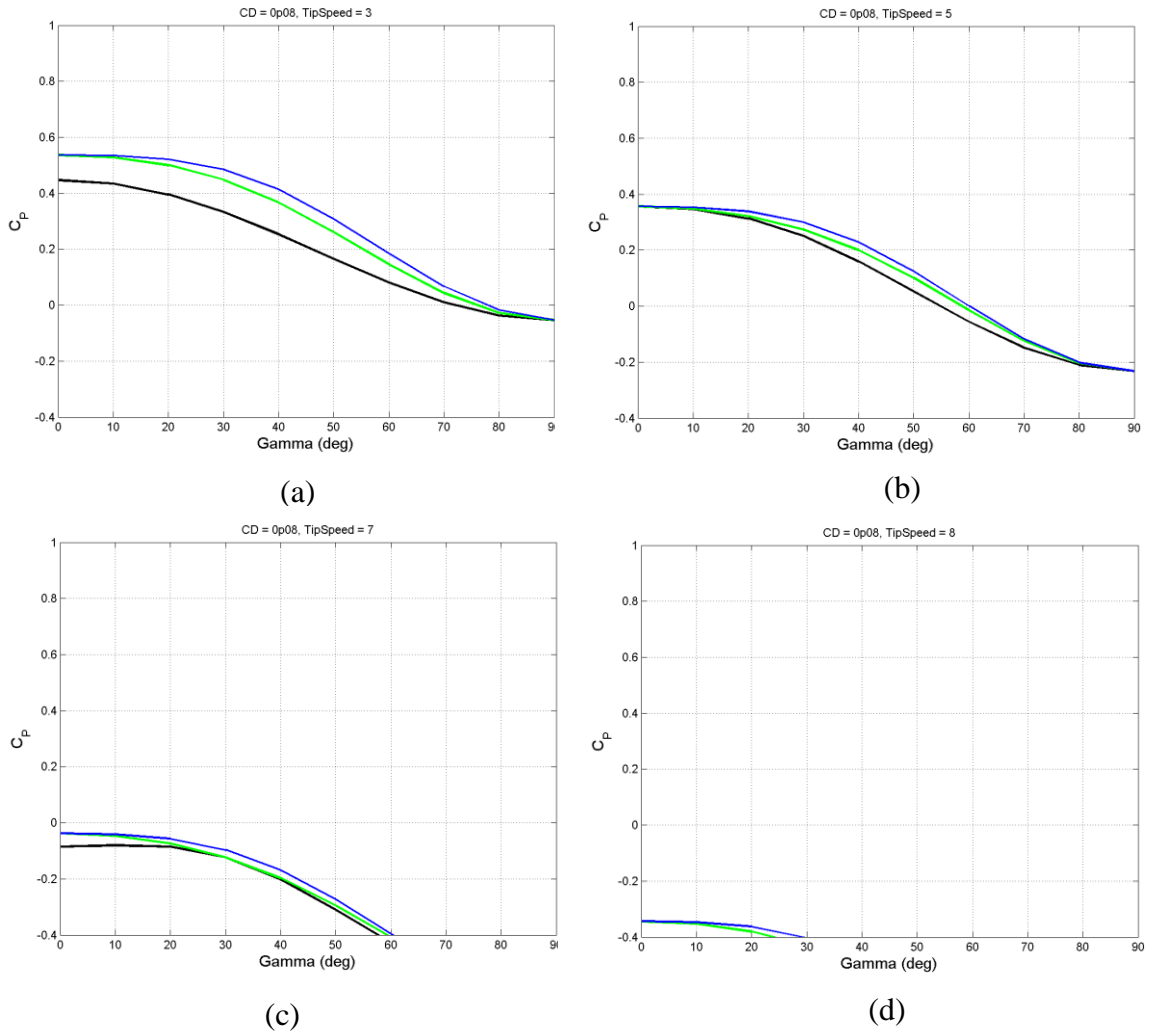


**Figure 6.9 Optimal CP as a function of Yaw Angle,  $\gamma$ , for  $C_D = 0.08$ , and (a)  $J = 3$ , (b)  $J = 5$ , (c)  $J = 7$  and (d)  $J = 8$**

Figures 6.8 and 6.9 show the relative improvements in the power coefficient as a function of yaw angle. Improvements in the optimal value of the power coefficient are observed for nearly all yaw angles and tip speeds over the fixed pitch case. The improvements are more pronounced between the tip speed range of 3-6. The optimization of the collective pitch alone does increase the power coefficient in yawed flow, however the data also shows using cyclic pitch extends the improvements over a wide range of yawed wind conditions.

In addition to the trends of the optimal power coefficient it is insightful to review the data trends for the optimal solutions as well, namely the optimal values for  $\theta_O$ ,  $\theta_S$  and  $\theta_C$ . Figures 6.10 – 6.13 show the optimal values computed as a function of tip speed for yaw angles of 0, 20, 40 and 60 degrees respectively.

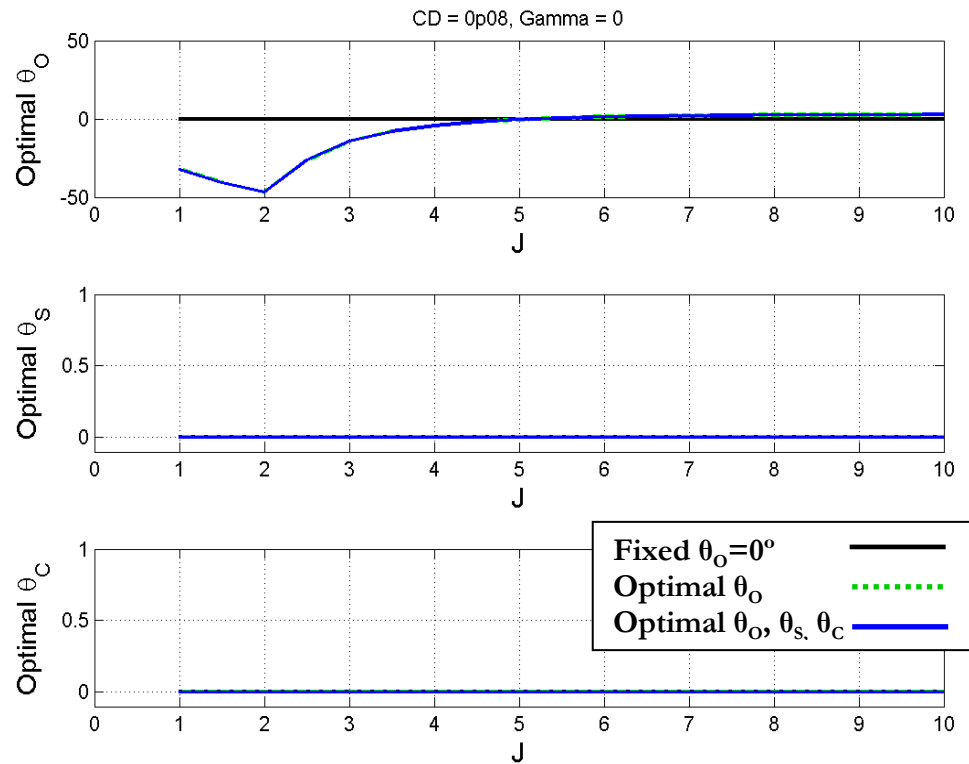


Figure 6.10 Optimal Values as a function of tip speed, J, for  $C_D = 0.08$ , and  $\gamma = 0^\circ$



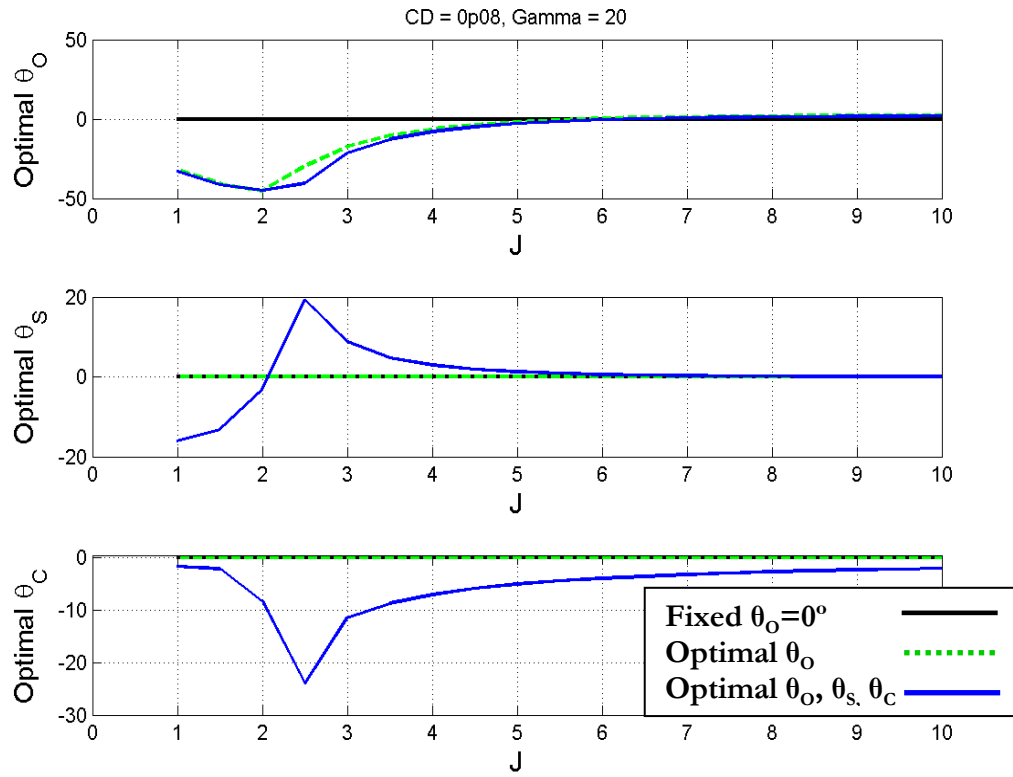


Figure 6.11 Optimal Values as a function of tip speed,  $J$ , for  $C_D = 0.08$ , and  $\gamma = 20^\circ$

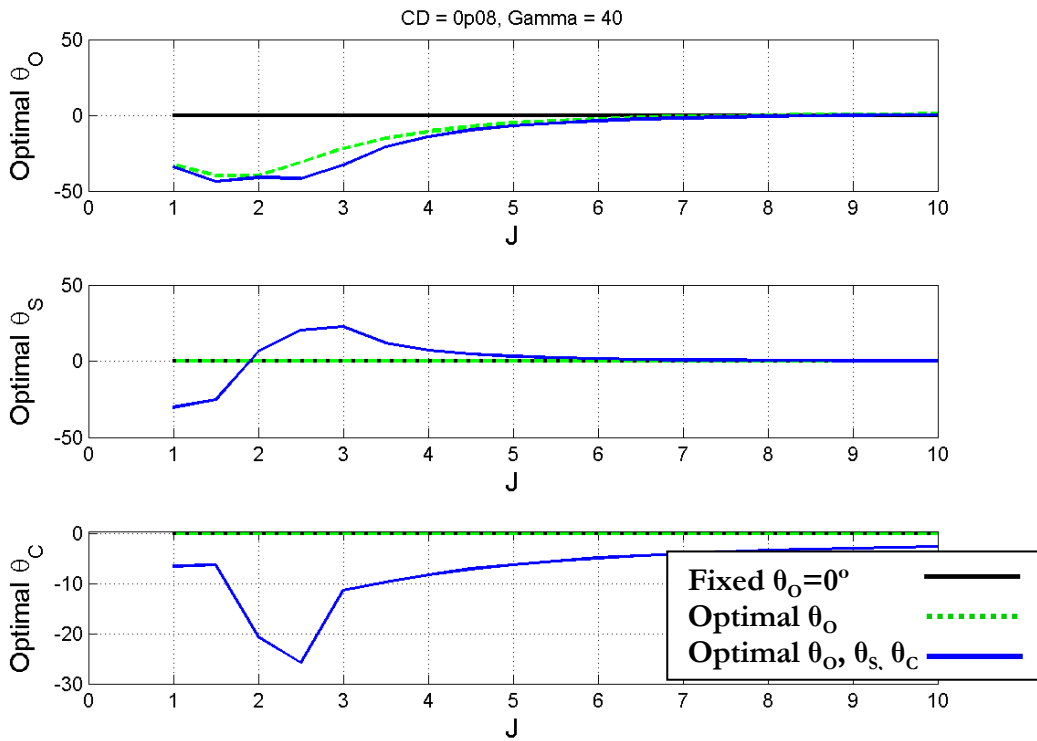
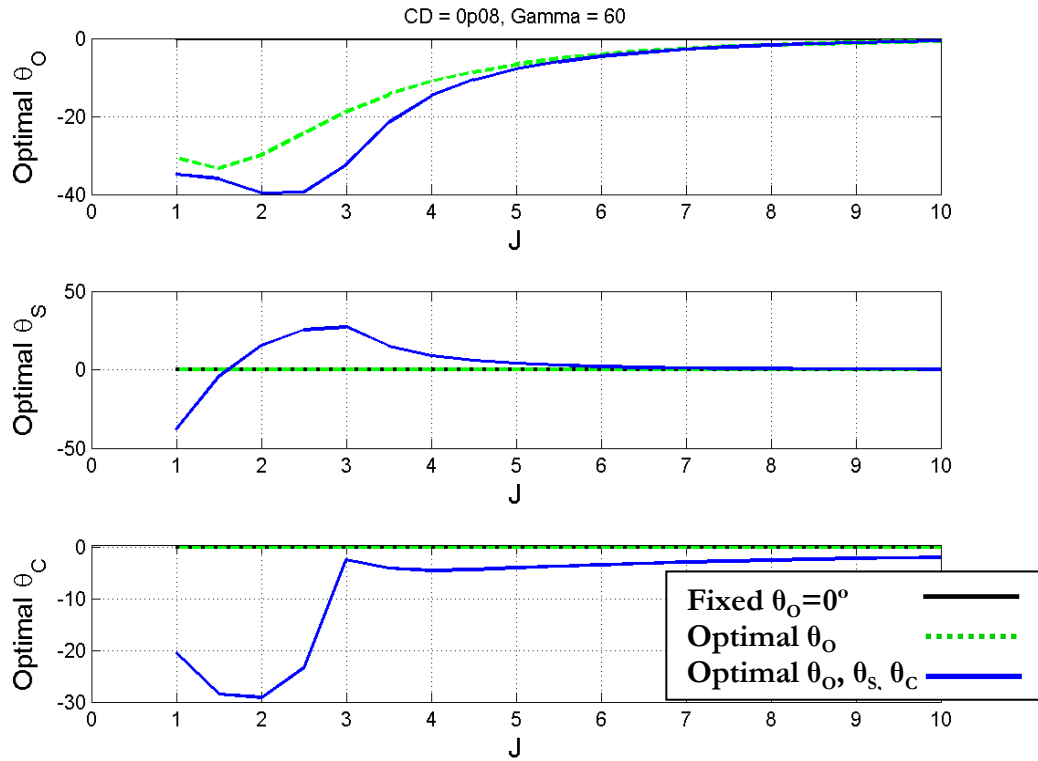


Figure 6.12 Optimal Values as a function of tip speed,  $J$ , for  $C_D = 0.08$ , and  $\gamma = 40^\circ$



**Figure 6.13** Optimal Values as a function of tip speed,  $J$ , for  $C_D = 0.08$ , and  $\gamma = 60^\circ$

Figure 6.10 shows again that for axial flow, the optimal values match for the collective only case and collective with cyclic pitch case. Figures 6.11 – 6.13 show the results for yawed flow and as expected, the optimal values of all control terms vary when both collective with cyclic pitch are part of the control space. The collective pitch tends to decrease (to a greater negative value) with small tip speed. The optimal value for the cyclic pitch terms  $\theta_S$  and  $\theta_C$  actively change with tip speed.

It is important to remember that, for this unconstrained optimization problem, the cost function seeks only to optimize the power coefficient (that is to minimize negative  $C_P$ ). There are no additional limitations put on a realistic value for theta or a design goal of having small moments. The side to side cyclic pitch term  $\theta_S$  tends to peak on the positive side at a tip speed of about 3, which corresponds with the peak of the power coefficient when plotted with tip speed for this case. As the tip speed decreases from 3 to 0,  $\theta_S$  decreases until it becomes negative. As for  $\theta_C$ , the optimal results for this model indicate that it will remain negative. The optimal values obviously

vary more at tip speeds of 5 and smaller as the power coefficient is changing rapidly in this tip speed range.

It should be noted that for this unconstrained case, the magnitude of the control terms has increased to a point where it is likely they would encounter stall. As the pitch value increases the corresponding angle of attack will increase and at some large value (depending on the airfoil being analyzed) the linear assumption of lift with angle of attack will break down. In practice additional steps are taken to address stall such as adding twist to the blade. Some preliminary work was done with this model to determine if twist would help reduce the magnitude of the control terms for the unconstrained case. However the dynamic inflow model used, the non-linear Pitt Peters model, does not have a radial component so the positive effects of twist would not show up in the results.

The results for this unconstrained case provide a solid starting point for further investigation into improving the optimal power that can be realized in a system by opening the control space. Future work can be done to implement an alternative dynamic inflow model, such as the Generalized Dynamic Wake Model, to evaluate if twist can reduce the magnitude of the optimal values and preserve the improvements of the power coefficient.

# Chapter 7

## Results for Optimal Power Coefficient in Trimmed State

The previous chapter showed that opening a wind turbine's control space does indeed improve the achievable power coefficient for a system by increasing the control space. For some boundary conditions then, such as a fixed tower, it may be useful to use cyclic pitch to improve power output, especially with varying wind direction. As posited by Hohenemser, another possible use for cyclic pitch is to control the yaw angle by controlling the moments of the system and using them to trim at a specific attitude relative to the wind. The intent of selecting a specific yaw angle is to keep the induced flow through the disk within a desired design range that works best for the turbines rotor capacity. Too little induced velocity results in low power, too high can result in hardware damage.

A broader study on this problem would require a validated plant in a real-time simulation with feedback control, which is one of the long-term development goals of WT\_3DOF. In the near term, it is useful to know what happens to the optimal power curves when the blades are also being used to trim the system. For any desired state (RPM, yaw angle relative to the wind), the collective and cyclic pitch settings will be required to drive the pitch and roll moments to zero. This will compete with the settings which could result a larger power coefficient. This chapter will add to the progression in chapter 6 by adding a case where the power coefficient is being optimized, varying collective and cyclic pitch but with an additional constraint – the optimal solution should also have small pitch and roll moments.

## 7.1 Optimization Set up and Check out

This optimization problem will again take the general form of:

$$\begin{aligned} & \text{minimize } f_0(x) \\ & \text{subject to } f_i(x) \leq b_i, i = 1, 2, \dots, m \end{aligned} \tag{7.1}$$

where  $x = (\theta_o, \theta_s, \theta_c)$ ,  $f_0$  is the objective function to be minimized and  $f_i$  is the constraint function with boundaries  $b_i$ . To gain understanding of what the optimal values and power coefficient are for various conditions when the system is in a pseudo-trimmed state, the objective function can be modified to minimize the pitch and roll moments. The objective function to be minimized is:

$$f_0(x) = -C_p + k*(M^2+L^2) \tag{7.2}$$

where  $C_p$  is the power coefficient,  $M$  is the system pitch moment,  $L$  is the system roll moment and  $k$  is a scale factor to adjust the weight of the moment minimization. For this study there again will be no constraints on the system such as pitch magnitude limits or assumptions of dynamic stall. It is at this point an investigation into what design space exists in an idealized case.

It would be helpful—before starting any optimization—to see how the second term  $(M^2+L^2)$  changes with the variables  $\theta_o$ ,  $\theta_s$  and  $\theta_c$ . To do this, the scalar  $k$  is defined as  $k = 1$  just to gain an appreciation of how this term in the objective cost function behaves and the term will be plotted. Figure 7.1-7.3 shows a plot of this term that squares the moments as a function of the control terms  $\theta_o$ ,  $\theta_s$  and  $\theta_c$ .

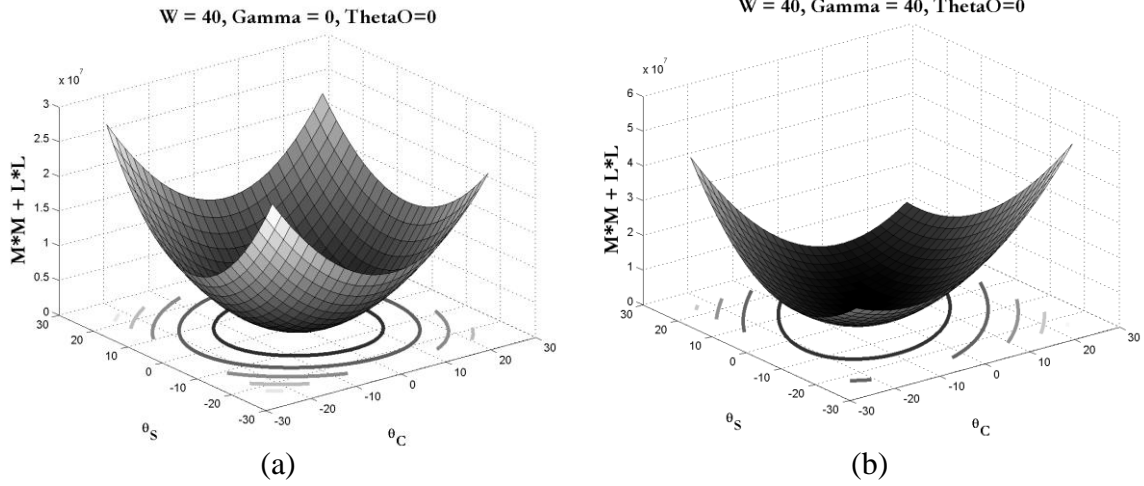


Figure 7.1  $M^2+L^2$  as a function of  $\theta_S, \theta_C$ , for  $J=3, C_D = 0.08, \theta_O = 0^\circ$  and (a)  $\gamma = 0^\circ$  and (b)  $\gamma = 40^\circ$

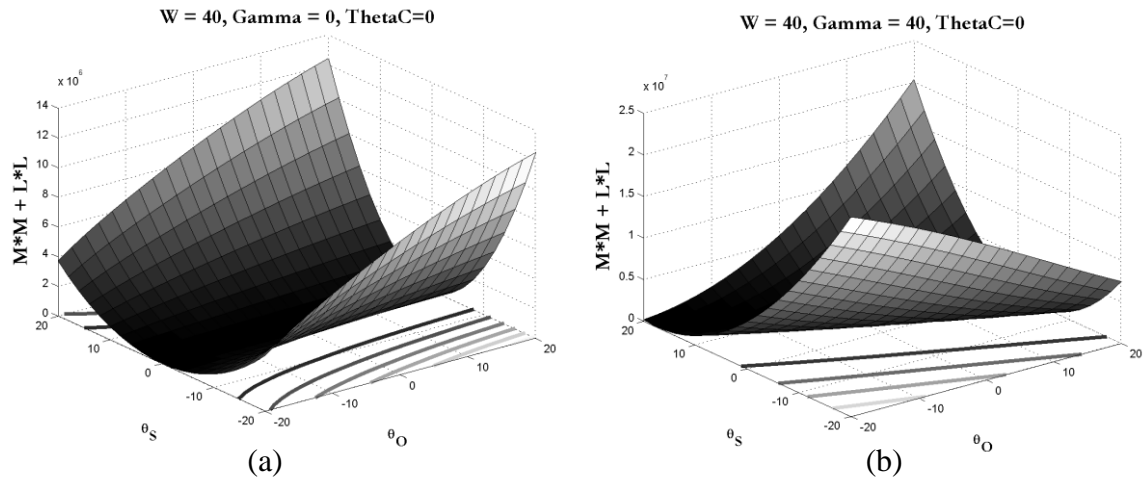


Figure 7.2  $M^2+L^2$  as a function of  $\theta_S, \theta_O$ , for  $J=3, C_D = 0.08, \theta_C = 0^\circ$  and (a)  $\gamma = 0^\circ$  and (b)  $\gamma = 40^\circ$

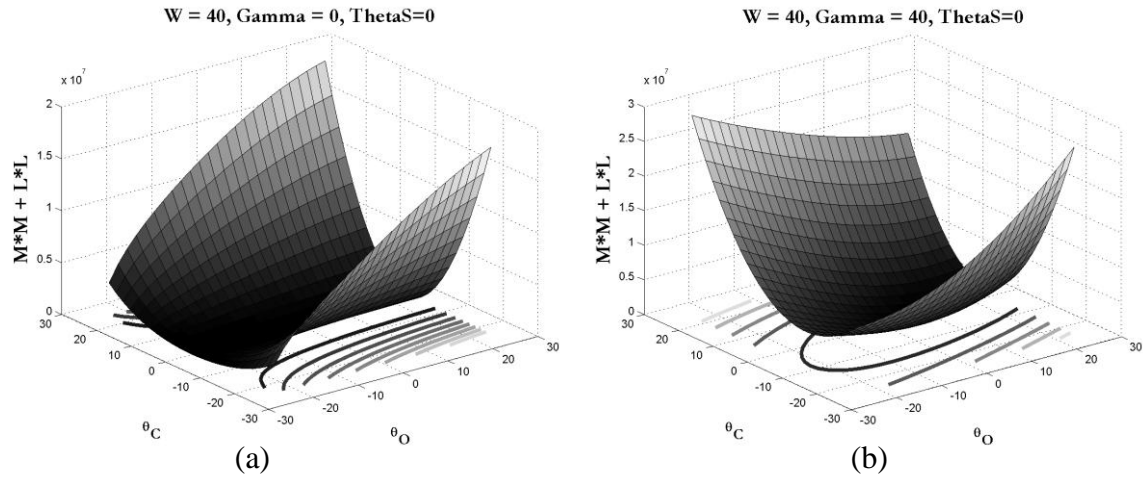
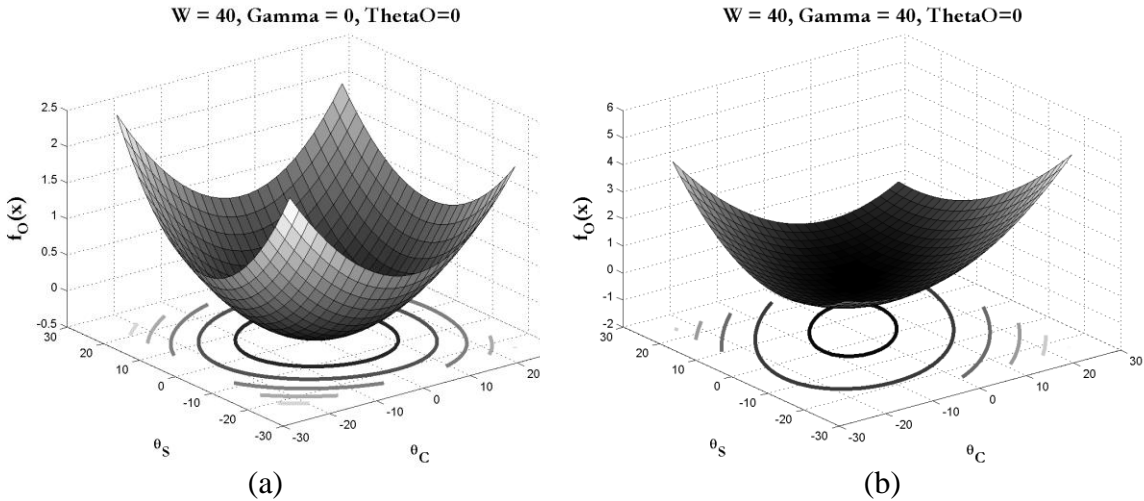


Figure 7.3  $M^2+L^2$  as a function of  $\theta_O, \theta_C$ , for  $J=3, C_D = 0.08, \theta_S = 0^\circ$  and (a)  $\gamma = 0^\circ$  and (b)  $\gamma = 40^\circ$

It is observed that the square of the moments changes smoothly as the control terms are varied. Just as in Chapter 6, this moment term in the objective function is well suited to the gradient search type optimization.

The value of  $k$  is a design choice that will have some bearing on the results. A very large value for  $k$  will reduce the importance of the power coefficient while a value of 0 would result in the chapter 6 results. A small trade study was performed to choose an appropriate value. The design goal was to keep the weighting of  $k$  as small as possible (while not being zero) and keep all the moments less than 1-2% of the system thrust times rotor radius. Reviewing Figures 7.1-7.3 shows that the pitch moment squared plus the roll moment squared can increase to a magnitude of  $10^7$  within the analysis domain. Thus a weight of  $1e-7$  would scale the moment terms to be close enough to the scale of the power coefficient. Figure 7.4 shows the objective function defined in equation 7.2 with  $k = 1e-7$ .



**Figure 7.4**  $f_0(x)$  as a function of  $\theta_s, \theta_c$ , with  $k=1e-7$ , for  $J=3, C_D = 0.08, \theta_0 = 0^\circ$  and (a)  $\gamma = 0^\circ$  and (b)  $\gamma = 40^\circ$

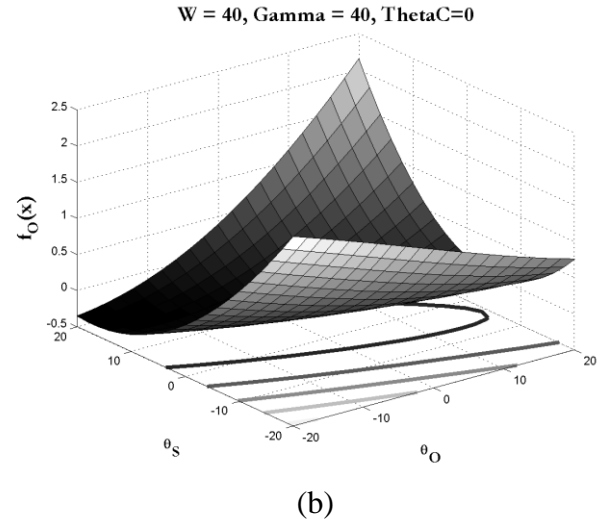
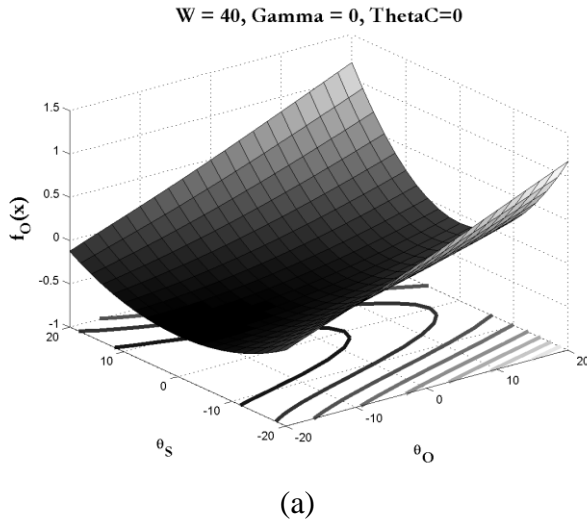


**Figure 7.5**  $f_O(x)$  as a function of  $\theta_O, \theta_S$ , with  $k=1e-7$ , for  $J=3, C_D = 0.08, \theta_C = 0^\circ$  and (a)  $\gamma = 0^\circ$  and (b)  $\gamma = 40^\circ$

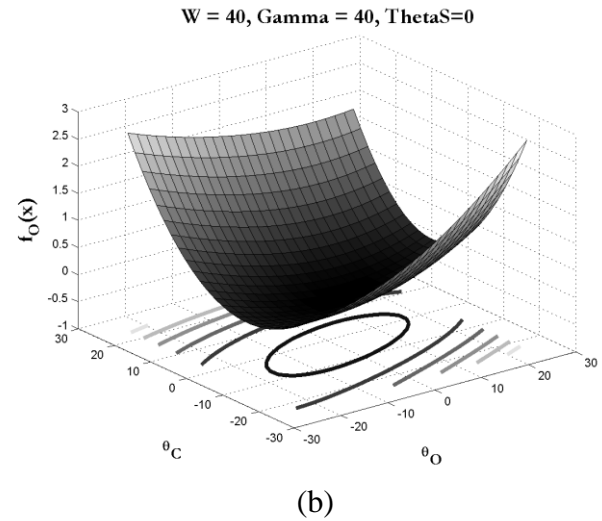
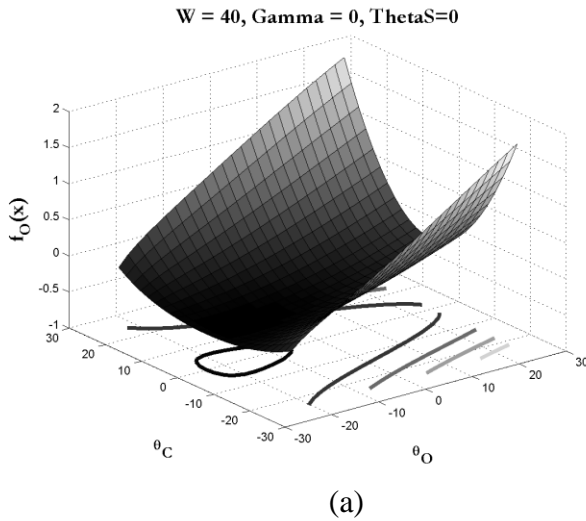


**Figure 7.6**  $f_O(x)$  as a function of  $\theta_O, \theta_C$ , with  $k=1e-7$ , for  $J=3, C_D = 0.08, \theta_S = 0^\circ$  and (a)  $\gamma = 0^\circ$  and (b)  $\gamma = 40^\circ$

This objective function will be satisfactory for this feasibility study as the objective function changes smoothly, appears suitable to find a global minimum with a gradient search technique and it puts the power coefficient and the magnitude of the moment terms on approximately the same scale.

Before running the optimization routine over the entire domain, some test cases were run to verify that the optimization routine did successfully find the optimal solution for the new objective function defined in equation 7.2. The routine ran for 15



or more test grid cases such as those plotted in Figures 7.4 – 7.6 and results compared well with the graphical plots upon inspection. For example the results for Figure 7.4 were (a)  $\theta_s = 0^\circ$  and  $\theta_c = 0^\circ$ , (b)  $\theta_s = 5.1^\circ$  and  $\theta_c = -0.3^\circ$ . The results for Figure 7.6 were (a)  $\theta_o = -14^\circ$  and  $\theta_c = 0^\circ$ , (b)  $\theta_o = 0.4^\circ$  and  $\theta_c = -2.3^\circ$ . In both cases, the resultant moments verified to be less than 1% of the system thrust times rotor radius. Test cases such as this indicate that the optimization routine is working as intended.

The final concern is that the scale factor  $k=1e-7$  may not successfully reduce the resultant moments of the system sufficiently across the entire domain. Using data from Chapter 6 a “worst case” example was chosen for having large moments and analyzed for several values of  $k$ . A sample worst case chosen was for a drag coefficient of 0.08, tip speed of 8 and a yaw angle of 40 degrees. Figure 7.7 shows a plot of the moment design criteria as a function of  $\log_{10}(k)$ .

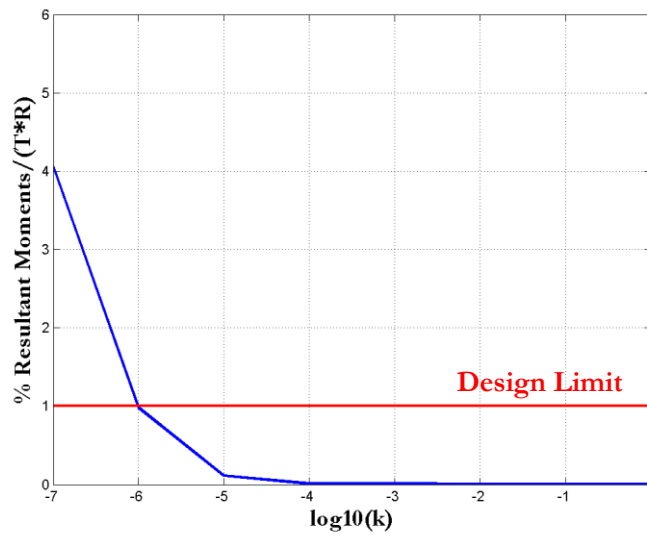


**Figure 7.7 Moment design criteria as a function of  $\log_{10}(k)$  for  $J=8$ ,  $C_D = 0.08$ ,  $\gamma = 40^\circ$**

Again the design criteria, keeping the resultant moments less than  $\sim 1\%$  of the system thrust times rotor radius, is shown in red on Figure 7.7. While the value  $k=1e-7$  generally will reduce the moments below the design criteria across the domain, there do exist some worst cases that will require a larger value of  $k$  and a greater weigh on the moments in the objective function. Thus the analysis steps taken are to run the optimization with  $k = 1e-7$ , and if the moments violate the design criteria, to change  $k$  to  $1e-5$  and re run that test point to find the optimal values. Note this constraint is only

placed on the case where both collective and cyclic pitch terms are variables for optimization. Collective pitch alone is not able to meet the defined design criteria.

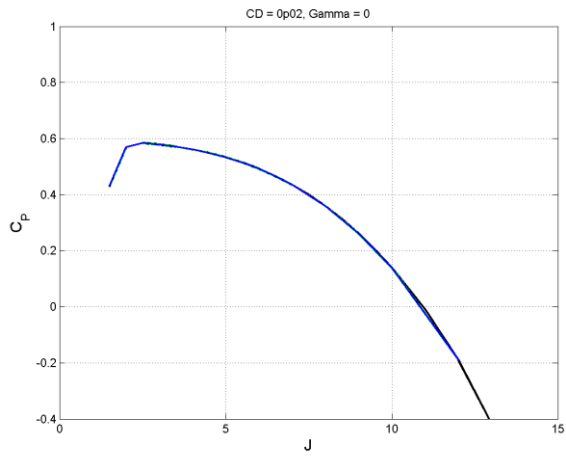
## 7.2 Optimization Results

With the checkout complete, the optimization routine as formed in Section 7.1 was run and data recorded on the optimal power coefficient and corresponding optimal solution (i.e. the optimal  $\theta_o$ ,  $\theta_s$  and  $\theta_c$ ). The results are evaluated here with parameter sweeps of tip speed and yaw angle ( $\gamma$ ). The optimal value for the control terms will be reviewed with tip speed as well.

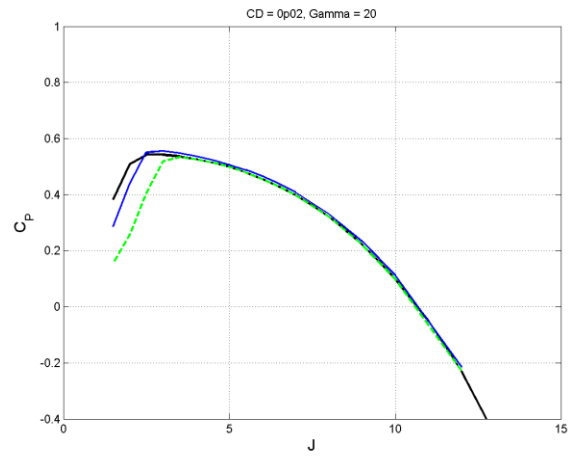
The plots in this section show a progression of three curves to observe the impact of first imposing the moment constraint, then the change that occurs when the full control space is available. The three curves represent: (1) the chapter 6 results that optimize the power coefficient only for the case where only collective pitch is a variable, (2) the optimal results where only collective pitch is a variable but using the objective function in this chapter, equation 7.2 (minimizing the negative power coefficient and moments) and (3) the optimal results using equation 7.2 but with collective and cyclic pitch as variables.

The rationale for starting with the collective only case is that varying collective pitch to improve power output is already an established practice in industry and provides a reasonable benchmark for the results. As a stepping stone to the final result, the collective only case is recomputed using the new objective function 7.2, or attempting to put the system in a pseudo-trimmed state. Then the results present what, if any, improvements can be realized by opening up the control space, using collective and cyclic pitch for this new constraint of system trim.

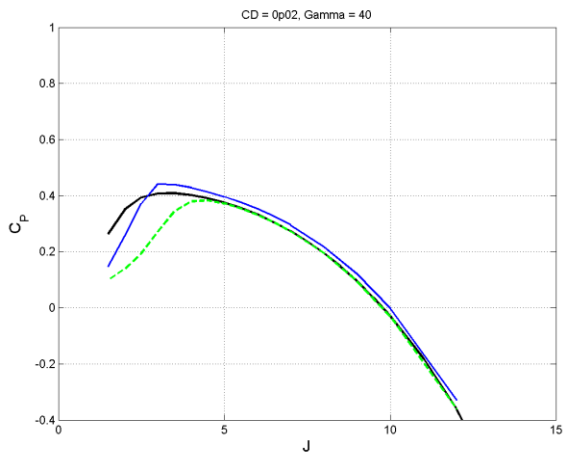
Figures 7.7 – 7.9 show the optimal power coefficient as a function of tip speed for drag coefficients of 0.02, 0.04 and 0.08 respectively. The black line is case 1, when collective pitch is a variable and only  $C_p$  is optimized, the green line shows the results for collective pitch-trim optimization and the blue line shows the results for both collective and cyclic pitch-trim optimization.



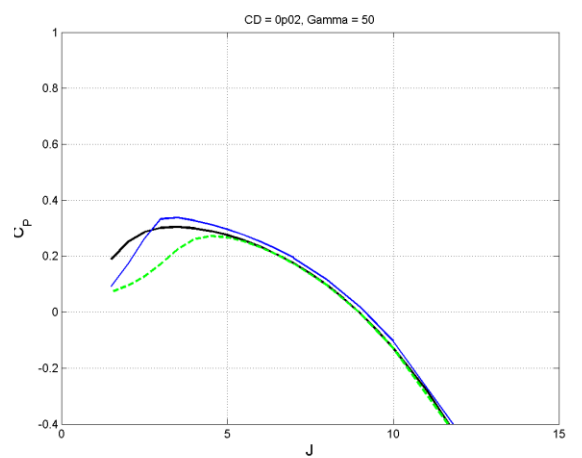
(a)



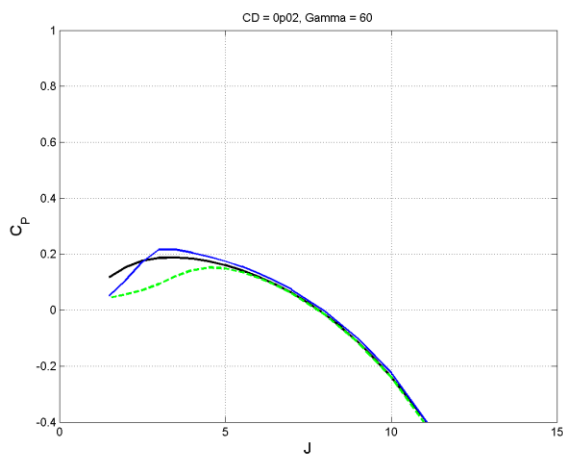
(b)



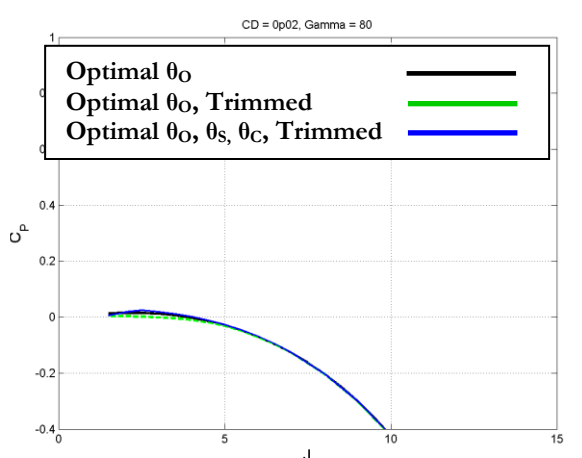
(c)



(d)

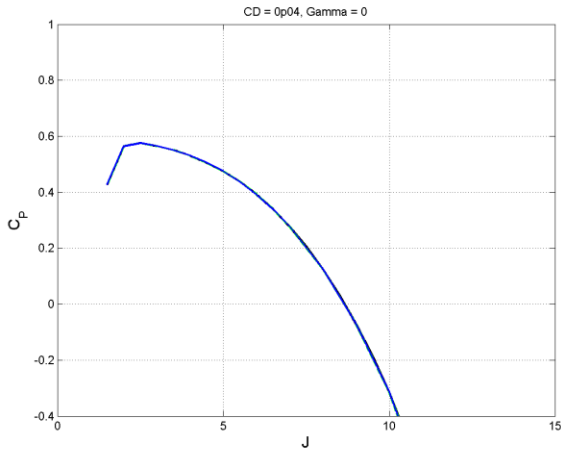


(e)

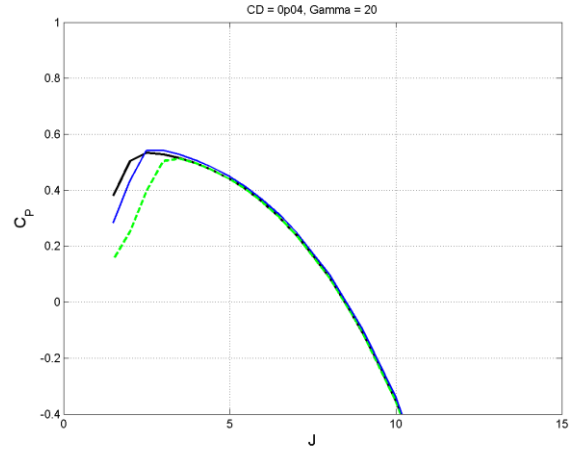


(f)

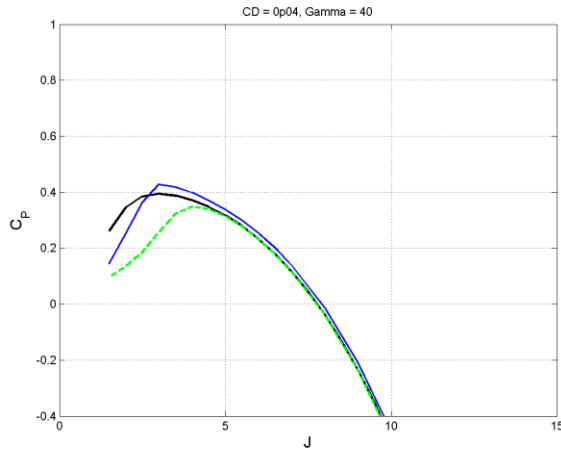
**Figure 7.8 Optimal CP as a function of tip speed, J, for  $C_D = 0.02$ , and (a)  $\gamma = 0^\circ$ , (b)  $\gamma = 20^\circ$ , (c)  $\gamma = 40^\circ$ , (d)  $\gamma = 50^\circ$ , (e)  $\gamma = 60^\circ$ , (f)  $\gamma = 80^\circ$**



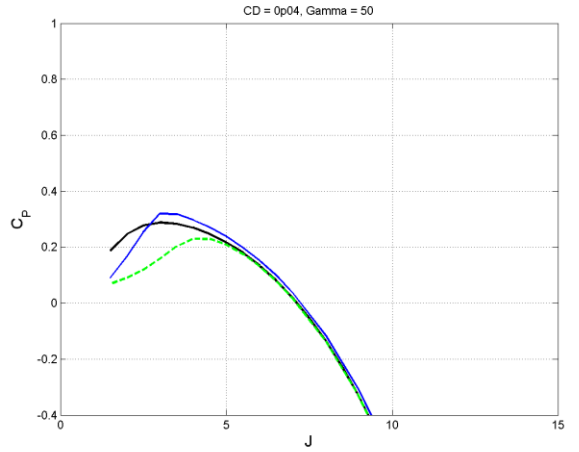
(a)



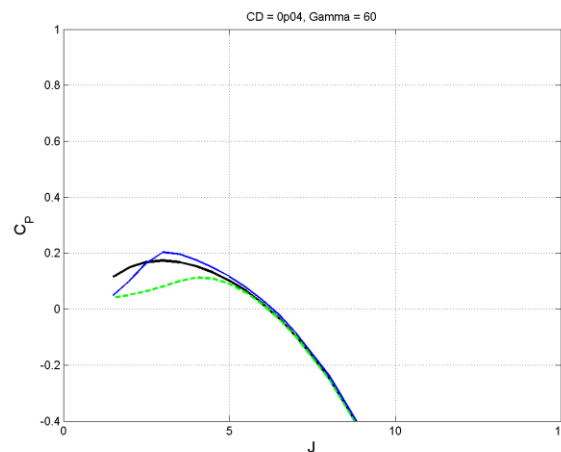
(b)



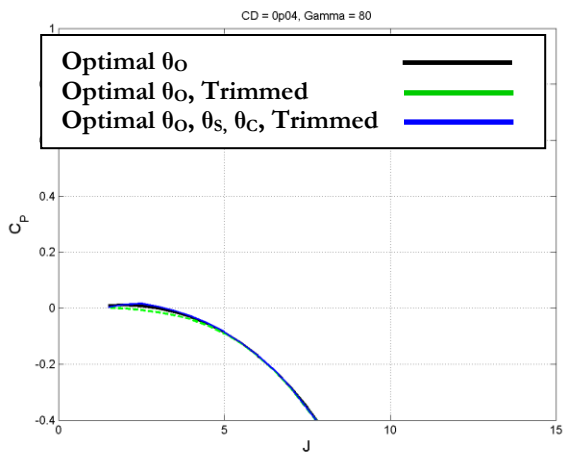
(c)



(d)



(e)



(f)

**Figure 7.9 Optimal CP as a function of tip speed, J, for  $C_D = 0.04$ , and (a)  $\gamma = 0^\circ$ , (b)  $\gamma = 20^\circ$ , (c)  $\gamma = 40^\circ$ , (d)  $\gamma = 50^\circ$ , (e)  $\gamma = 60^\circ$ , (f)  $\gamma = 80^\circ$**

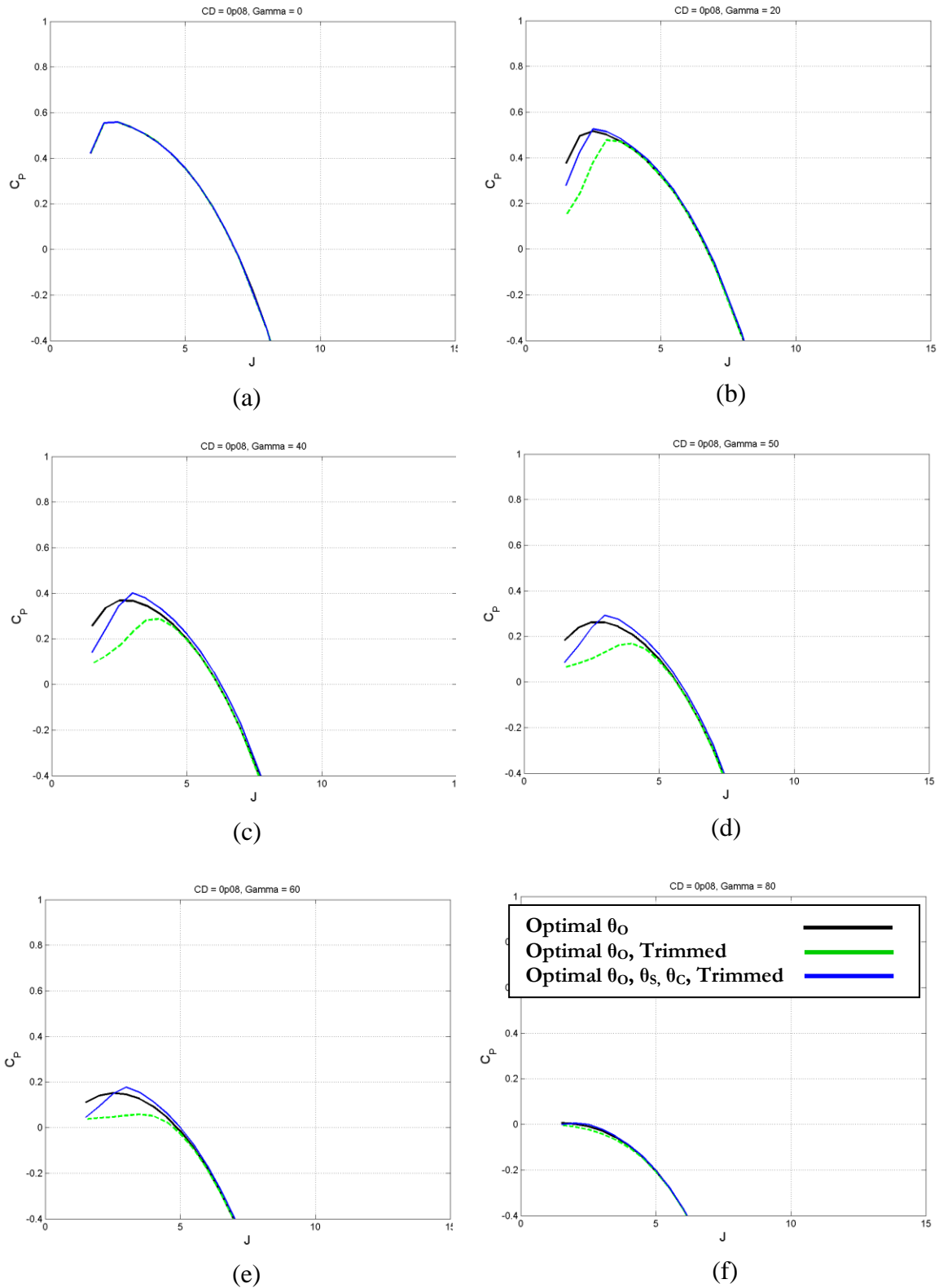


**Figure 7.10** Optimal  $C_P$  as a function of tip speed,  $J$ , for  $C_D = 0.08$ , and  
 (a)  $\gamma = 0^\circ$ , (b)  $\gamma = 20^\circ$ , (c)  $\gamma = 40^\circ$ , (d)  $\gamma = 50^\circ$ , (e)  $\gamma = 60^\circ$ , (f)  $\gamma = 80^\circ$

In Figures 7.8-7.10, plots (a) verify that the solutions are the same in axial flow which is expected as the grid plots show that both the optimal power coefficient and the smallest moments exist for zero cyclic pitch in axial flow. Plots (f) show the point of diminishing return in yawed flow, namely, there is some large yaw angle (in this case  $80^\circ$ ), for which the increased control cannot help increase power output.

Plots (b) – (e) show that, when a system uses cyclic pitch, the turbine can optimize the power coefficient, reduce the system moments and still meet or exceed the peak power coefficient compared to the black line (the notional industry standard). The green line shows the impact of applying the trim constraint, which in some instances is severe. It is observed that the peak power coefficient drops, in some cases, more than 50%. This shows that the design objective of trimming a system can significantly impact the peak power output of a wind turbine. The blue line, optimizing collective and cyclic pitch while meeting the trim constraint, shows that only with the full control space can the system stay trimmed and meet standard expectations for power output.

One of the principal ideas being studied in this research is whether the use of cyclic pitch will enable a system to simultaneously put the turbine at a desired yaw angle with the wind, keep the system trimmed and yield a reasonable power output. Controlling the yaw angle can effectively control the magnitude of flow through the disk and thus keep the system at an optimal tip speed ratio  $J$ . A concern is that in using the blades to trim in yawed flow would significantly compete with the objective of maximizing power output, making the concept infeasible for practice. However these results suggest that it is feasible for a wind turbine to trim at a desired yawed flow angle and achieve nearly the same power coefficient as the notional industry standard, (i.e. optimizing collective pitch with disregard for moment constraints).

It is observed that at low tip speeds (1-2), opening the control space did not result as great of an improvement. In this condition the RPM is very low relative to the wind magnitude, applying the trim constraint degrades the performance more significantly. Besides low tip speeds, the use of cyclic pitch generally increases the power coefficient elsewhere.

Of interest is how the power coefficient changes in yawed flow. Figures 7.11 – 7.12 show the optimal power coefficient as a function of yaw angle ( $\gamma$ ) for a variety of tip speeds and for drag coefficients of 0.04 and 0.08 respectively.

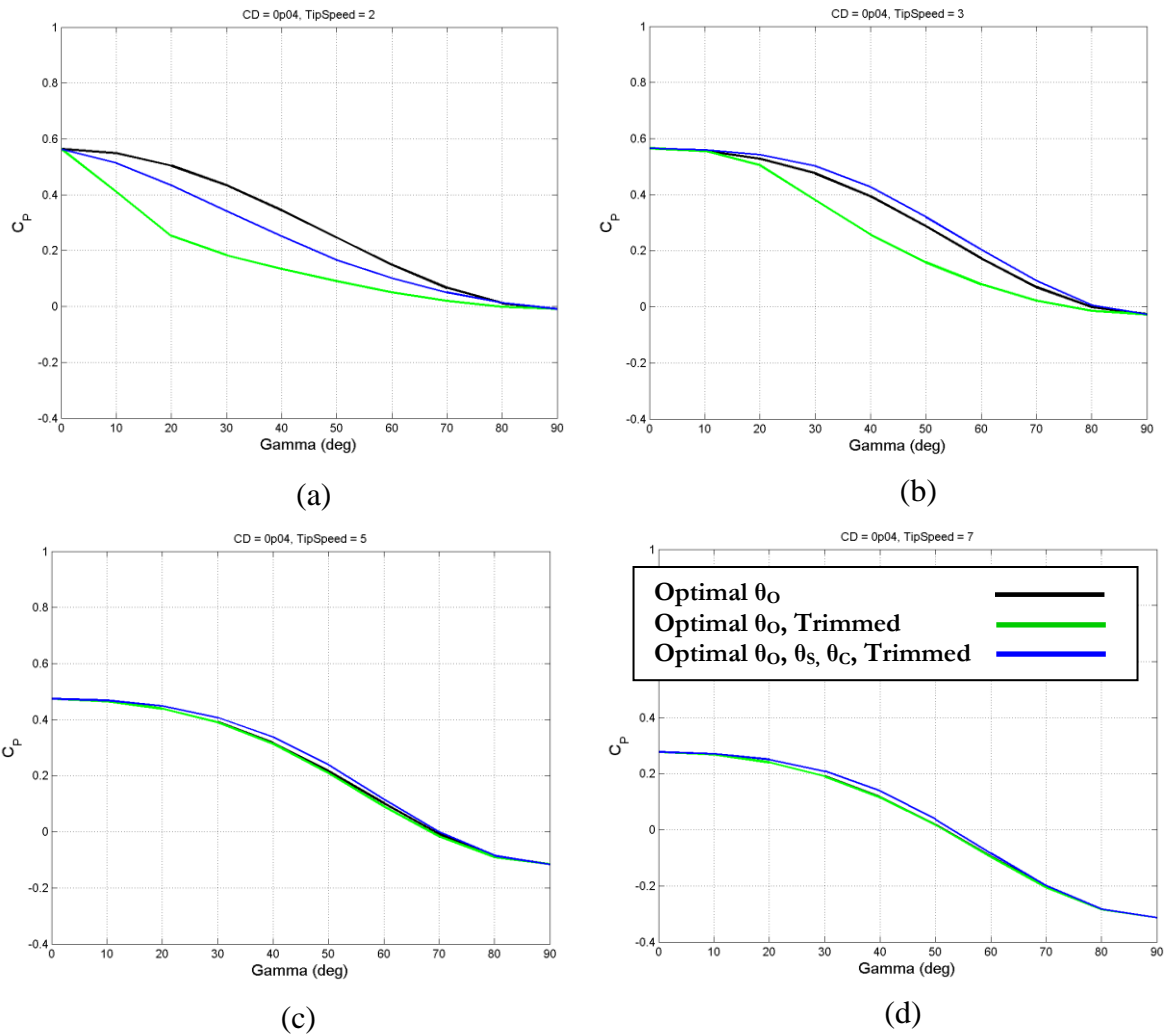


**Figure 7.11** Optimal  $C_P$  as a function of Yaw Angle,  $\gamma$ , for  $C_D = 0.04$ , and (a)  $J = 2$ , (b)  $J = 3$ , (c)  $J = 5$  and (d)  $J = 7$

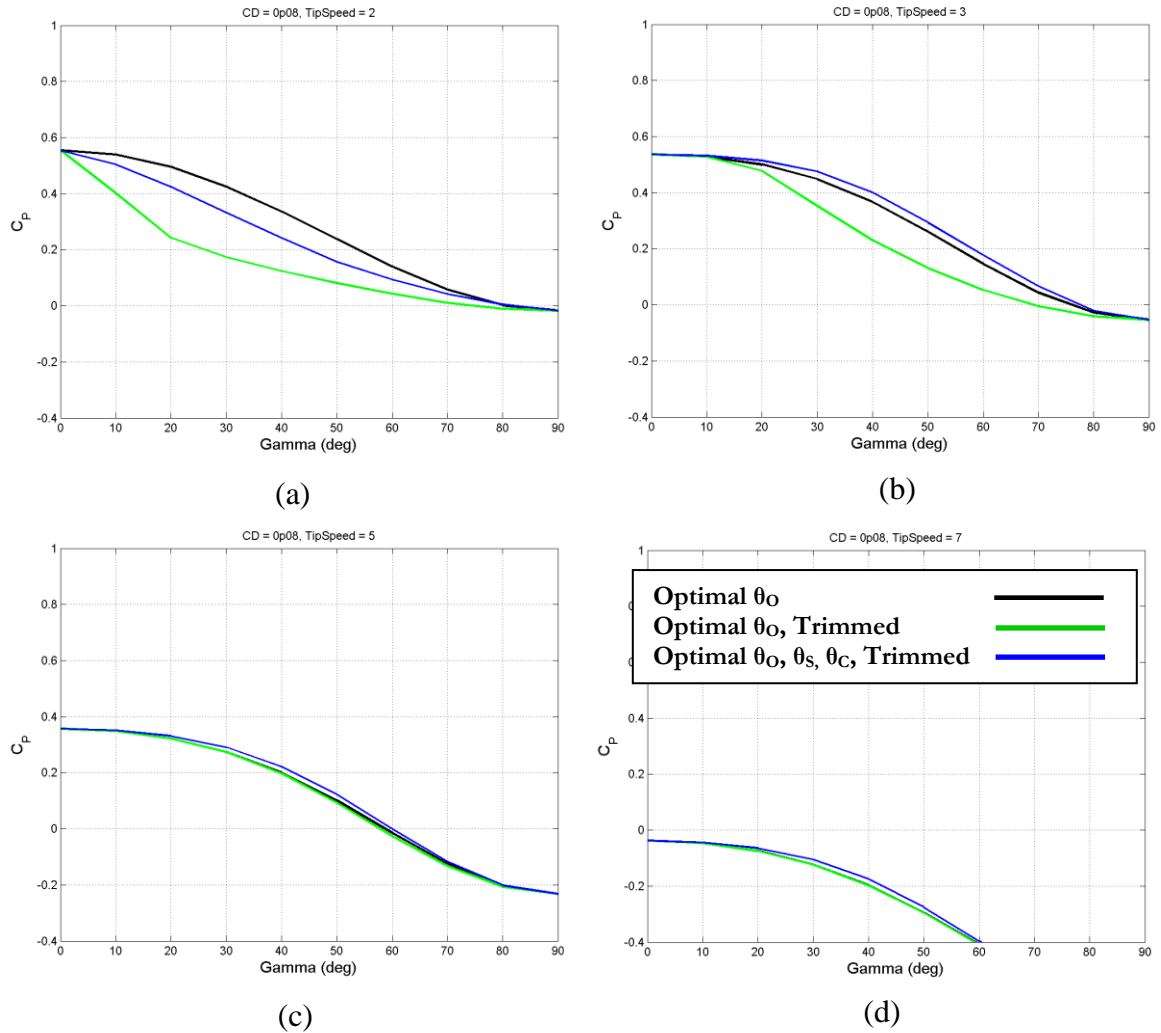


**Figure 7.12 Optimal CP as a function of Yaw Angle,  $\gamma$ , for  $C_D = 0.08$ , and (a)  $J = 2$ , (b)  $J = 3$ , (c)  $J = 5$  and (d)  $J = 7$**

In Figures 7.11 – 7.12, plot (a) shows the result that at low tip speeds, the objective of finding small moments degrades the power coefficient at all yaw angles. The results for tip speeds of 3-7 show that in yawed flow, the use of cyclic pitch increases the power coefficient over the case of collective only without trim. Thus in yawed flow, the use of cyclic pitch does increase the feasible power output.

It is also useful to review the optimal values  $\theta_0$ ,  $\theta_s$  and  $\theta_c$ , computed by the optimization routine. Figures 7.13 – 7.16 show the optimal values as a function of tip speed for yaw angles of 0, 20, 40 and 60 degrees respectively.



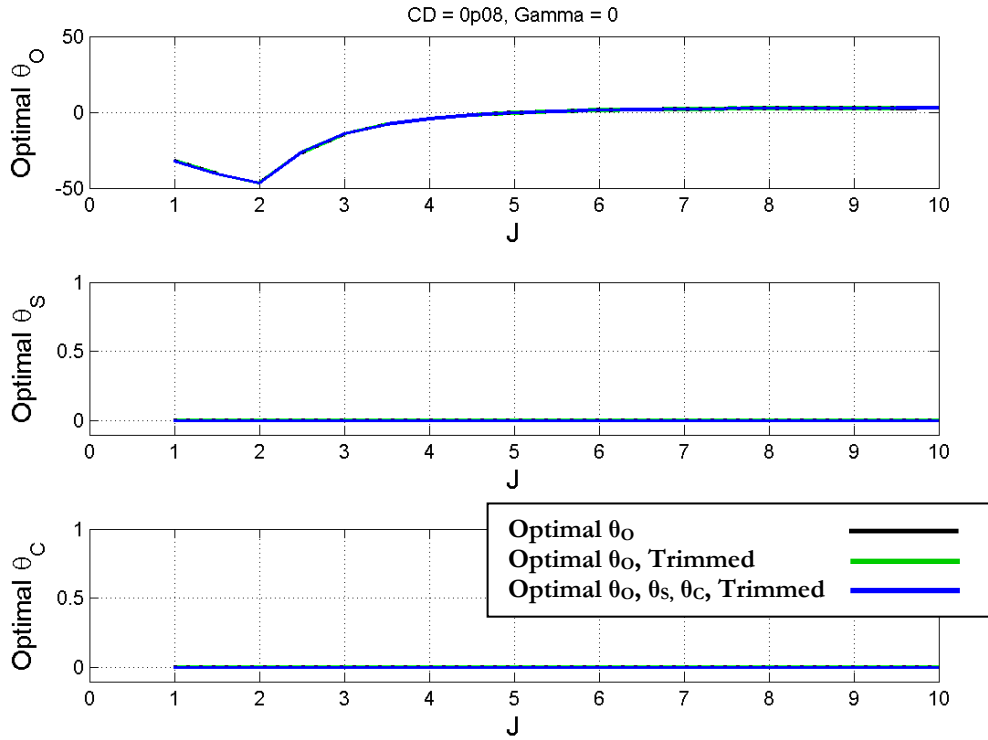


Figure 7.13 Optimal Values as a function of tip speed, J, for  $C_D = 0.08$ , and  $\gamma = 0^\circ$

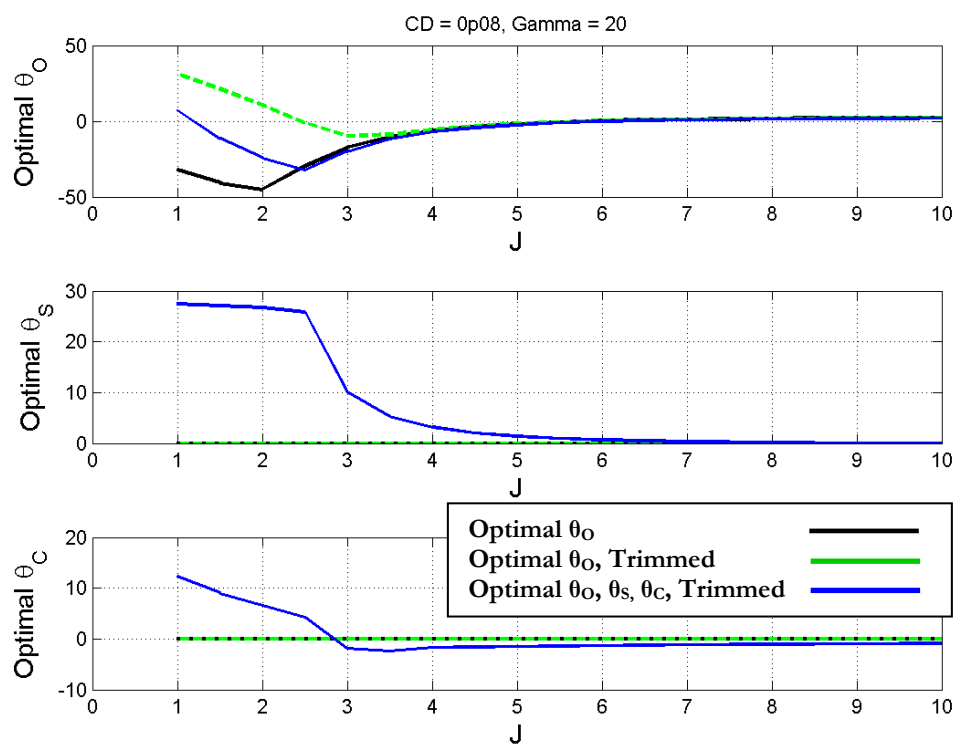


Figure 7.14 Optimal Values as a function of tip speed, J, for  $C_D = 0.08$ , and  $\gamma = 20^\circ$

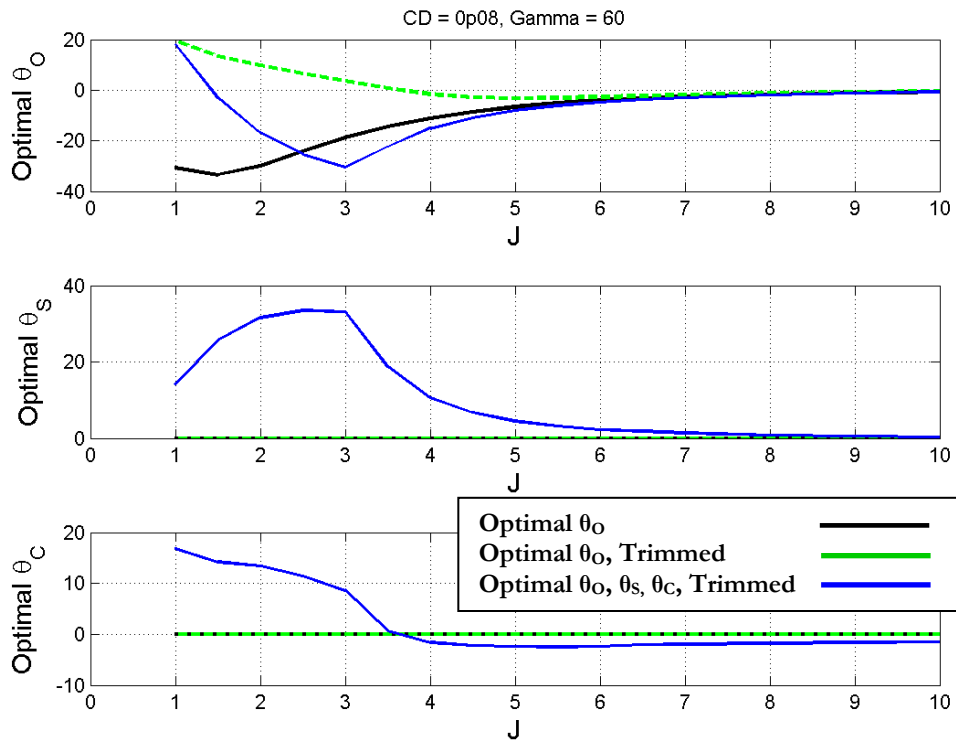


Figure 7.15 Optimal Values as a function of tip speed,  $J$ , for  $C_D = 0.08$ , and  $\gamma = 40^\circ$

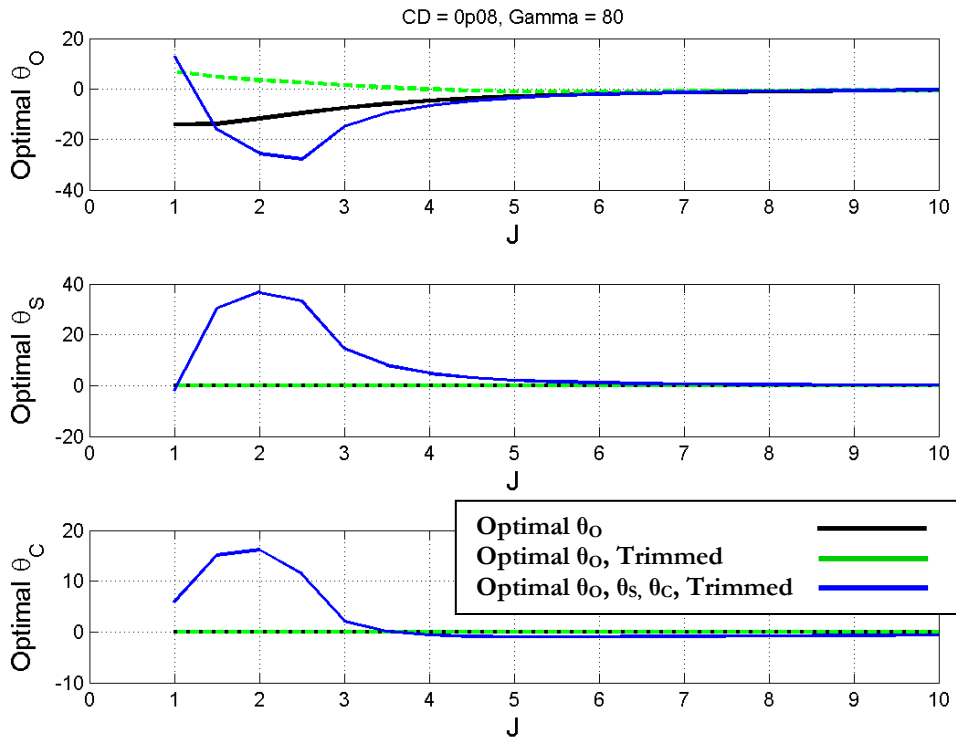
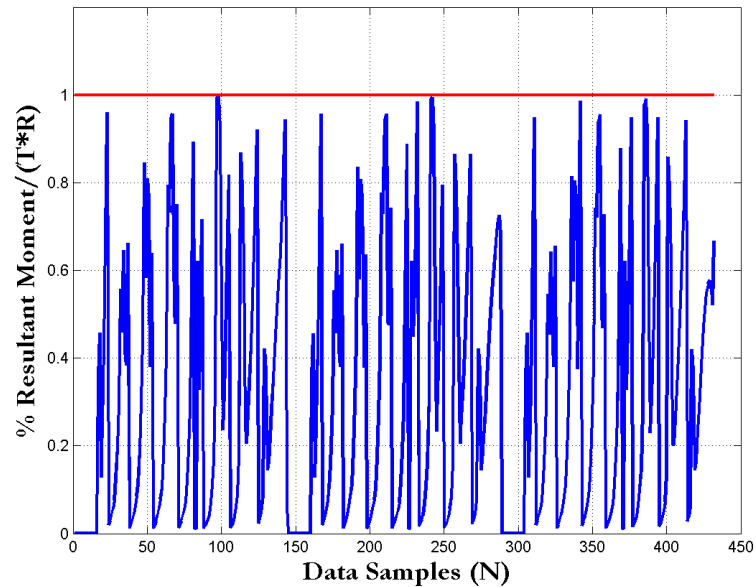


Figure 7.16 Optimal Values as a function of tip speed,  $J$ , for  $C_D = 0.08$ , and  $\gamma = 60^\circ$

The data generally show larger blade deflections at lower tip speeds, where the system forces and moments are increasing. As the optimal power changes and system forces and moments grow, it is natural to expect more dynamically changing optimal values. The optimal results require all three control terms be active (nonzero) from tip speeds of 1-5 to accomplish the pseudo-trimmed state. Generally the peak deflections increase with the yawed flow angle. It is also observed that the magnitude of the blades can become large and thus the results can be degraded should stall be included in the model (which is future work for improving WT\_3DOF). Interestingly enough, the objective of reducing the moments did decrease the magnitude of the optimal values over chapter 6, reducing the potential impact of stall or dynamic stall on these results.

A final check to be accomplished is to make sure the optimization routine met the design criteria for reducing the system moments while optimizing the power coefficient. Figure 7.17 shows the percentage ratio of the system's resultant moments divided by the instantaneous thrust times rotor radius for all data samples presented in this chapter.



**Figure 7.17 % Resultant Moment/(T\*R) for Optimal Results Using Collective and Cyclic Pitch in Trimmed State**

Figure 7.17 shows that the data meet the design criteria of being less than 1%. This result shown is for the case where both collective and cyclic pitch are optimization variables. When only collective pitch is a variable for optimization, the resultant moments were quite large and unable to meet this criterion.

Hohenemser hypothesized that cyclic pitch could be used to control the yaw angle of a wind turbine with respect to the wind. To fully investigate this idea would require a feedback control simulation to evaluate the full system performance. However the results in this chapter encourage the idea. The objective of trimming the system in yawed flow did not render impossible the realization of a feasible power coefficient (i.e. comparable to a turbine optimizing collective pitch without trim.) At low tip speed, the trimmed condition impacts the power coefficient more significantly. But the use of cyclic pitch increases the range of tip speeds for which a decent power coefficient can be achieved in yawed flow. It is also able to meet the competing objective of reducing the system moments. This increases the design space for further study in control methods, such as real-time adjustments to the turbine yaw angle to keep the system in a desired tip speed range.

# Chapter 8

## Conclusions and Future Work

The objective of this research is to numerically determine the value of the parameters required to optimize a wind turbine's power output using the traditional rotary-wing control terms of collective and cyclic pitch. The primary objective is to optimize the power coefficient using collective and cyclic pitch, in the presence of axial or yawed wind inflow, and evaluate what effect increasing the control space has on the optimal power coefficient. A secondary objective of this research is to investigate the effect of cyclic pitch on the power coefficient if it were being used to both reduce the system moments of a wind turbine at a specific yaw angle and optimize the power coefficient.

To accomplish these objectives a literature review was performed documenting the relevant previous work. Special attention was paid to the available wind turbine codes that are available for industrial use. To perform the analysis, a wind turbine simulation called WT\_3DOF was developed that included a blade element theory and the nonlinear form of the Pitt Peters dynamic inflow model. Although this simulation is currently very simple and can be greatly improved, the model showed good agreement with NREL's WT\_PERF simulation in axial flow for a set of test cases presented and is considered sufficient for use in this feasibility study. In chapter 5, WT\_3DOF was used to provide design space plots for the optimal power coefficient. The results showed that varying cyclic pitch could result in larger power coefficients than a case where cyclic pitch is fixed. Grid surface plots were presented to show that the design space was well suited for a gradient search type optimization routine.

Regarding the primary objective, chapter 6 presents numerical results for the optimal power coefficient as the system control space is opened. Three cases were compared to evaluate the change in control space: a fixed pitch case ( $\theta=0$ ), a case where only the collective pitch is a variable and a case where both collective and cyclic pitch are variables. The results show conclusively that in yawed flow, the use of cyclic pitch can result in a larger optimal power coefficient.

Increasing the power coefficient in yawed flow can result in more cumulative power output as wind changes direction with respect to a turbine. As discussed, yaw angle can be used as a regulator to control the magnitude of air flowing through the turbine disk. This can be valuable in making sure the airflow is consistent with the rotor rating or optimal tip speed for the hardware and operating conditions. The chapter 6 results would suggest that for any system using this technique, the use of cyclic pitch would produce more power than a fixed pitch turbine or one that optimizes collective pitch only. It was observed that the magnitude of the blade deflections became large and could be affected by dynamic stall, which is currently not modeled in WT\_3DOF.

Regarding the secondary objective, chapter 7 extends the results of chapter 6 by modifying the objective function in the optimization to reduce the system moments. This is intended capture how the optimal power coefficient will generally change when the cyclic pitch has competing priorities: optimizing power and holding the system in a pseudo-trimmed state. Three cases were again compared to evaluate how the power coefficient changes when blades are trimming the system and the control space opens. The first case is the optimal results with only collective pitch as a variable and no trim constraint. The second case is the optimal results with only collective pitch as a variable and with a trim constraint. The third case is the optimal result with collective and cyclic pitch as variables with a trim constraint.

The chapter 7 results show that, except for low tip speeds, it is feasible for cyclic pitch to both trim a system and provide the same level of power as the first case, where collective pitch is optimized without trim. This is an interesting result for any turbine design that seeks to optimize the power coefficient in axial or yawed flow while keeping the moments small. Hohenemser posited that cyclic pitch could be used to control the yaw angle of a wind turbine with respect to the wind. The chapter 7 results suggest that

this could be accomplished without serious degradation to the optimal power coefficient. Although just a feasibility study in its current form, the results do provide an encouraging result for Hohenemser's idea. As in chapter 6, it is observed that the magnitude of the blade deflections became large and could be affected by stall, which is currently not modeled in WT\_3DOF. Also the objective of trimming the system did degrade the power coefficient at low tip speeds. Additional study is required to see if improvements can be made at low tip to wind speed ratios.

There is no shortage of future work available. As mentioned, to fully investigate this idea would require a feedback control simulation to evaluate the full system performance. Many wind turbine codes are available, however none of them model cyclic pitch. Thus to add fidelity to the results presented in this thesis, and to determine how much cyclic pitch can improve power output in a time domain with realistic wind models, more simulation work is required. This can be done using the available turbine codes such as those developed at NREL, however they would need to be modified with new control terms and recompiled.

Alternatively, improvements could be made to WT\_3DOF in the MATLAB environment. Improvements to WT\_3DOF need start with the wind turbine plant and include an improved dynamic inflow model (such as the Generalized Dynamic Wake model) to account for radial changes in induced velocity, a dynamic stall model for large blade deflections and a code improvements to simplify how airfoil data is loaded into the simulation. Once improvements are made to the plant, the model would need some level of validation by comparing the simulation results to actual wind turbine data. And once the plant is validated a control loop could be added for analysis. This application for studying how control methods can optimize power can be used to analyze specific turbine systems. A possible extension of the code is analyzing ocean turbines that collect power from strong ocean currents. Perhaps in such an environment the use of improved control methods may result in greater power output as flow through the turbine disk is balanced.

# Appendix A

To compute the element value of  $dF_1^i$  and  $dF_2^i$ , the equations (3.12) and (3.13) are used. Substituting (3.5), (3.10) and (3.11) gives the blade element lift and drag force for that section of the blade in terms of  $W_T$  and  $W_p$ . Substituting (3.8) and (3.9) into (3.12) and (3.13) yields:

$$dF_1 = \frac{1}{2} \rho c dx [\cos\theta W_p W_T - \sin\theta W_T^2] + \frac{1}{2} \rho c dx [W_p \sqrt{W_T^2 + W_p^2}] C_D \quad (A.1)$$

$$dF_2 = \frac{1}{2} \rho c dx [\cos\theta W_p^2 - \sin\theta W_p W_T] - \frac{1}{2} \rho c dx (W_T \sqrt{W_T^2 + W_p^2}) C_D \quad (A.2)$$

which represents  $dF_1^i$  and  $dF_2^i$  in terms of  $W_T$  and  $W_p$  (presuming  $C_D$ ,  $\rho$ ,  $a$ ,  $c$  and  $dx$  are known.) Some simplifying assumptions are:

$$\sqrt{W_T^2 + W_p^2} = W_T \quad (A.3)$$

$$\sin\theta = 0 \quad (A.4)$$

$$\cos\theta = 1 \quad (A.5)$$

$$\frac{C_D}{a} = 0 \quad (A.6)$$

which when put into (A.1) and (A.2) yield:

$$dF_1^i = \frac{1}{2} \rho a c dx [-(W_T^i)^2 \theta + W_p^i W_T^i] \quad (A.7)$$

$$dF_2^i = \frac{1}{2} \rho a c dx [-(W_T^i)^2 \frac{C_d}{a} - W_p^i W_T^i \theta + (W_p^i)^2] \quad (A.8)$$

which are equations (3.14) and (3.15).



# Appendix B

WT\_3DOF is a MATLAB Simulink program that, in its current state, simply combines a blade element theory and the nonlinear Pitt Peters dynamic inflow model to evaluate aerodynamic performance of wind turbines. This simplified version of a wind turbine simulation was developed due to the non-existence of wind turbine code that could evaluate cyclic pitch. Industry codes could be modified to account for cyclic pitch, but none of them were, at the time of this thesis work, available to the author for use or develop. Descriptions of the simulation inputs and outputs are shown in Tables 4.1 and 4.2. Figure B.1 shows the top level system blocks of WT\_3DOF.

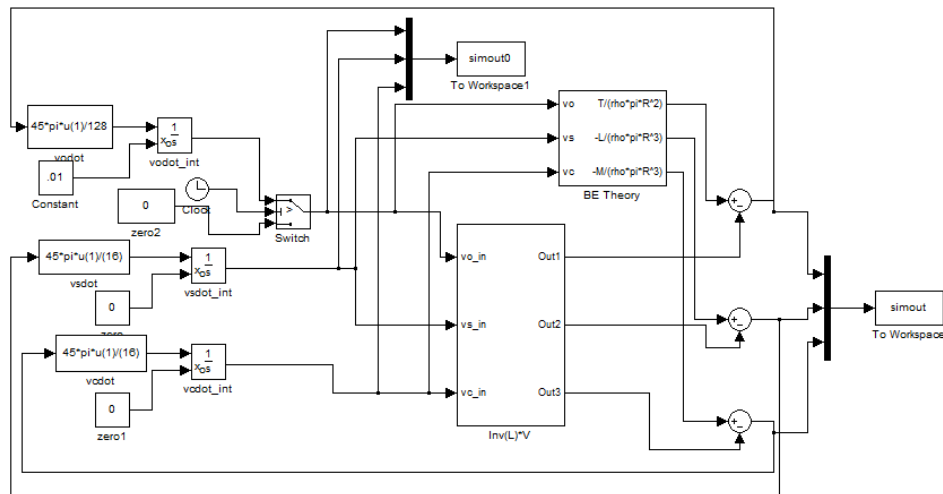


**Figure B.1 Top Level Blocks of WT\_3DOF**

Figure B.2 shows the BE Theory Block.

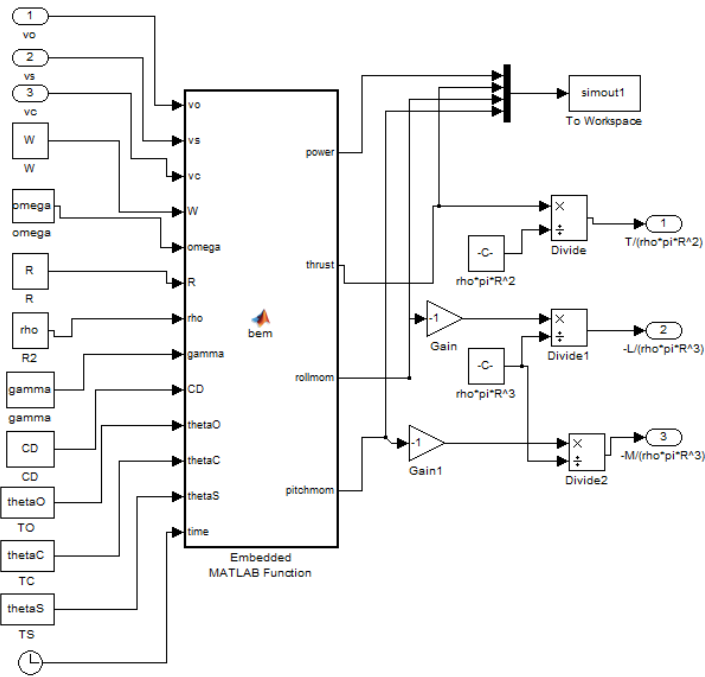


**Figure B.2 Blade Element Theory Block in WT\_3DOF**

Because the non-linear solution of the Pitt-Peters model is dependent upon the instantaneous thrust, pitch and roll moment, the dynamic inflow model and blade element theory are coupled. For each run the simulation is initialized and allowed to converge to a solution for the defined parameters. The “BEM” block in Figure B.2 is a simple routine that sums the moments and forces along all the blade elements using all the inputs shown. The clock is used as a simple means to simulate blade rotation.

# References

- [1] "20% Wind Energy by 2030: Increasing Wind Energy's Contribution to the U.S. Electricity Supply", The U.S. Department of Energy, December 2008.
- [2] "2008 Wind Technologies Market Report", The U.S. Department of Energy, July 2009.
- [3] [www.baseloadenergy.com](http://www.baseloadenergy.com)
- [4] [http://baseloadenergy.com/blog\\_beblog/](http://baseloadenergy.com/blog_beblog/)
- [5] Hohenemser, K. H. and Swift, A. H. P., "Torque Control by Yawing of a Constant Speed Two-Bladed Wind Turbine with Passive Cyclic Pitch Variation," Proceedings of the Sixth Biennial Wind Energy Conference and Workshop, Minneapolis/St. Paul, June 1983, pp. 277-287.
- [6] Wilson RE, Lissaman PBS. Applied aerodynamics of wind power machines. PB 238595, Report No. NSF-RA-N-74-113, NTIS, Springfield, Virginia, 1974.
- [7] Rankine, W. J., Transactions, Institute of Naval Architects, Vol. 6, 1865.
- [8] Froude, W., Transactions of Naval Architects, Vol 19, 1878.
- [9] Froude, W., Transactions of Naval Architects, Vol 30, 1879.
- [10] Betz, A. *Windenergie und Ihre Ausnutzung durch Windmullen*. Vandenhoeck and Ruprecht, Gottingen, 1926.
- [11] Glauert, H., *Aerodynamic Theory*, Vol. 6, Division L, p. 324. Julius Springer, Berlin 1935.
- [12] Glauert, H., *The Analysis of Experimental Results in the Windmill Break and Vortex Ring States of an Airscrew*, Br. R & M 1026, 1926.
- [13] Joukowski, N. E., *Travaux du Bureau des Calculs et Essais Aeronautiques, de l'Ecole Supérieure Technique de Moscou*, 1918.
- [14] Prandtl, L., Appendix to *Schraubenpropeller mit geringstem Energieverlust*, by A. Betz, *Gottinger nchr.* P. 193-217, 1919.
- [15] Wilson, R. E., Lissaman, B. S. & Walker, S. N. Aerodynamic Performance of Wind Turbines, Report No. EDRA/NSF/0414-76/1, Oregon State University, June 1976.

- [16] Wilson RE, Lissaman PBS, Walker SN. Aerodynamic performance of wind turbines. Report No. NSF/RA-760228, NTIS, Chapters I–III, Oregon State Univ., June 1976.
- [17] Wilson, R. E., "Aerodynamics Potpourri", Wind Turbine Dynamics Workshop, Cleveland, Ohio, February 1981.
- [18] T. Burton, D. Sharpe, N. Jenkins, and E. Bossanyi. Wind Energy Handbook. Jon Wiley & Sons, 2001.
- [19] Manwell, J. F., McGowan, J. G. and Rogers, A. L. *Wind Energy Explained: Theory, Design and Application*, Second Edition. John Wiley & Sons, Ltd, Chichester, UK. 2009.
- [20] Swift, Andrew H.P., *The Effects of Yawed Flow on Wind Turbine Rotors*, D.Sc. Dissertation, Washington University in St. Louis, May, 1981.
- [21] Pitt, D.M. and Peters, D.A. March 1981. "Theoretical Prediction of Dynamic Inflow Derivatives," *Vertica*, Vol.5. (1), pp.21-34.
- [22] Swift, Andrew H.P., "Extensions to the Wilson-Lissaman Prop Code for Steady and Dynamic Rotor Performance Prediction", Presentation at Energy Sources Technology Conference & Exhibition, Houston, Texas, January 30th - February 3rd, 1983.
- [23] Viterna, L.A. and Corrigan R. D., "Fixed Pitch Rotor Performance of Large Horizontal Axis Wind Turbines", Large Horizontal Axis Wind Turbines Conference, Cleveland, Ohio, July 1981.
- [24] Snel, H. and Schepers, J.G. (ed.). "JOULE 1: Joint Investigation of Dynamic Inflow Effects and Implementation of an Engineering Method", ECN-C-94-107, December 1994.
- [25] Suzuki, A. *Application of Dynamic Inflow Theory to Wind Turbine Rotors*, Ph.D. Dissertation, University of Utah, August 2000.
- [26] Peters, D.A, and He, Cheng Jian, "Correlation of Measured Induced Velocities with a Finite-State Wake Model," *Journal of the American Helicopter Society*, Vol.36(3). July 1991.
- [27] Hansen, A.C. Yaw Dynamics of Horizontal Axis Wind Turbines. NREL/TP-442-4822. Golden, CO: National Renewable Energy Laboratory, 1992. Work performed by the University of Utah, Salt Lake City, Utah.

- [28] D. A. Peters, J. Loyet, W. Chan, and L. Ahaus, "Optimum operational parameters for tethered yawed wind turbines," in *Proceedings of the 29<sup>th</sup> Applied Aerodynamics Conference*, Honolulu, Hawaii, June, 27-30, 2011.
- [29] D.A. Peters, X. Rong, "Optimal Operational Parameters for Yawed Wind Turbines," *International Journal of Aerospace Engineering*, Volume 2011, Article ID 635750, April 7<sup>th</sup>, 2011.
- [30] Hohenemser, Kurt H., Swift, Andrew H. P., and Peters, David A., A Definitive Generic Study for Sailwing Energy Systems, Final Report, SERI Subcontract No. AH-9-8003-5, SERI/TR-8003-02, October 1979.
- [31] Hohenemser, K. H., "Analysis and Test Results for an Improved Constant Speed Passive Cyclic Pitch Wind Turbine," Final Subcontractor Report, SERI Subcontract XE-2-02054-01, SERI STR-217-3002, DE87001135, January 1987.
- [32] Hohenemser, Kurt H., Analysis and Test Results for a Two-bladed, Passive Cyclic Pitch, Horizontal-Axis Wind Turbine in Free and Controlled Yaw, NREL/TP-442-7391, National Renewable Energy Lab, October 1995.
- [33] <http://www.metaefficient.com/news/new-record-worlds-largest-wind-turbine-7-megawatts.html>
- [34] Passon P., Kühn M., Butterfield S., Jonkman J., Camp T., Larsen T. J., "OC3– Benchmark Exercise of Aero-elastic Offshore Wind Turbine Codes." *Journal of Physics: Conference Series* 75. 2007.
- [35] <http://wind.nrel.gov/designcodes/>
- [36] NWTC Design Codes (WT\_Perf by Marshall Buhl). <http://wind.nrel.gov/designcodes/simulators/wtperf/>. Last modified 17-February-2011; accessed 17-February-2011.
- [37] [http://wind.nrel.gov/designcodes/papers/GL\\_Certific.pdf](http://wind.nrel.gov/designcodes/papers/GL_Certific.pdf)
- [38] NWTC Design Codes (AeroDyn by Dr. David J. Laino). <http://wind.nrel.gov/designcodes/simulators/aerodyn/>. Last modified 03-February-2011; accessed 03-February-2011.
- [39] <http://www.windwardengineering.com/>
- [40] Gaonkar, G.H. and Peters, D.A. "Review of dynamic inflow modeling for rotorcraft flight mechanics". *Vertica*, Vol. 12, No. 3, pp. 213-242, 1988.
- [41] HaQuang, N. and Peters, D.A. "Dynamic Inflow for Practical Applications". *Journal of the American Helicopter Society*, Vol. 33, No. 4, October 1988, pp. 64-68.

- [42] <http://wind.nrel.gov/designcodes/simulators/wtperf/verification/>
- [43] Boyd S. & Vandenberghe L., *Convex Optimization*. Cambridge University Press, 2004.

# Vita

## Robert Isaac Liebschutz

<b>Date of Birth</b>	August 27, 1973
<b>Place of Birth</b>	Iowa City, Iowa
<b>Degrees</b>	B.S. Summa Cum Laude, Mechanical Engineering, December 2000 M.S. Mechanical Engineering, December 2002 D.Sc. Mechanical Engineering, May 2012
<b>Professional Societies</b>	American Society of Mechanical Engineers American Institute of Aeronautics and Astronautics

May 2012